High-speed optical fibre transmission using advanced modulation formats

Sergejs Makovejs

A thesis submitted to the University College London for the degree of Doctor of Philosophy (Ph.D.)

Department of Electronic and Electrical Engineering
University College London
July 2011

I, Sergejs Makovejs, confirm that the work presented in this thesis is my own. Where information has been deri ved from other sources, I confirm that this has been indicated in this thesis.

To my parents and Tillie

Abstract

The rapid growth in interactive bandwidth-hungry services demands ever higher capacity at various stages of the optical network, leading to a potential capacity exhaust, termed the *capacity crunch*. The main aim of the research work described in this thesis was to help solve the potential capacity crunch by exploring techniques to increase the data rate, spectral efficiency and reach of optical fibre systems. The focus was on the use of advanced signal modulation formats, including optical time-division multiplexing (OTDM), quadrature phase shift keying (QPSK), and 16-state quadrature amplitude modulation (QAM16). QPSK and QAM16 modulations formats were studied in combination with coherent detection and digital signal processing (DSP) for the compensation of transmission impairments. In addition, return-to-zero (RZ) pulses were explored to increase the tolerance towards nonlinearity for coherently detected signals, and nonlinearity compensation (NLC) through the DSP.

Initially, to maximise the bit-rate, research was focused on the study of OTDM transmission at 80Gbit/s with the aim to optimise the phase difference between the adjacent OTDM channels. A new technique to achieve bit-wise phase control using a phase-stabilised fibre interferometer was proposed. Faced with a limited fibre capacity, the need to maximise the spectral efficiency became paramount, and thus the need to use phase, amplitude and polarisation domains for signal transmission. In combination with coherent detection the research focused on the performance of optical fibre systems using QPSK and QAM16 modulation formats, including their generation, transmission and detection in single-channel and WDM regimes. This included the study of the impact of pulse shapes, and the mitigation of linear and nonlinear transmission impairments with receiver-based DSP at bit-rates ranging from 42.7 to 224Gbit/s. The technique demonstrated for bit-wise phase control for OTDM was successfully used to demonstrate a new method for QAM16 signal generation. Longest transmission distances (up to 10160km in 112Gbit/s QPSK, 4240km in 112Gbit/s QAM16, and 2000km in 224Gbit/s QAM16) have been achieved with the use of NLC and RZ pulses. The efficiency of these two techniques is explored through a comprehensive set of experiments in both single-channel and WDM transmission experiments. The results can be used in the design of future optical transmission systems.

Acknowledgments

I am profoundly grateful to Professor Polina Bayvel for giving me the opportunity to pursue my PhD at UCL, and for her constant support and guidance throughout my research. Her uncompromising quest for truth has been a constant source of inspiration, and has helped me to remain motivated for the past four-and-a-half years. I have a great deal of respect for Polina in many senses and I sincerely hope we will remain friends for years to come.

Amongst others, I would particularly like to thank Dr. Giancarlo Gavioli for supervising my initial activities in the Optical Networks Group transmission laboratory and for being my mentor. Our close collaboration has gradually turned into strong friendship. I am also grateful to Dr. Vitaly Mikhailov for frequent technical discussions, which helped me refine the process I used for my problem-solving. Vitaly also showed a great deal of interest in my research work after he left UCL, which I am very thankful for. I would also like to thank other academics in the department: Dr. Robert Killey, Dr. Seb Savory and Dr. Benn Thomsen for their support and helpful technical discussions.

I also feel lucky and grateful for the chance to have worked with my colleagues David Millar, Carsten Behrens and Enrico Torrengo – they all brought their invaluable complementary expertise into the research project. I would also like to acknowledge Carsten for letting me use some of his simulation results in my PhD thesis (Section 6.3) to support my experimental results.

I would also like to thank Yokogawa for providing my studentship, without which this research work would not have been possible. Finally, I can't express enough how fortunate I am to have such strong support from my parents and my loving wife Tillie, for whose understanding and encouragement I am very grateful.

Table of Contents

1. Introduction

1.1. Motivation for High-Speed Optical Fibre Transmission

As well put in [1], "optical fibre communication is firmly entrenched as part of the global information infrastructure", that is high performance optical networks are essential for economic growth and well-being of communities. The attraction of transmission over an optical fibre is mainly in its much larger capacity compared to copper counterparts and immunity to electromagnetic interference and other external influence. At present, optical fibre transmission is seen as a dominant technology for both long-haul and short-haul broadband transmission.

Following the "bubble burst" of the early 2000's, the revival in research into optical fibre communication has been remarkable. It is now becoming increasingly apparent that the reason partially lies within social behaviour, that is the desire for new interactive bandwidth-hungry services, such as video-on-demand, high-definition 3D television, online gaming and others. It has also become clear that what was previously thought to be plentiful capacity could gradually result in a capacity exhaust, if no actions are taken. Ironically, the flattening of the increase in the optical bit-rate of commercially deployed systems due to the "bubble burst" in combination with the continuing increase in the clock speed of silicon chips, facilitated the convergence of the silicon chip speed with optical line-rates. This has helped coherent detection with DSP gain momentum and become a practical technique to mitigate fibre impairments, demodulate advanced modulation formats and perform many other functions that were previously performed optically or using analogue electronics. Coherent detection and subsequent DSP has also revolutionised the way the system designers and researchers can solve the limitations of fibre impairments and other functionality, such as polarisation tracking and phase recovery.

Over its history optical fibre system development has mainly been aided by the reduction of losses in optical fibres [2] and the invention of optical amplifiers, which in turn facilitated the use of the WDM technology. WDM, initially performed for intensity modulated (IM) signals with direct detection (DD), has allowed different wavelength channels to be densely packed to enhance the utilisation of the available bandwidth, which is fast becoming a limited and, therefore, a precious resource. The subsequent growth in the channel bit-rate and overall capacity can be attributed to the development of optical time-division multiplexing (OTDM), advanced modulation formats, and coherent detection with DSP.

OTDM was initially proposed as a laboratory technique to overcome the limited bandwidth of available electronics by increasing the bit-rate optically. This approach was used in the early 40Gbit/s IM-DD OTDM experiments, which were assembled from 4x10Gbit/s base-rate channels. With the further development and refinement of electrical components the generation of a 40Gbit/s signal using a fully electrical time-division multiplexing (ETDM) has become feasible. The ETDM bit-rates are currently limited to 56Gbit/s, therefore, to understand the transmission limitation at higher IM-DD speeds the use of an OTDM technique is essential.

In contrast, advanced modulation formats – the ones that make use of not only amplitude, but also other signal domains, such as phase and the state of polarisation, are more sophisticated techniques to encode the electrical data pattern onto an optical carrier. This yields an enhancement in the functionality and an increase in the spectral efficiency, compared to the conventional IM-DD schemes used for the majority of optical fibre communication systems to date. Advanced modulation formats can also have improved noise characteristics and increased tolerance towards nonlinearity due to the more optimum allocation of symbols on the complex plane. A “constellation diagram” is typically used to represent the signal as a two-dimensional diagram on a complex plane, and allows visualisation of both amplitude and phase modulation. In addition, the use of coherent detection and DSP takes full advantage of the benefits of advanced modulation formats and allows functionality, previously unavailable for systems with direct detection.

The main aim of the research work described in this thesis was to investigate the techniques, which allow an increase in the bit-rate and/or transmission distance of existing and future optical transport systems. At the start of this research work OTDM

was seen as a driving technology to satisfy an increase in the signal bit-rates, and initial research activities of this work were, therefore, focused on the techniques to increase the transmission distances of OTDM signals. The initial goal of this research work was to investigate the generation and transmission of OTDM signals at 160Gbit/s, and exploring the techniques of bit-wise phase control that would allow a greater range of modulation formats to be implemented. At the time 160Gbit/s was seen as the bit-rate of the next-generation optical fibre systems, following the traditional four-fold increase in the bit-rate, according to synchronous digital hierarchy (SDH). However, by 2008 it has become apparent that the future long-haul optical fibre transmission systems are likely to be based on the emerging technology, consisting of the symbiosis of advanced modulation formats, coherent detection and DSP, and accumulating the advantages brought by these individual techniques. The research was then re-focused towards the study of advanced modulation formats with coherent detection. However, the phase-stabilisation technique, initially developed during the work on bit-wise OTDM signal generation, has also proved to be invaluable for all the subsequent research on the generation and transmission of advanced modulation formats.

It should be noted, however, that prior to 2008 limited experimental work was published in the area on the advanced modulation formats, primarily employing quadrature phase-shift keying (QPSK) modulation and conventional non-return-to-zero (NRZ) pulses. The aim of the research work described in this thesis was, therefore, to carry out a comprehensive study of transmission performance of not only QPSK signals, but also more spectrally efficient 16-state quadrature amplitude modulated (QAM16) signals. The research focused on the experimental implementation of these formats and their transmission to maximise both bit-rate and distances over which these could be transmitted on standard single-mode fibre (SMF) with Erbium-doped fibre amplifiers (EDFAs) only.

The advantage of QAM16 is a twice lower symbol rate, required to achieve the same overall bit-rate as in the case of QPSK, which means that the lower-bandwidth electrical components can be used for QAM16. The advantage of QAM16 format, however, comes at the expense of the increased required optical signal-to-noise ratio (OSNR), reduced tolerance towards nonlinearity and the complexities, associated with its generation. While QPSK coherent optical transport systems have recently become available from Ciena [3] and were also tested by Opnext/AT&T/Cisco in field trials [4],

the QAM16 technology still remains largely unavailable even in optical fibre transmission research laboratories. QAM16 is also a very promising modulation format to obtain a 400Gbit/s per carrier – the likely bit-rate of the 2nd generation future optical fibre transmission systems [5]. The constellation diagrams of currently most widespread modulation formats are shown in Figure **1**.

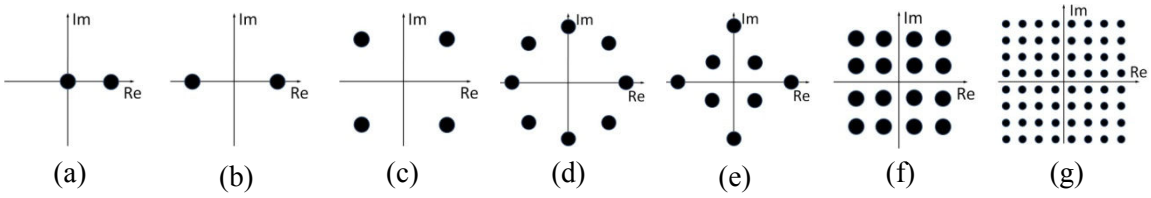

Figure 1: Constellation diagrams of various modulation formats; (a) OOK (b) BPSK (c) QPSK (d) PSK8 (e) QAM8 (f) QAM16 (g) QAM64

The ways to further increase the bit-rate to 1Tbit/s per optical carrier is currently a topic of active research, and a solution to efficiently generate and receive a 1Tbit/s signal is being actively sought after. Overall, it is clear that optical fibre communication technology is entering a stage where the combination of all possible innovations in the field must be applied to improve the capacity of optical fibre networks. It should also be noted that in practical systems, such considerations as floor space, system complexity, cost of the terminal equipment and power consumption need to be taken into account, in addition to the technological benefits any new techniques offer.

This research work also provides the first comprehensive analysis of the two techniques to increase the maximum reach (defined as the maximum achievable transmission distance for a given system design): return-to-zero (RZ) pulses instead of NRZ, and digital back-propagation for nonlinearity compensation (NLC). The investigation of these techniques is carried out for both QPSK and QAM16 transmission.

The rest of this PhD thesis is structured as follows. Chapter 2 provides a background on the techniques used in this research work, such as the design of OTDM subsystem blocks and the operational principle of the Mach-Zehnder and electro-absorption modulators (MZMs and EAMs, respectively). The understanding of MZM operation principle is important for the generation of QPSK and QAM16 signals, and also for the return-to-zero (RZ) pulse shaping. Section 2.3 describes the hardware part of a digital

coherent receiver and the subsequent DSP, which is carried out offline in Matlab. The DSP used in this research work was implemented in a parallel PhD work by my colleague David Millar, as a part of our collaborative work. Section 2.4 outlines the sources of transmission impairments, which are relevant to the specific experiments carried out in this research work. Chapter 2 also summarises the results previously reported by other research groups in the area of OTDM with direct detection (section 2.1.4), advanced modulation formats with coherent detection (section 2.2.6), and OTDM with advanced modulation formats and coherent detection (section 2.1.5).

Chapter 3 is focused on the investigation of 80Gbit/s OTDM (2x40Gbit/s) transmission performance by varying the phase relationship between the adjacent OTDM tributaries. To emulate long-haul transmission, a recirculating fibre loop was used for all transmission experiments carried out in this PhD work (described in Appendix A). The details on the technique used to generate bit-wise OTDM signals are given in section 3.2. The further characterisation of 80Gbit/s OTDM transmission was carried out using simulations by varying the data pulse width and the receiver filter bandwidth, and calculating the maximum achievable transmission distance (section 3.5).

Chapter 4 describes the single-channel back-to-back and transmission experiments and the obtained results for both QPSK (section 4.1) and QAM16 (section 4.2) signals. The QPSK transmission was carried out at 42.7, 85.4 and 112Gbit/s, while QAM16 signals were characterised at 112Gbit/s and 224Gbit/s (this is one of only 4 demonstrations of 224Gbit/s QAM16 transmission reported to date). The bit-rates of 42.7 and 112Gbit/s for QPSK transmission were chosen from a practical perspective, since these are the bit-rates on which the next generation of coherent transponders are currently being developed. The QAM16 transmission at 112Gbit/s allowed for the comparison of its performance with the QPSK transmission at the same bit-rate to identify an optimum modulation format for 100Gbit/s applications. The QAM16 transmission is further studied at the bit-rate of 224Gbit/s; this is an interim step towards a 400Gbit/s – the likely bit-rate for the 2nd generation of future optical networks. Therefore, understanding an upper bound of 224Gbit/s transmission would also help estimate the transmission limits at higher bit-rates and refine experimental techniques required to generate and receive a higher bit-rate signal. The benefit of using return-to-zero with 50% duty cycle (RZ50) pulses instead of non-return-to-zero (NRZ)

pulses is further quantified in the QPSK (section 4.1.3) and QAM16 (section 4.2.3) transmission experiments. A possibility to generate a QAM16 signal at the symbol rate of up to 42Gbaud is investigated in section 4.2.4.

Finally, chapter 5 extends the results obtained in chapter 4 to the WDM generation and transmission of QPSK and QAM16 signals at 112 and 224Gbit/s. As in the case of single-channel transmission, NRZ and RZ50 pulse shapes were compared for all bit-rates investigated in this chapter. At 224Gbit/s the experimentally obtained results are further extended using Matlab simulations, which also investigate an impact of using RZ pulses with 33 and 67% duty cycles (RZ33 and RZ67, respectively) and variable number of WDM channels (3,5,7,9) (sections 5.1, 5.2). These simulations were carried out by my colleague Carsten Behrens, as a part of our collaborative work.

1.2. Original Contributions

The following original contributions to the field of optical fibre communication have been made in the course of this research work, giving rise to the cited publications:

- Development of a novel design and construction of an OTDM multiplexer based on a phase stabilised fibre interferometer, which enabled bit-wise OTDM transmission for enhanced performance [6] (section 3.2)

- Optimisation of phase difference between the adjacent OTDM tributaries to reduce an impact of intra-channel nonlinearity [7] (sections 3.4, 3.5)

- Quantification of the impact of intra-channel four wave mixing (IFWM) using computer simulations for different pulse width and phase values between adjacent OTDM tributaries [7] (section 3.5)

- Development and demonstration of a new technique to generate a QAM16 signal, which is simpler to implement, less noisy than previously reported, and could be assembled from commercially available components [8] (section 4.2.1)

- The first comprehensive comparison of return-to-zero (RZ) and non-return-to-zero (NRZ) pulse shapes in QPSK and QAM16 transmission; RZ yields a ~20% increase in the maximum reach compared to NRZ [9] [10] (sections 4.1.3, 4.2.3, 5.1, 5.2)

- Several demonstrations of record transmission distances for QPSK and QAM16 modulation formats for SMF links with EDFAs [10] [11] [12]. 13600km for 42.7Gbit/s QPSK; 10160km for 112Gbit/s QPSK; 4240km for 112Gbit/s QAM16; 2000km for 224Gbit/s QAM16 (sections 4.1.1, 4.1.2, 4.2.2, respectively)

- Experimental demonstration of a new way to generate a WDM comb for QAM16 modulation format, which utilises the concept of free-spectral range of a phase-stabilised fibre interferometer [10] (section 5.2)

1.3. List of Publications

1) S**ergejs Makovejs**, Giancarlo Gavioli, Polina Bayvel, **"Characterisation and comparison of bitwise phase-control OTDM signals in 80Gbit/s transmission"**, *Proceedings of European Conference on Optical Communication 2008, We.2.E.7.*

2) **Sergejs Makovejs**, Giancarlo Gavioli, Vitaly Mikhailov, Robert I. Killey, Polina Bayvel, "**Experimental and numerical investigation of bit-wise phase-control OTDM transmission**", *Optics Express, Vol. 16, No. 22, pp. 18725-18730, 2008.*

3) David S. Millar, **Sergejs Makovejs**, Vitaly Mikhailov, Robert I. Killey, Polina Payvel, Seb J. Savory, "**Experimental comparison of nonlinear compensation in long-haul PDM-QPSK transmission at 42.7 and 85.4 Gb/s**", *Proceedings of European Conference on Optical Communication 2009, Paper 9.4.4.*

4) Polina Bayvel, Carsten Behrens, Robert I. Killey, **Sergejs Makovejs**, David S. Millar, Seb J. Savory, "**Coherent electronic compensation techniques for long-haul optical fibre transmission – opportunities and challenges**", *Proceedings of European Conference on Optical Communication 2009, Paper 10.7.2.*

5) **Sergejs Makovejs**, David S. Millar, Vitaly Mikhailov, Giancarlo Gavioli, Robert I. Killey, Seb J. Savory, Polina Bayvel, "**Novel method of generating QAM-16 signals at 21.3 Gbaud and transmission over 480 km**", *IEEE Photonics Technology Letters, Vol. 22, No. 1, pp. 36-38, 2010.*

6) **Sergejs Makovejs**, David S. Millar, Vitaly Mikhailov, Giancarlo Gavioli, Robert I. Killey, Seb J. Savory, Polina Bayvel, "**Experimental investigation of PDM-QAM16 transmission at 112 Gbit/s over 2400km**", *Technical Digest of Optical Fiber Communication Conference 2010, OMJ6.*

7) **Sergejs Makovejs**, David S. Millar, Domanic Lavery, Carsten Behrens, Robert I. Killey, Seb J. Savory, Polina Bayvel, "**Characterization of long-haul 112 Gbit/s PDM-QAM16 transmission with and without digital nonlinearity compensation**", *Optics Express, Vol. 18, No. 12, pp. 12939-12947, 2010.*

8) David S. Millar, **Sergejs Makovejs**, Carsten Behrens, Stephan Hellerbrand, Robert I. Killey, Polina Bayvel, Seb J. Savory, "**Mitigation of fiber nonlinearity using a digital coherent receiver**", *IEEE Journal of Selected Topics of Quantum Electronics, Vol. 16, No. 5, pp. 1217-1226, 2010.*

9) David S. Millar, **Sergejs Makovejs**, Irshaad Fatadin, Robert I. Killey, Polina Bayvel, Seb J. Savory, **"Experimental characterisation of QAM16 at Symbol Rates up to 42Gbaud",** *Proceedings of European Conference on Optical Communication 2010, P3.20.*

10) Enrico Torrengo, **Sergejs Makovejs**, David S. Millar, Irshaad Fatadin, Robert I. Killey, Seb J. Savory, Polina Bayvel, **"Influence of Pulse Shape in 112-Gb/s WDM PDM-QPSK Transmission",** *IEEE Photonics Technology Letters, Vol. 22, No. 23, pp. 1714-1716, 2010.*

11) Domanic Lavery, Maria Ionesku, **Sergejs Makovejs**, Enrico Torrengo, Seb J. Savory, **"A long-reach ultra-dense 10 Gbit/s WDM-PON using a digital coherent receiver"**, *Optics Express, Vol. 18, No. 15, pp. 25855-25860, 2010.*

12) **Sergejs Makovejs**, Enrico Torrengo, David S. Millar, Robert I. Killey, Seb J. Savory, Bayvel P., **"Comparison of pulse shapes in a 224Gbit/s (28Gbaud) PDM-QAM16 long-haul transmission experiment"**, *Technical Digest of Optical Fiber Communication Conference 2011, OMR5.*

13) David Millar, Domanic Lavery, **Sergejs Makovejs**, Carsten Behrens, Benn Thomsen, Polina Bayvel, Seb Savory, **"Generation and transmission of polarization-switched QPSK at 42.9 Gb/s"**, *Optics Express, Vol. 19, No. 10, pp. 9296-9302, 2011.*

14) Carsten Behrens, **Sergejs Makovejs**, Robert I. Killey, Seb J. Savory, Polina Bayvel, **"Pulse shaping versus digital backpropagation in 224Gbit/s PDM-16QAM transmission"**, *Optics Express, Vol. 19, No. 14, pp. 12879-12884, 2011.*

15) Carsten Behrens, Domanic Lavery, David S. Millar, **Sergejs Makovejs**, Benn C. Thomsen, Robert I. Killey, Seb J. Savory, Polina Bayvel **"Ultra-long-haul transmission of 7x42.9Gbit/s PS-QPSK and PM-BPSK"**, *accepted for publication in Proceedings of European Conference on Optical Communication 2011.*

2. Subsystem Design and Literature Review

The purpose of this chapter is to give an overview of the subsystems, used in the transmission experiments in this work. The techniques described in this chapter are: optical time-division multiplexing (OTDM), amplitude and phase modulation techniques, and coherent reception of optical signals. Finally, a short overview on the limiting transmission impairments, specific to the experiments carried out in this research work, is given.

2.1. Optical Time-Division Multiplexing (OTDM)

Although an optical fibre is a very broadband medium for information transmission, it is currently technologically impossible to modulate the full optical bandwidth at once. This is because an optical signal is initially generated from an electrical data pattern and converted back into an electrical signal after transmission for the recovery of the transmitted data. The bandwidth limitation of most electronic and opto-electronic components (currently ~ 50-60GHz) consequently sets the limit on the maximum achievable optical bit-rate. For example, the current state-of-the-art pulse pattern generators (PPGs) can provide a maximum binary electrical bit rate of 56Gbit/s. Current attempts towards achieving maximal information throughput involve WDM, where the whole optical bandwidth (e.g. of the C-band) is broken up into disjoint frequency bands, each of which is modulated separately [13]. By combining these separately modulated channels a very high optical capacity could be achieved [14] [15] [16]. At the receiver the WDM signal is demultiplexed back into the separately modulated channels using a tunable optical filter (or, an array waveguide grating) for the bit error rate (BER) measurements (Figure **2(a)**).

An alternative to WDM in increasing the overall information capacity is an optical time-division multiplexing (OTDM) technique (Figure **2(b)**). OTDM is a powerful tool that allows the bandwidth limitation of electronic and opto-electronic components to be overcome and can significantly increase the transmitted signal bit-rate. While WDM utilises the frequency domain to increase the overall transmitter capacity, the OTDM technique uses solely a time domain approach. The idea behind OTDM is to optically interleave several base-rate data streams (e.g. 40Gbit/s) in the time-domain to achieve a larger aggregate bit-rate (multiples of 40Gbit/s in this example – 80Gbit/s, 160Gbit/s etc.). At the receiver, the OTDM signal is separated into original multiple base-rate channels for the BER measurements.

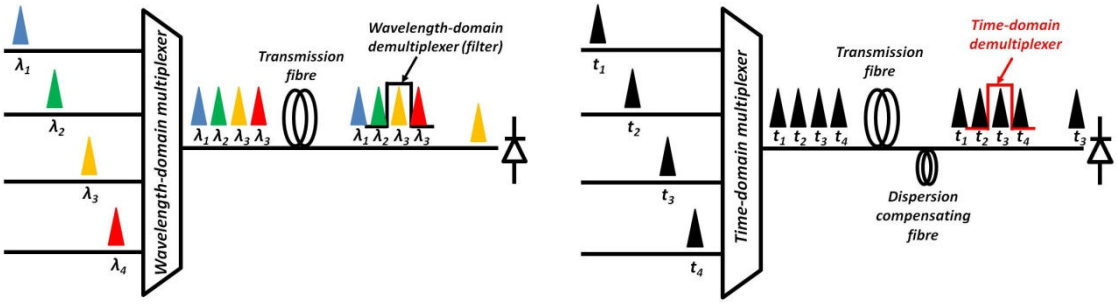

(a) (b)

Figure 2: Schematic diagrams of (a) WDM and (b) OTDM signal generation and reception

2.1.1. Pulse source for an OTDM transmitter

The most important prerequisite for an OTDM transmitter is the use of short return-to-zero (RZ) pulses instead of conventional non-return-to-zero (NRZ) pulses to carry the binary signal information. Since the RZ pulse energy is concentrated within a time window shorter than a bit period, the time separation between the two consecutive data pulses can be efficiently utilised for multiplexing multiple streams of data together (Figure **3**). Hence, there is a certain requirement on the pulse width (typically defined as full-width half-maximum (FWHM)); the shorter the pulse width the more data streams could be potentially multiplexed together. To multiplex four 40Gbit/s data streams into

a 160Gbit/s OTDM signal, the pulse width should be 2ps or less to avoid major signal degradation due to time-channel crosstalk from overlapping wings of adjacent pulses after multiplexing [1]. Figure **3(c)** shows an example of an increased crosstalk between the OTDM channels when the pulse width is not sufficiently short. To measure the width of such short pulses an intensity autocorrelator can be used; more detailed information about the pulse intensity and phase profile can be obtained using advanced pulse measurement techniques, such as frequency resolved optical gating (FROG) [17]. To further suppress the time-channel cross-talk and interferometric noise (also known as incoherent interference) due to fluctuating phase difference between the neighbouring OTDM channels, a transmitter must ensure an extinction ratio of ~35-40dB [18] [19]. The requirement for the extinction ratio is reduced for the OTDM experiments with phase control applied on a bit-by-bit basis (or, bit-wise), since the effect of the fluctuating phase between OTDM channels (and, hence, interferometric noise) is cancelled in this case.

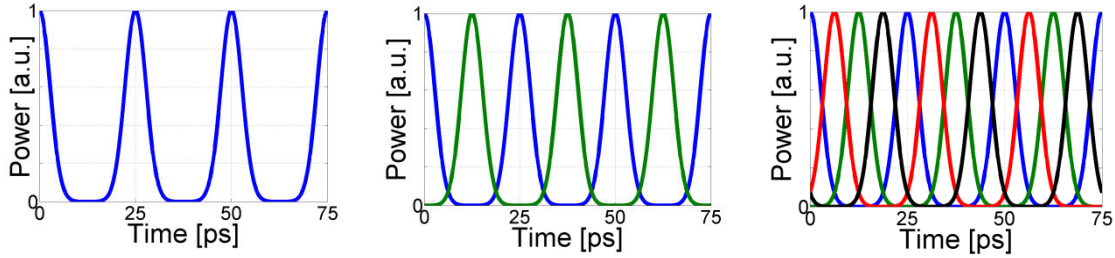

Figure 3: Generation of a higher bit-rate binary signal using the OTDM technique. Pattern "111" was used as an example. (a) 40Gbit/s base rate signal; (b) 80Gbit/s OTDM signal; (c) 160Gbit/s OTDM signal.

A short-pulse train can be obtained using a mode-locked laser diode (MLLD), a mode-locked fibre ring laser (ML-FRL) or by a continuous wave (CW) laser externally carved by an electro-absorption modulator (EAM) or Mach-Zehnder modulator (MZM). In the case of an external pulse carving a cascade of two or more modulators can be used to decrease the pulse width. At the start of this research work the significance of the 160Gbit/s bit-rate was seen from the historic four-fold increase in bit-rate, as specified in SDH (e.g. 2.5Gbit/s to 10Gbit/s; 10Gbit/s to 40Gbit/s), giving rise to a possible future upgrade from 40Gbit/s to 160Gbit/s. The generation of sub-picometer

pulses is also possible using various laboratory pulse compression techniques, like those described in [20] [21].

2.1.2. OTDM multiplexer design

To multiplex the base-rate RZ signal into a higher-rate OTDM signal several techniques can be used. The first way to generate an 80Gbit/s OTDM signal can be achieved by splitting a 40GHz RZ optical pulse train equally in two via a 3dB coupler, after which the two signals are modulated with two independent data patterns and two separate EAMs or MZMs. The 40Gbit/s RZ signals are then temporarily interleaved with respect to each other by half a bit period using an adjustable delay line; the residual difference in optical powers within the two interferometer arms is equalised with an tunable optical attenuator. Then the two 40Gbit/s RZ-OOK signals are recombined using a 3dB coupler to obtain an 80Gbit/s OTDM signal (Figure **4(a)**). Several stages of OTDM can be cascaded to obtain a higher aggregated bit-rate (e.g. 160, 320Gbit/s). The highest achieved OTDM bit-rate to date is 1.28Tbit/s using on-off-keying (OOK), polarisation division multiplexing (PDM) and direct detection [21]; and 10.2Tbit/s using advanced modulation formats, PDM and coherent detection [22].

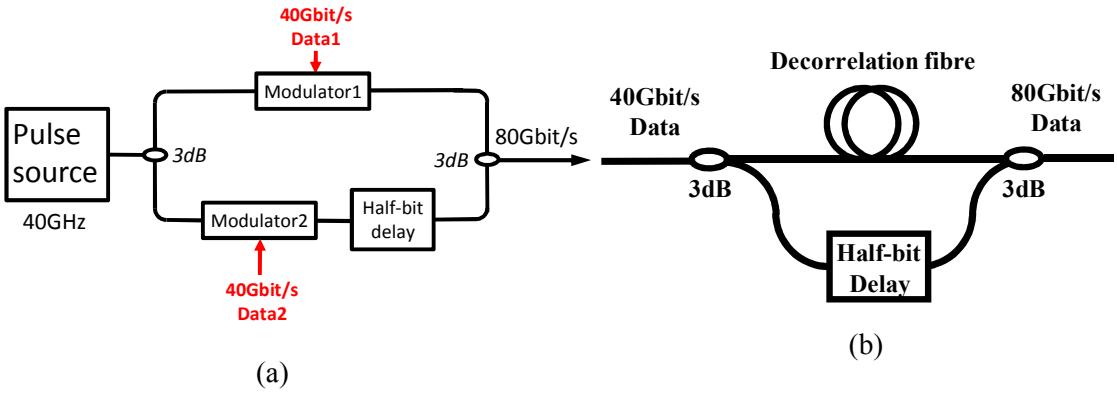

Figure 4: Schematic diagram of an 80Gbit/s OTDM signal generation from 40Gbit/s base rate signal (a) using independent electrical data patterns; (b) using a delay-line multiplexer.

In transmission laboratories, however, the generation process of an OTDM signal could be simplified by using a single modulator and a delay-line interferometer to

synthesise the OTDM signal (Figure **4(b)**). This is a widely accepted experimental technique amongst researchers and allows emulation of the behaviour of a OTDM transmitter, which would consist of independent data modulators. However, the delay-line interferometric configuration would also imply that the two OTDM tributaries carry the same data, which would incorrectly represent the behaviour of a real OTDM transmitter. The spectral content of non-decorrelated sequences is reduced compared to that of a true pseudo-random binary sequence (PRBS) (Figure **5**) and such sequences will yield a conservative estimate of system performance as shown in [23]. To solve this problem the two 40Gbit/s OTDM tributaries can be decorrelated within the OTDM multiplexer by changing the optical paths difference for two propagating signals. The most common way of implementing it would be to insert a piece of fibre in one of the interferometer arms to optically delay one signal with respect to each other, as shown in Figure **4**. In order to maintain true PRBS structure of the generated sequence the relative delay between the OTDM channels must be equal to half the pattern length of the initial PRBS sequence [24]. Taking into account that the light propagation speed in optical fibre equals to ~2×10^8 m/s and that the operating bit rate is 40Gbit/s, it has been found that the data propagation in 1 meter of optical fibre corresponds to the delay by ~200 bits. For a 2^7-1 PRBS sequence, this corresponds to 32cm of fibre needed to fully decorrelate two OTDM data tributaries.

Pattern length	2^7	2^9	2^{11}	2^{15}	2^{23}	2^{31}
Fibre length	32cm	1.28m	5.12m	81.92m	20.97km	5368.7km

Table 1 Optical fibre length needed to fully decorrelate different PRBS patterns

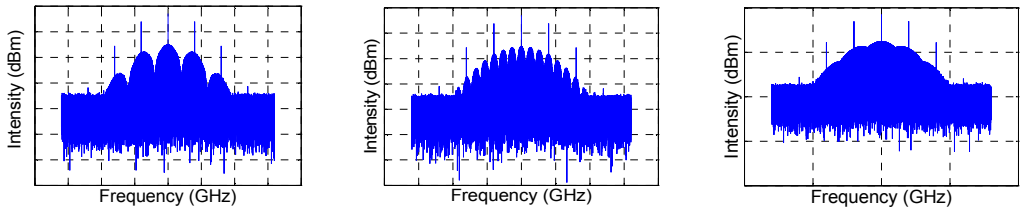

(a) (b) (c)

Figure 5: Simulated RF spectra for 80Gbit/s OTDM signal (2^7-1 PRBS); (a) No OTDM channel decorrelation; (b) 2bit decorrelation; (c) Half PRBS decorrelation.

However, since the required length of the decorrelation fibre (and hence, the loss) increases with the pattern length, it becomes impractical to fully decorrelate very long PRBS patterns, as shown in Table 1. In addition, the difference between the two interferometer arms must not exceed the coherence length of the source laser to allow coherent interference, required for the generation of bit-wise OTDM signals, as will be described in section 3.2. Also, the full decorrelation is available for one particular bit-rate at the time and, therefore, limits an experimental flexibility. Fortunately, it turns out that even a very modest decorrelation by several bits (a few tens of bits for very long patterns) is sufficient to reliably represent distribution of the signal transitions, and this is a widely accepted experimental technique amongst various research groups [25] [26] [27]. The length of a PRBS pattern in the previously reported OTDM experiments varied from as little as 2^7-1 to 2^{31}-1; e.g. 2^{15}-1 pattern was used in the OTDM experiment with the highest bit-rate reported to date for OOK and direct detection. The simulated RF spectra of an 80Gbit/s OTDM signal with no decorrelation between adjacent bits and ~1.2ns of decorrelation (corresponding to the decorrelation by 46 bits at such bit rate) are shown in Figure **6**. The decorrelation value of 46bits was also chosen for all the experiments to represent nearly half-pattern decorrelation for the shortest PRBS of 2^7-1 available from the PPG, and reasonable decorrelation for longer patterns. In order to measure the relative bit decorrelation of two patterns, the data sequence entering the OTDM multiplexer was pre-programmed to contain a single '1' bit within the PRBS length; the time response of the OTDM multiplexer is then measured using a real-time oscilloscope.

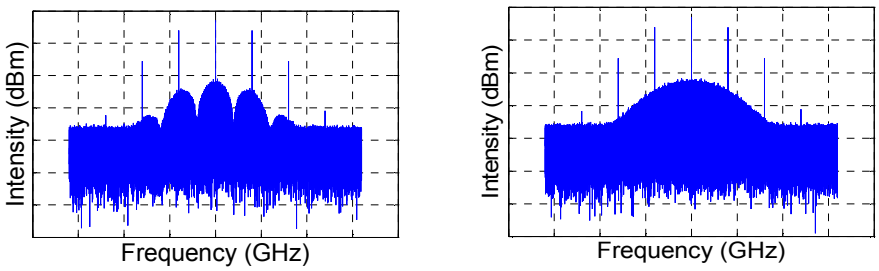

(a) (b)

Figure 6: Simulated RF spectra for 80Gbit/s OTDM signal (2^{31}-1 PRBS); (a) No OTDM channel decorrelation; (b) 45bit decorrelation.

One of the potential drawbacks of a conventional OTDM multiplexer is the inability to control optical phase between adjacent OTDM channels, which makes it impossible

to implement advanced modulation formats based on fixed phase relationships. This arises from the fact that ambient temperature deviations cause random optical path difference inside a fibre delay-line multiplexer and, therefore, leads to random phase fluctuations between adjacent OTDM channels. Another cause of phase fluctuations is the wavelength drift of the source laser. Both the temperature and wavelength drift severely affect the interferometers with short free-spectral range (this will be covered in detail in section 4.3).

Several techniques were previously used to control the phase between adjacent OTDM bits, such as using a free-space optical arrangement with EAMs [28] or planar lightwave circuit (PLC) technology [29] [30]. The problem is that the development of a prototype for such an OTDM transmitter can be expensive and requires a significant expertise in device design and fabrication.

2.1.3. OTDM receiver design

At OTDM bit-rates of 80Gbit/s and above a conventional receiver is not capable of directly detecting an OTDM signal due to the limited electrical bandwidth of components at the receiver. The solution to this is to optically demultiplex an OTDM signal prior to sending it to a 40Gbit/s receiver, where the BER can be measured directly. The clock recovery in OTDM experiments must not only provide the clock signal for the BER measurements, but also the timing for demultiplexing.

For experiments with direct detection the optical gate (or, switching window) for demultiplexing can be generated using cross-phase modulation (XPM) or four-wave mixing (FWM) effects in a semiconductor optical amplifier (SOA), or highly nonlinear fibre in conjunction with interferometric arrangements [31] [32] [33] [34]. These include the nonlinear optical loop mirror (NOLM), gain-transparent ultrafast nonlinear interferometer (GT-UNI) and hybrid integrated symmetric Mach-Zehnder (HI-SMZ) interferometer. NOLM is currently the only technique that allows to demultiplex an OTDM signal of up to 640Gbaud, which corresponds to 640Gbit/s for OOK or differential phase-shift keying (DPSK) [21] and 1.28Tbit/s for differential quadrature phase-shift keying (DQPSK) [35] signals. The difference between *Gbaud* and *Gbit/s* is

that the former represents the number of distinct *symbol* changes per second in a digitally modulated signal, while the latter defines a number of *bit* changes per second. For OOK or DPSK signal one symbol carries the information about only one bit, thus, the symbol rate is equal to bit-rate. In a DQPSK modulation one symbol consists of two information bits, which means that the DQPSK bit-rate is twice its symbol rate. Alternatively, a simpler technique employing an EAM, sinusoidally driven by the recovered electrical signal at the receiver, can be also used to generate a switching window. Similarly to the transmitter design, two or more EAMs at the demultiplexer can be cascaded to reduce the width of the switching window. Although an EAM-based demultiplexer can be very compact and easy to implement, the disadvantage of this approach is the limited width of the switching window (2-3ps, hence, the operation speed is typically limited to 160Gbit/s) and the fact that the switching window is not tunable. The latter means that the width of the switching window has to be designed for a particular bit rate. For experiments with coherent detection a pulsed local oscillator with a delay line can be used to directly demultiplex the channel of interest.

While in conventional non-OTDM experiments a clock recovery unit (CRU) can be realised using a voltage controlled oscillator (VCO) with a phase comparator or a high Q-filter to directly extract clock from the signal spectrum, the CRU design must be adjusted for OTDM experiments, where the timing for the demultiplexer must be also extracted. Various approaches have been proposed: bi-directionally operated EAM [36], phase-locked loop with optical phase comparators, exploiting nonlinearity in SOAs [37] and phase-locked loop in combination with high-Q filter [38]. A modified version of the latter algorithm is used for OTDM experiments, carried out in this work.

After down-conversion from the OTDM rate to the base rate, a conventional receiver can be used. Such a receiver consists of a broadband 40GHz photodetector; depending on the front-end of an error detector, and additional broadband 40GHz radio-frequency (RF) amplifier may need to be used. An optional noise loading stage can be used to set the optical signal-to-noise ratio (OSNR) at the receiver. This typically consists of an additional Erbium doped fibre amplifier (EDFA) and an attenuator before the EDFA to control the input launch power and, hence, the OSNR. An additional attenuator after the EDFA may need to be used to limit the power to the photodetector. The BER measurements typically involve setting a decision threshold in terms of amplitude and sampling phase to determine an ideal sampling point. The received value can be

compared with the known transmitted, after which a decision on the presence of an error can be made.

2.1.3. Literature review on OTDM

The first introduction of optical multiplexing and demultiplexing principle goes back to 1968, when the generation of 5376Mbit/s bit stream from several interleaved 224Mbit/s base rate signals was proposed [39]. Back then the idea was revolutionary and allowed previously unimaginable bit-rates. The more contemporary description of an OTDM technique, on which many existing OTDM experiments are based, can be found in [40]. This paper was also the first one to mention the possibility of reaching the overall bit-rate of 100Gbit/s using the OTDM technique. During that time, OTDM was seen as the most promising technology to increase the system capacity since broadband optical amplifiers were not yet available for any effective WDM systems to be realised. The invention of the EDFA sparked the research in WDM systems, and the overall interest in high-speed OTDM systems somewhat diminished. However, the possibility of combining WDM and OTDM techniques to complement each other, has also become an active topic of research.

The first 160Gbit/s OTDM experiment was demonstrated in 1995 when Nakazawa et al. from NTT transmitted a 160Gbit/s soliton data signal through a 200km-long fibre [41]. In this experiment a 10Gbit/s signal was multiplexed to 80Gbit/s, after which polarisation division multiplexing was applied to increase the bit-rate to 160Gbit/s. Using essentially fibre-based optical signal processing, the group from NTT increased the OTDM bit rate to 1.28Tbit/s [21] in a number of breakthrough experiments and was the first one to demonstrate combined OTDM/WDM experiments, where 1.4Tbit/s [42] and, later, 3Tbit/s [43] total capacities were transmitted over short distances. Further combined OTDM/WDM experiments were conducted in [44] [45] [46].

Most recent OTDM experiments have been based on advanced modulation formats with both direct and coherent detection, which allows a further increase in the capacity and transmission distance. In the experiments with direct detection, RZ modulation formats with alternating phase between the adjacent pulses, such as 90°-RZ and carrier-suppressed (CS)-RZ, have been used to increase the tolerance towards intra-channel

four-wave-mixing (IFWM) and achieve longer transmission distances [44] [47] [48]. DPSK was also found to have an increased tolerance towards nonlinearity compared to a conventional RZ, in addition to a 3dB improvement in receiver sensitivity, when balanced detection was used [49]. Further increase in an overall bit-rate and spectral efficiency was possible using DQPSK modulation format, which carries 2 bits per symbol [35]. The largest values of transmission distance, bit-rate per channel and capacity-distance product obtained in OTDM experiments with direct detection are 4320km [49], 2.56Tbit/s [35] and 2.04 (Pbit/s • km) [45], respectively. A number of field OTDM experiments were performed too [38] [44] [50] to verify the behaviour of OTDM over installed fibres.

2.1.4. Potential future of OTDM

The past has shown that, OTDM has been typically considered as a useful interim experimental technique to investigate the limits of high bit-rate transmission and has been replaced by electrical time-division multiplexing (ETDM) as soon as the bandwidth of optoelectronic components allowed the desired bit-rate. ETDM-based devices can be preferable to the OTDM-based in terms of both stability and compactness – essential factors for commercial use. However, an upgrade from 40Gbit/s to higher bit-rates has been also proposed using OTDM-only approach, where the OTDM transmitter prototype used with direct detection can be assembled from free-space components [28] or as a photonic integrated circuit [44]. Owing to the recent developments in the generation and reception of spectrally-efficient modulation formats with coherent detection and elaborate digital signal processing used to mitigate transmission impairments, the future of OTDM with direct detection is questionable.

The potential future of OTDM technology could be assisting researchers with investigation of advanced modulation formats with coherent detection at high symbol rates (>30Gbaud). One of the reason for the lack of demonstrations of 400Gbit/s (per carrier) transmission employing coherent detection is the limited bandwidth and sampling rate of commercially available analogue-to-digital converters (ADCs) at the receiver, and the high cost of an electrical part at the transmitter. The use of OTDM would allow optical synthesis of a 56Gbaud RZ-QAM16 signal from 28Gbaud RZ-

QAM16 signal using a single-stage phase-stabilised multiplexer, which in combination with PDM yields the overall channel bit-rate of 448Gbit/s (400Gbit/s + FEC). To demultiplex an OTDM signal at the receiver, a pulsed local oscillator (LO) with a tunable delay line can be used to detect the channel of interest. The limitation of OTDM transmission with coherent detection is the fact that only fully dispersion-compensated link could be used due to the nature of the demultiplexing process at the receiver. The use of OTDM could also be important in investigating the potential for 1Tbit/s transmission per carrier using spectrally-efficient modulation.

The feasibility to combine OTDM and coherent detection has been recently shown in [51] [52] [53]. Results in [52] demonstrate the first use of OTDM with coherent reception, in which a 480Gbit/s 8-state phase shift keying (PSK8) was generated and detected. Subsequent demonstrations are described in [53], where a 5.1Tbit/s QAM16 signal was detected using a single coherent receiver and [54], where a 640Gbit/s QPSK signal was transmitted over 1073km. Further transmission of 960Gbit/s PSK8 and 1.28Tbit/s QAM16 signals – both over 480km, was shown in [55]. The highest OTDM bit-rate per carrier reported to date is 10.2Tbit/s obtained in [22]. Based on this review it is clear that more work needs to be done on OTDM transmission at "practical" bit-rates, such as 400Gbit/s and 1Tbit/s. Further techniques to achieve long-haul transmission distances also need to be tested.

2.2 Modulation Techniques

In optical fibres the electro-magnetic waves with frequencies of ~200THz are used to transfer information from one point to another. In order to convey a message signal, one or more of the parameters of the electro-magnetic wave can be changed (modulated) accordingly. In most conventional optical fibre communication systems modulation is achieved by varying the amplitude of the optical carrier wave. However, the modulation of both amplitude and phase of the carrier allows for an improved utilisation of the complex plane, where information symbols are mapped, yielding an increased spectral efficiency.

This section describes the modulation techniques used in the experiments, carried out in this research work. First, the concept of data modulation using electro-absorption and Mach-Zehnder modulators (EAMs and MZMs) is described. The operation principle of an MZM is described in greater details since MZM is the main building block in the transmitter design for the generation of advanced modulation formats; an MZM can also be used for generating RZ pulses with 33, 50 and 67% duty cycle (RZ33, RZ50 and RZ67, respectively). The rationale behind using RZ pulses instead of NRZ is their increased tolerance towards nonlinearity, which results in an increase in transmission distance and launch power margin. Next, the generation principles of QPSK and QAM16 signals are described; it is also pointed out that there is no standard way of generating a QAM16 signal and various laboratory techniques to generate QAM16 signals are described. Although the experimental generation of higher-order modulation formats, such as QAM64 were outside the scope of this research work, section 2.2.6 describes the ways to generate QAM64 for the completeness of section 2.2.

2.2.1 Electro-absorption modulator (EAM)

The EAM principles of operation as a data encoder and a pulse carver are shown in Figure **7**. The optical modulation in an EAM arises from a periodic change in the waveguide loss in the presence of a periodical electrical field (sine-wave for pulse carving or data pulses for encoding), applied with a reversed bias voltage [56]. This

means that an electrical data pattern can be translated into the optical domain by driving the EAM between two discrete points, typically chosen to be located on the nonlinear part of the EAM transfer function (Figure **7(a)**). The latter can be particularly apparent in the presence of overshoots in the amplified RF signal. The strength of an electrical driving data signal is measured in $V_{p\text{-}p}$, which is equivalent to the swing between the maximum and the minimum points of the signal. To shift a point at which an electrical driving signal is applied, a direct-current (DC) bias (V_{bias}) must be combined with the RF signal – this function is achieved in the device called "bias tee". In a similar way an electrical clock signal can be applied to the EAM to provide an optical RZ pulse train. As illustrated in Figure **7(b)**, the operation in the nonlinear part of the EAM transfer function effectively reshapes the clock signal and removes some parts of it when seen in the optical domain. Both configurations were used in the OTDM experiment carried out in this research work to generate RZ pulses and encode the data (OOK modulation); this will be discussed in details in chapter 3.

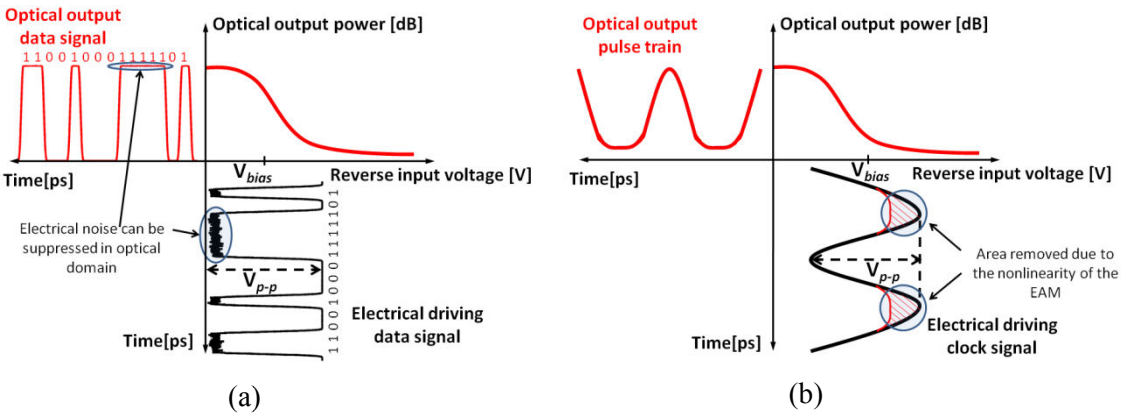

Figure 7: EAM principle of operation for (a) OOK modulation (b) pulse carving.

2.2.2 Mach-Zehnder modulator (MZM)

Unlike EAMs, which work by the principle of absorption, MZMs work by the principle of interference, controlled through the modulation of optical phase [24]. The main building block of a MZM is a 3dB fibre coupler; provided that only one input of the MZM is used for the incoming CW light, the relationship between the output and input optical fields is given in **Figure 8**. An important feature of a MZM is a 90° phase

shift between the direct-pass and cross-coupling outputs; it is this 90° phase shift that allows phase diversity, and implement MZMs and 90° optical hybrids (required for a coherent receiver).

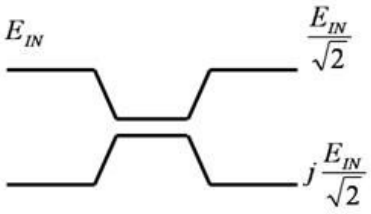

Figure 8: Transfer function of an optical fibre coupler

To create a MZM, the two optical fibre couplers are placed into an interferometric arrangement with the voltage-controlled phase shifters as shown in Figure **9**.

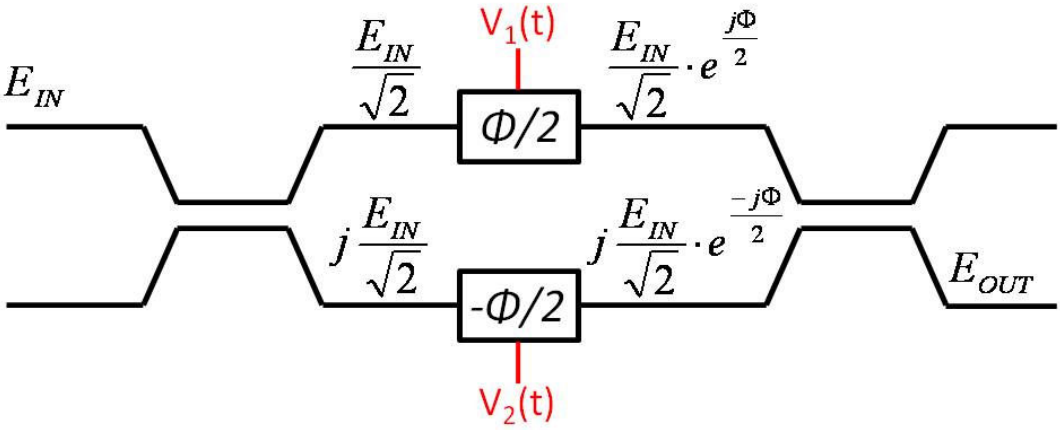

Figure 9: Relationship between optical fields within a MZM

The addition of the optical fields propagating through both arms the total optical output field is equal to:

$$\boldsymbol{E_{OUT} = \frac{1}{\sqrt{2}} j \frac{E_{IN}}{\sqrt{2}} e^{\frac{j\Phi}{2}} + \frac{j}{\sqrt{2}} \frac{E_{IN}}{\sqrt{2}} e^{\frac{-j\Phi}{2}} =} \quad \textbf{(1)}$$

$$\boldsymbol{= \frac{jE_{IN}}{2}\left(e^{\frac{j\Phi}{2}} + e^{\frac{-j\Phi}{2}}\right) = E_{IN} j cos\left(\frac{\Phi}{2}\right)}$$

This means that the ratio of output vs. input optical fields, and hence the field transfer function is represented by a periodic function, as shown in Figure **10(a)**. The amplitude transfer function is then the square of the modulus of the field transfer function

$\left|\frac{E_{OUT}}{E_{IN}}\right|^2$ (Figure **10(a)**), and the phase transfer function is a sign of the field transfer function $arg\left(\frac{E_{OUT}}{E_{IN}}\right)$ (Figure **10(b)**). An important conclusion of this is that both amplitude and phase of the signal can be modulated, depending on driving conditions. Another important application of a MZM is the generation of RZ pulses, when the MZM is driven by a sinewave.

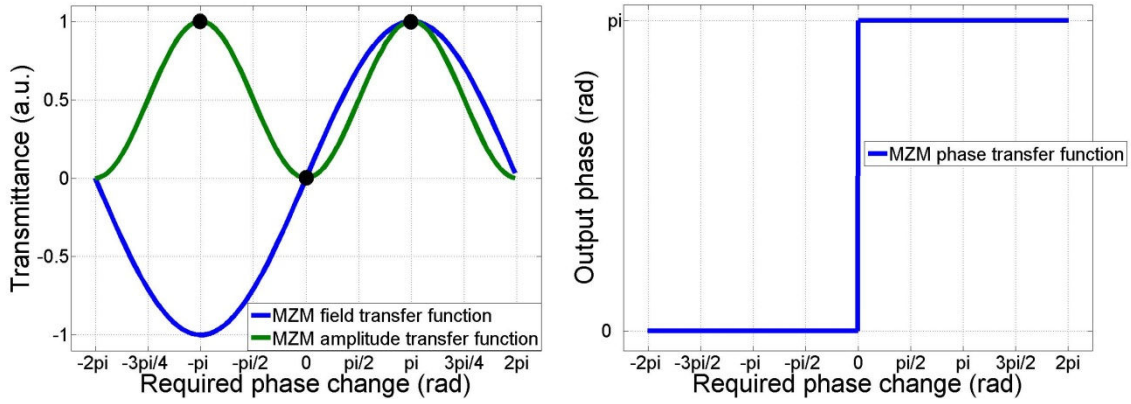

(a) (b)

Figure 10: MZM transfer functions (a) Field and amplitude function (b) Phase function.

MZMs can be manufactured using materials that exhibit the Pockels effect, such as lithium niobate ($LiNbO_3$), gallium arsenide (GaAs) and indium phosphide (InP). The InP technology is currently seen to be dominant in manufacturing small size devices, leading to the possibility of large-scale monolithic integration [57]. In transmission laboratories, where small size of the transmitter/receiver is not a crucial, $LiNbO_3$ and GaAs modulators are more common. The Pockels effect manifests itself as a linear change in refractive index in the presence of an electric field. The periodically changing refractive index causes the difference in signal propagation speed and, hence, induces a periodically varying phase shift. The phase modulation can be converted into an amplitude modulation, when using the interference between the two arms in a Mach-Zehnder configuration. Such modulators can be used in a single-sided operation (only one voltage source) or push-pull operation (two voltage sources operated with opposite phases). The advantage of a push-pull MZM is the smaller driving voltage required and the reduced footprint due to the smaller size of the MZM.

2.2.3. Diverse functionality of a MZM

2.2.3.1. Data modulation

As mentioned previously a MZM can be used for the generation of OOK or binary phase-shift keyed (BPSK) signals, when an electrical data pattern is applied at its input, and for the generation of RZ33, RZ50 and RZ67 pulses, when an electrical clock signal is applied. To generate an OOK signal, a MZM should be biased exactly in the middle of its transfer function and driven with a binary electrical signal over V_π for best performance. Figure **11** illustrates this process for a randomly chosen segment of a PRBS pattern. The difference between the maximum and minimum points of the transfer function determines the extinction ratio of the resulting signal, and is a unique feature of a particular modulator. Using the complete swing between the two extreme points yields the highest modulation depth for a given modulator; the nonlinearity of the MZM also results in the suppression of electrical noise transfer into the optical domain.

A MZM can be also used to modulate the phase of the optical field when the modulator is biased at the null of the transfer function (in terms of amplitude) and driven over $2V_\pi$ (Figure **12**). Although twice as much RF power is needed to achieve phase modulation, the current generation of modulators has $2V_\pi$ of around 5V [57], which can be easily generated using commercially available broadband amplifiers. As in the case of OOK, the nonlinearity of the modulator transfer function allows for the suppression of the electrical noise transfer into the optical domain. In theory, the generated optical BPSK signal should have a single intensity level since no amplitude modulation is present. In practice, the electrical driving signal has finite rise and fall times, which results in the presence of transitions through the minimum point of the transfer function (Figure **12**).

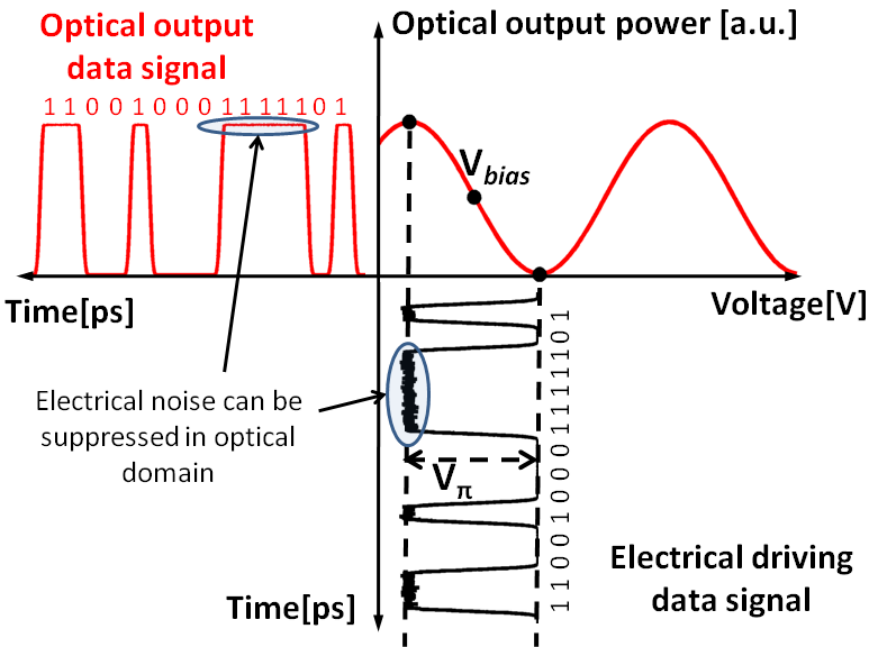

Figure 11: Generation of an OOK modulated signal

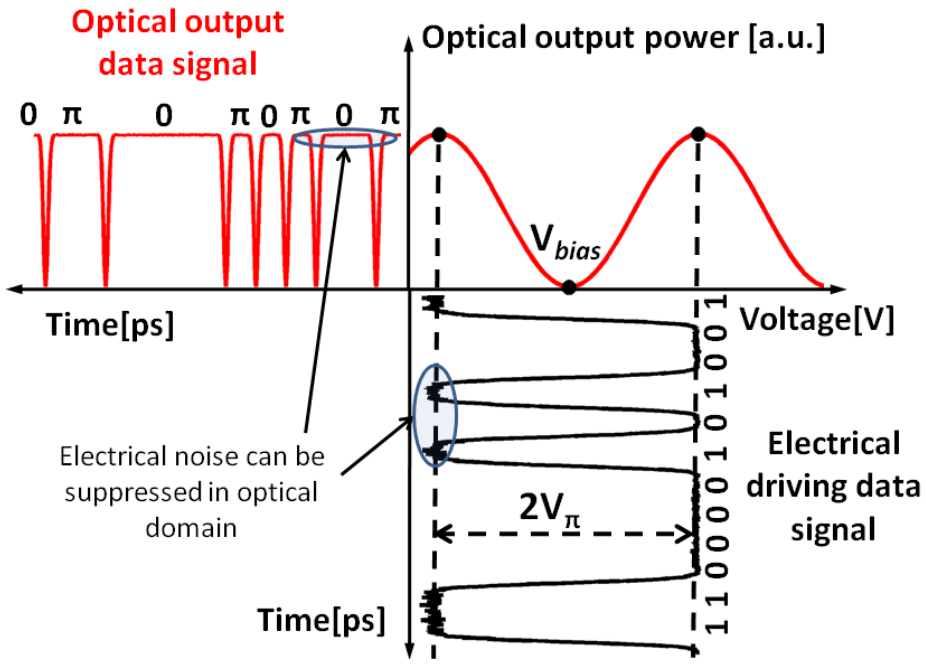

Figure 12: Generation of a BPSK modulated signal

A convenient representation of amplitude- and phase-modulated signals can be obtained via a constellation diagram – the representation of signal symbols on a complex plane. For a binary intensity-modulated signal the two constellation points

(that is, logical ‘ones’ and ‘zeros’) are located at (0,0) and (1,0) to emphasise that no phase modulation is present (Figure **13(a)**). For BPSK signals the two constellation points are at (1,0) and (-1,0) due the presence of π phase shift between the two (Figure **13(b)**).

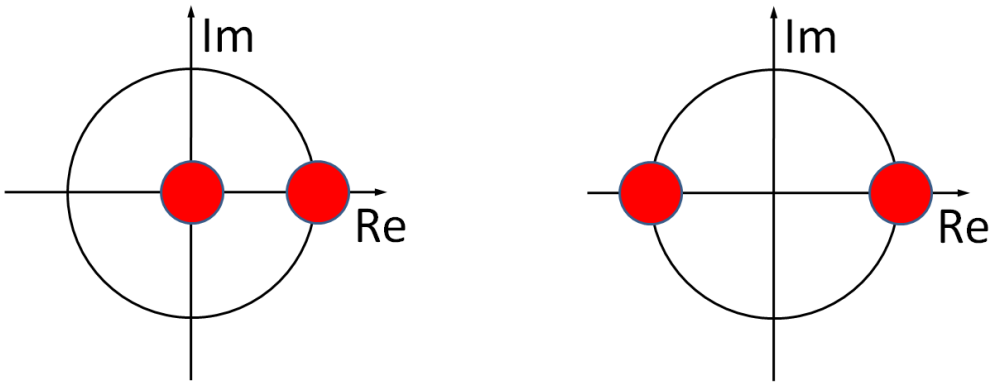

(a) (b)

Figure 13: Constellation diagrams of (a) OOK and (b) BPSK signals

2.2.3.2.Pulse shaping

The receiver sensitivity benefit by using RZ pulses instead of NRZ is well studied for optically pre-amplified systems with direct detection [58] [59]. This benefit of RZ pulses stems from the fact that for the same average optical power at the output of an EDFA, an RZ data signal has a higher peak power than an NRZ data signal. For instance, RZ signal with 50% duty cycle (RZ50) have twice the NRZ signal peak power. Since the optical receiver respond to peak optical power, rather than average optical power, the use of RZ50 signals yields a theoretical 3dB advantage in receiver sensitivity. In practice, due to the increased shot noise associated with a higher peak power, the actual benefit in receiver sensitivity is reduced to ~2dB. Another advantage of RZ signals in systems with direct detection is the presence of a clock tone in the RZ spectrum, which could simplify the design of the clock recovery.

However, unlike systems with direct detection both NRZ and RZ pulse shapes provide very similar receiver sensitivities when coherent detection is used [60] [61]. For systems employing coherent detection the main advantage of using RZ data pulses is their higher tolerance towards nonlinearity due to reduced phase-matching between adjacent frequency components during propagation over a dispersive medium [62]. This

means that more optical power can be launched into the fibre, hence, the maximum reach and the launch power margin can be improved. It must be noted that the broader spectrum of RZ data pulses compared to NRZ is also a cause of the disadvantages of RZ over NRZ, such as reduced spectral efficiency, increased WDM cross-talk and the need for higher-bandwidth analogue-to-digital converters (ADCs) at the receiver [9].

The use of RZ pulses in transmission over an uncompensated link and coherent detection, however, is not well-studied experimentally. Notable exceptions are [61] [63], where the benefit of using RZ pulses with 50% duty cycle (RZ50) was investigated for experimental configurations involving the interleaved, rather than aligned, polarisations. An interesting conclusion was also given in [64] - the performance of NRZ, RZ50 and RZ with 67% duty cycle (RZ67) pulses (both for aligned and interleaved polarisations) strongly depends on the bandwidth of the optical filtering in the WDM multiplexer. The results in [64] show that the RZ modulation prefers a narrower optical bandwidth compared to NRZ, and the advantage of using RZ instead of NRZ is apparent also when tight filtering is present. The latter is in agreement with the experimental results carried out in this research work. This is due to the fact that the narrow optical filtering converts an RZ pulse into a high-quality NRZ signal with less inter-symbol interference, compared with a conventional NRZ signal subjected to narrow optical filtering [64].

RZ50, RZ67 and RZ with 33% duty cycle (RZ33) pulses can be generated by driving a MZM with a clock signal at appropriate frequency, $V_{p\text{-}p}$ and the bias condition. To generate RZ33 pulses the MZM must be biased at the maximum point of its transfer function with a clock signal equal to $2V_{\pi}$ (Figure **14**). The generation of RZ67 pulses requires the MZM to be biased at the minimum point of its transfer function with a clock signal also equal to $2V_{\pi}$ (Figure **15**). An interesting conclusion is that for both RZ33 and RZ67 pulse train generation only a half-clock rate is needed (e.g. 14GHz clock signal is needed for 28Gbaud signals), which could reduce the cost of the components used at the transmitter. However, the use of RZ33 and RZ67 pulse shapes also requires the RF amplifier with twice the output voltage (compared to RZ50), therefore, creating a practical trade-off between the reduced bandwidth and an increased power of the driving signal.

To generate RZ50 pulses, the MZM needs to be biased in the middle of its transfer function (in terms of amplitude) and driven symmetrically by a full-clock rate over V_{π} –

that is between maximum and minimum points of the transfer function (Figure **16**). While the clock frequency required to generate an RZ50 signal is twice the frequency required for RZ33 and RZ67 signals, the required strength of the clock signal for RZ50 signal generation is only half that needed for the generation of other duty cycles. In the course of this research work the experimental investigation was focused on RZ50 pulses; the further comparison between RZ33 and RZ67 pulses was carried out in the simulations (section 5.2).

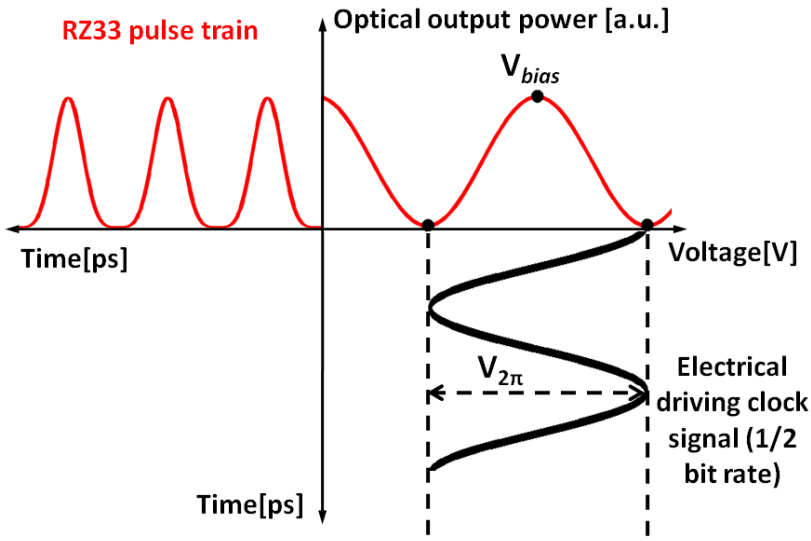

Figure 14: Generation of RZ33 pulse train

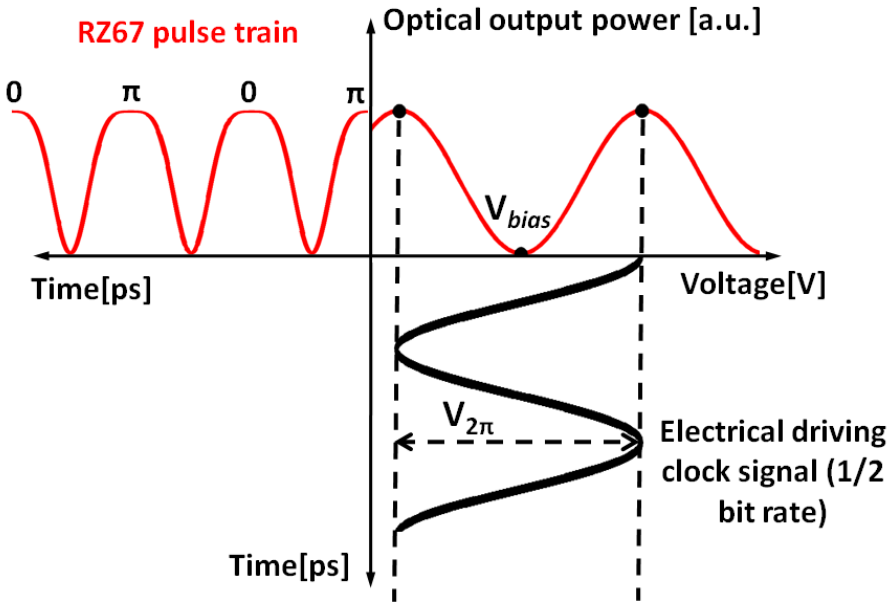

Figure 15: Generation of RZ67 pulse train

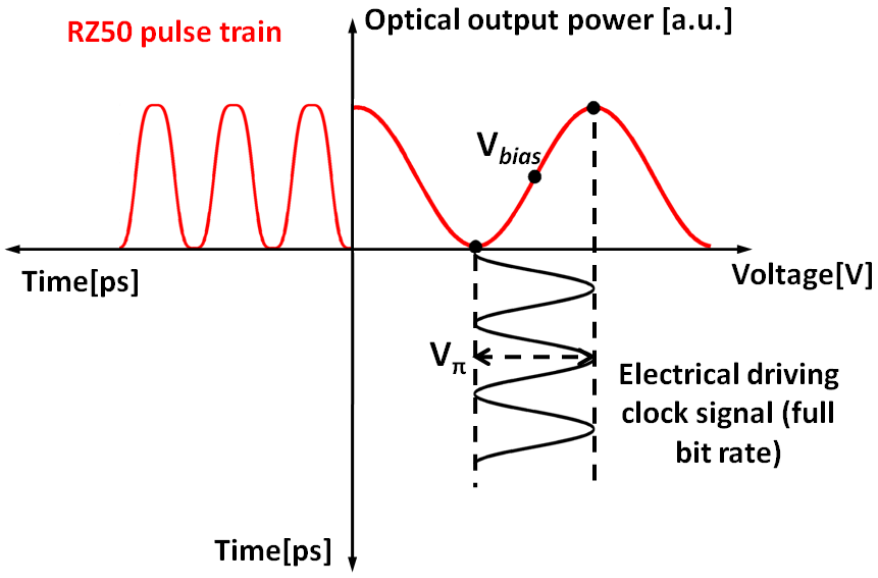

Figure 16: Generation of RZ50 pulse train

The experimental comparison of RZ pulses vs. NRZ is carried out in this research work for both QPSK (sections 4.1.3 and 5.1) and QAM16 (sections 4.2.3 and 5.2 signals) transmission. The obtained results represent the first comprehensive experimental comparison of two pulse shapes in terms of the maximum reach, in both QPSK and QAM16 transmission.

2.2.4. QPSK generation

An advantage of QPSK modulated signals over OOK or BPSK signals is twice higher spectral efficiency and twice lower symbol rate to obtain an equivalent overall bit-rate. A QPSK signal can be generated using a phase modulator or in a nested structure employing three MZMs. While the former option requires only one modulator and, hence, is cheap to implement, it also suffers from the conversion of phase noise into intensity noise. For this reason, most QPSK transmitters are based on the nested structure with 3 modulators.

In the nested structure (Figure **17**) voltages $V_1(t)$, $V_2(t)$, $V_3(t)$ and $V_4(t)$ need to be adjusted to obtain π phase difference between the two arms of the inner MZMs and,

hence, generate two BPSK signals. Within the outer MZM the two BPSK signals are shifted by π/2 with respect to each other by varying the voltages $V_5(t)$ and $V_6(t)$. The interference of the two BPSK signals with π/2 phase difference yields a QPSK signal, as shown in Figure **18**. During the interference the two BPSK signals shown in red and blue disappear to produce QPSK symbols (shown in black).

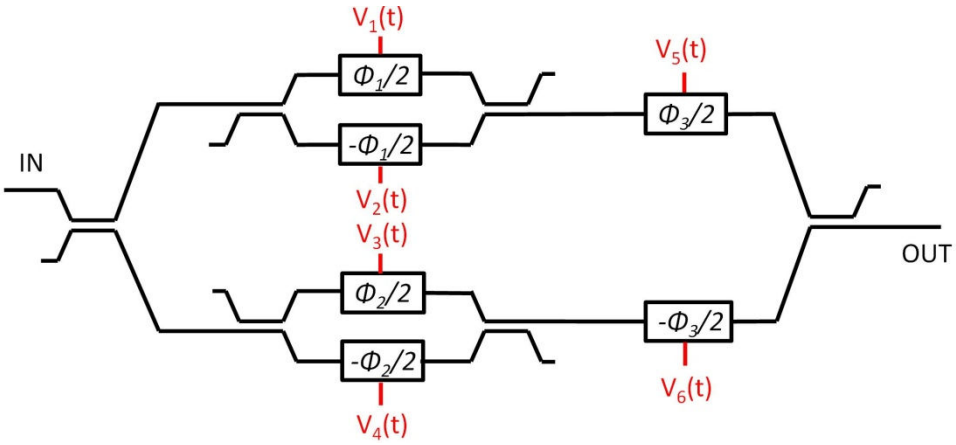

Figure 17: Structure of an in-phase and quadrature (I-Q) modulator

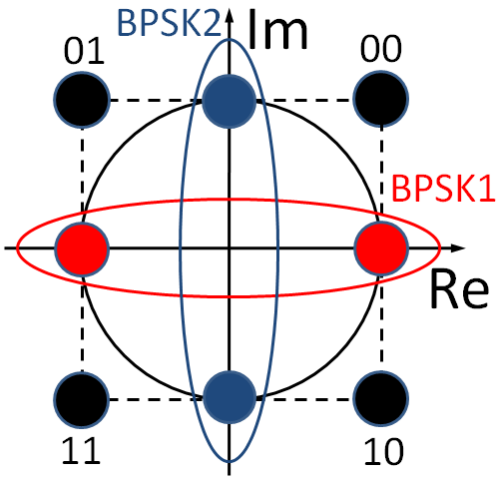

Figure 18: QPSK signal generation concept

Such a modulator for QPSK signal generation was first proposed in [65]. A QPSK signal can have one of four phase values at a time [0, π/2, π, 3π/4], which means that each symbol can transmit two bits of information. The QPSK symbols are inherently Gray coded (e.g. the adjacent symbols have only one bit difference), since the transition between neighbouring quadrants is equivalent to the change in state of only one MZM, while the transition between the opposite quadrants is equivalent to both MZMs

changing their states. The Gray coding is important to minimise the BER when a symbol error occurs. For non-Gray-coded signals the BER could be increased by up to two times for QPSK, four times for QAM16, six-times for QAM64 etc.

2.2.5. QAM16 generation

QAM16 modulation offers twice higher spectral efficiency than QPSK and further reduces the required symbol rate to obtain the equivalent overall bit-rate, albeit, at the expense of an increased required OSNR, and worse performance in the linear and nonlinear transmission regime. A QPSK signal has 6.8dB lower required OSNR than QAM16 signal for the same symbol rate of 28Gbaud, and also 3.8dB lower required OSNR for the same bit rate of 112Gbit/s, as shown in **Figure 19**. The theoretical back-to-back dependence of BER vs. OSNR is calculated according to [66]. QAM16 will also have reduced tolerance towards nonlinearity than QPSK because of the presence of 3 intensity levels and, hence, higher peak-to-mean ratio. Also, as will be described in section 2.3.1 the DSP for QAM16 signals is more complicated than for QPSK, in particular, adaptive equalisation and carrier phase estimation.

To date, few techniques have been proposed to generate QAM16 signals. Perhaps the most prominent generation technique involves the synthesis of two 4-level electrical signals to drive the two arms of an I-Q modulator. In the simplest implementation an I-Q modulator is driven by two electrical signals with equally spaced amplitude levels over the linear part of its transfer function. In such configuration, the equally spaced electrical amplitude levels are linearly converted into the optical domain creating two 4-state amplitude shift keyed (4-ASK) signals (**Figure 20(a)**). An alternative to equally spaced amplitude levels is to pre-distort a 4-level electrical driving signal in order to drive an I-Q modulator over $2V_{\pi}$, as shown in **Figure 20(b)**. Although in both cases the generated 4-ASK signal contains equally spaced optical levels, the latter configuration allows to exploit the full modulation depth of the modulator and suppress the noise in some of the QAM16 symbols, albeit, at the expense of increased transmitter complexity.

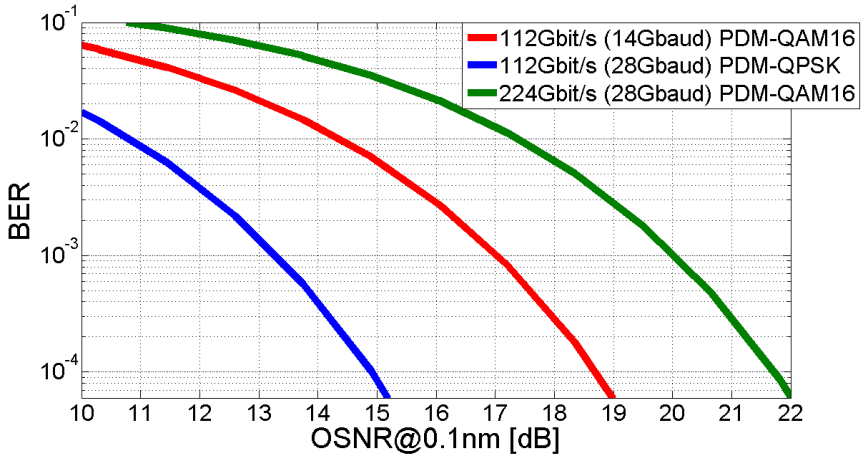

Figure 19: Comparison of theoretical linear performance of QAM16 vs. QPSK

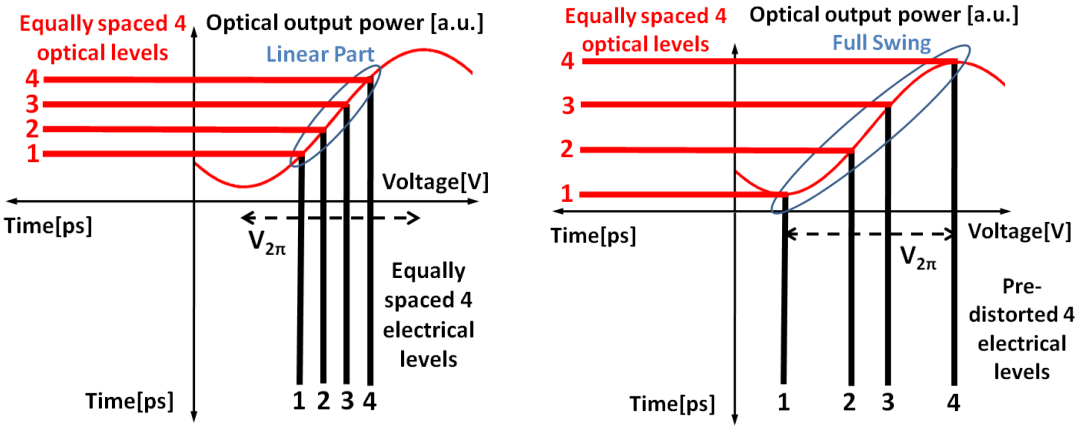

(a) (b)

Figure 20: Generation of 4-ASK optical with a 4-level electrical signal with (a) equally spaced electrical levels; (b) pre-distorted electrical levels

Within the I-Q modulator the two 4-ASK signals are then phase shifted by π/2, so when two 4-ASK signals interfere at the output of a Mach-Zehnder interferometer (MZI) a QAM16 signal is generated (**Figure 21**). In a similar way as in QPSK generation, the generation mechanism can be considered as superposition of vectors on a complex plane. As a result of the interference, the 'red' and 'blue' constellation points in **Figure 21** disappear.

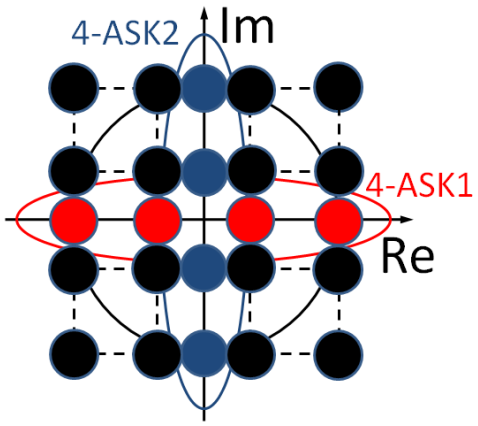

Figure 21: An illustration of QAM16 signal generation using two 4-level electrical driving signals

The 4-level electrical signals can be obtained either by combining two NRZ electrical signals with different intensity levels from the pulse pattern generator (PPG) or using an arbitrary waveform generator (AWG). The first approach is typically limited by the signal-to-noise ratio (SNR) of the 4-level electrical signal and the fact that the I-Q modulator is driven in the linear part of its transfer function, leading to electrical noise transfer into the optical domain. The limitation in the SNR of the 4-level electrical signal is due to the fact that the power dividers, used to combine two binary signals with different amplitude levels, are symmetric devices and, therefore, also act as splitters (**Figure 22**). Because of this property, part of the RF power from port 1 will exit through port 2 and reach the output of the RF amplifier, causing distortions (**Figure 23**). Although this could be mitigated by placing additional attenuator after the RF amplifier to reduce the reflected power, this will inevitably reduce the peak-to-peak voltage of the 4-level electrical NRZ signal and, hence, the modulation depth (**Figure 24**). QAM16 signal generation using 4-level driving signals from a PPG was first proposed in [67], followed by the demonstrations in [68] [69].

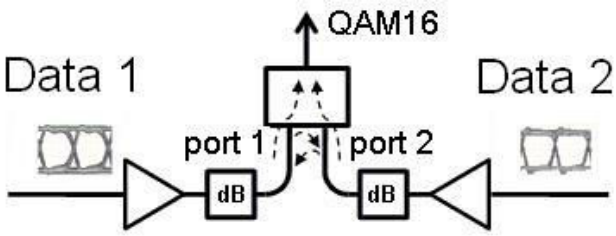

Figure 22: Back-reflections as a result of combining two binary signals

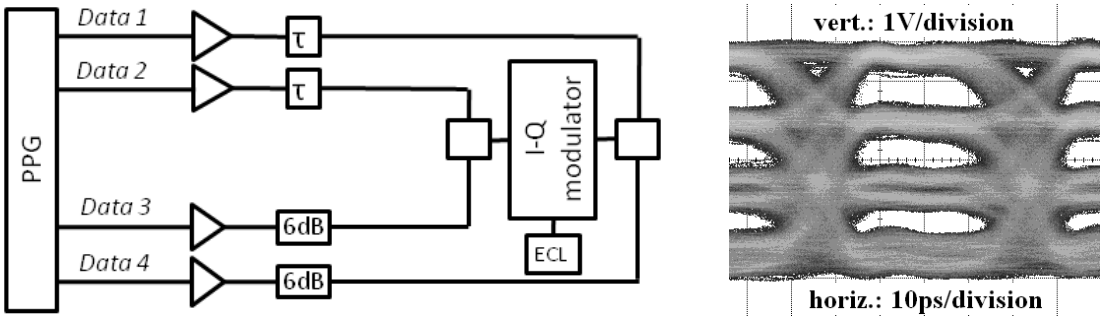

(a) (b)

Figure 23: (a) Schematic diagram of the generation of two high-power/low SNR driving signals in the QAM16 transmitter; (b) measured eye diagram of a corresponding 4-level electrical signal (V_{p-p} = 5.5V)

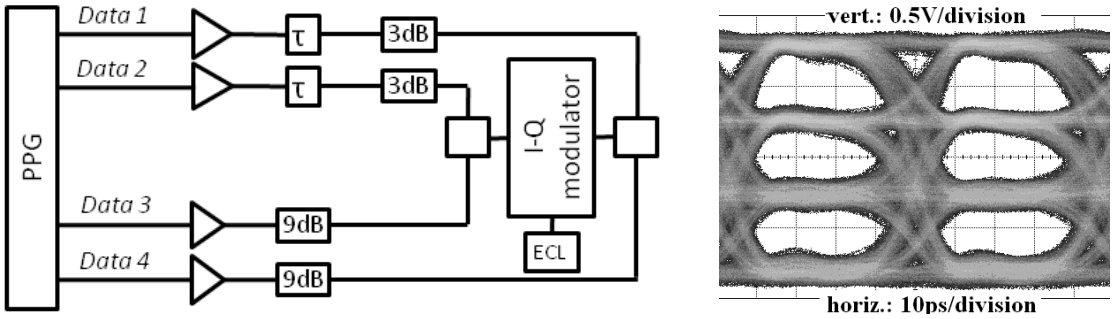

(a) (b)

Figure 24: (a) Schematic diagram of the generation of two low-power/high SNR driving signals for a QAM16 transmitter; (b) measured eye diagram of a corresponding 4-level electrical signal (V_{p-p} = 3V)

The disadvantage of the second approach is that the speed of current state-of-the-art AWGs is limited by the sampling rate (24GSamples/s), corresponding to a maximum of 24Gbaud assuming only 1 sample per symbol. In practice, however, the achievable symbol rate at the output of the AWG is lower due to its limited bandwidth (typically <10GHz). Another drawback of AWGs is the limited electrical output power (~1V_{p-p}), which means that a high-quality linear data amplifier may need to be used to fully exploit the modulation depth of an I-Q modulator.

Alternatively, QAM16 signals can be generated optically by combining two optical QPSK signals with different amplitude levels in a MZI. The inherent advantage of the optical generation of the QAM16 signal is that no complicated set-up for obtaining

multilevel electrical signal is needed. In other words, the complexity is shared between the electrical and optical domains. The principle of QAM16 signal generation by interfering two QPSK signals with 6dB difference in amplitude is shown in **Figure 25**, where the large-intensity ring is shown in solid line and small-intensity ring shown in dashed line. When two QPSK signals interfere, the large-amplitude QPSK signal determines the quadrant where a QAM16 symbol is mapped, while the small amplitude QPSK signal determines the phase within each quadrant ('red' constellation points in **Figure 25** disappear during interference).

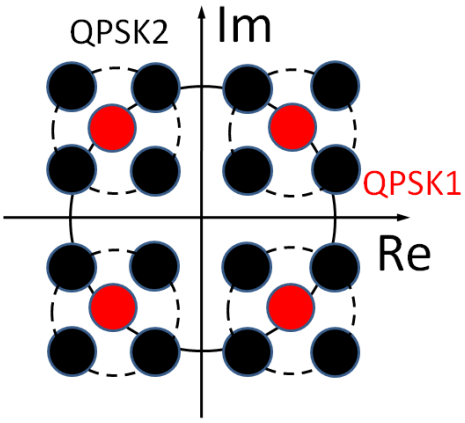

Figure 25: An illustration of QAM16 signal generation using two QPSK signals with 6dB difference between amplitude levels

Such a technique for QAM16 generation has been previously realised on a PLC-based platform at a symbol rate of 12.5Gbaud; however, the bias instability of the device affected the symmetry of the obtained QAM16 constellation [70]. The QAM16 constellation asymmetry has been recently solved in [71]. Other QAM16 generation techniques involve an in-series cascade of data modulators driven by binary electrical signals [26] [72], dual-drive MZM driven by 4-level signals [73], and an interference of 4 data streams in a photonic integrated circuit (PIC) [74].

2.2.6 Generation of higher-order modulation formats

The results of the laboratory experiments of QAM16 signal transmission show the feasibility of achieving up to 4240km at 112Gbit/s, 2000km at 224Gbit/s and 1200km at 448Gbit/s (all carried out as part of this research work). These transmission distances

are expected to be further increased with the technological advances in the generation and reception of high-speed QAM16 signals. The next logical research question is: what is the potential of the modulation formats with even higher spectral efficiency, such as QAM64? The QAM64 transmission experiments were outside the scope of this research work; however, this section briefly outlines the two techniques that could be used to generate a QAM64 signal. The techniques to generate a QAM64 signal are based on the extension of those used for QAM16 generation. Because of the 64 constellation points on the complex plane, one QAM64 symbol can encode 6 bits (i.e. 6 bits/symbol), which means that a 112Gbit/s bit-rate can be achieved at a symbol rate of only 9.3Gbaud employing polarisation division multiplexing (PDM).

The QAM64 signal can be generated by biasing an I-Q modulator at the minimum point of its transfer function and driving the modulator with two 8-level electrical signals. The principle of QAM64 signal generation using an interference of two 8-ASK signals is shown in Figure **26**. As in the case of QAM16 generation the 'blue' and 'red' constellation points disappear during the interference. In practice such generation technique can be realised using an AWG (albeit with limitation in speed and signal quality) or using a custom built digital-to-analogue converter (DAC), which has recently been successfully demonstrated in [75].

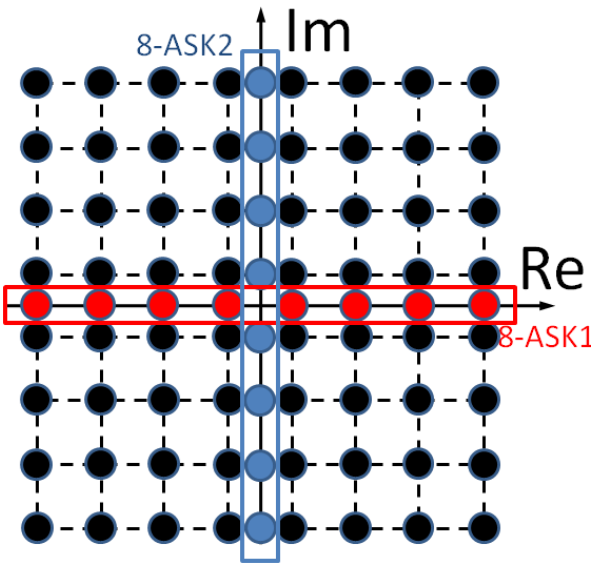

Figure 26: QAM64 signal generation using two 8-level electrical driving signals

The QAM64 signal can also be generated by interfering three QPSK signals, where two QPSK signals are attenuated by 6dB and 12dB with respect to the non-attenuated

QPSK signal. The amplitudes of three QPSK signals used in the interference are shown in **Figure 27** in 'red', 'blue' and 'black' colours. The large amplitude QPSK signal determines the quadrant where the QAM64 symbols are mapped, while two other QPSK amplitudes produce four QAM16 signals, as described previously.

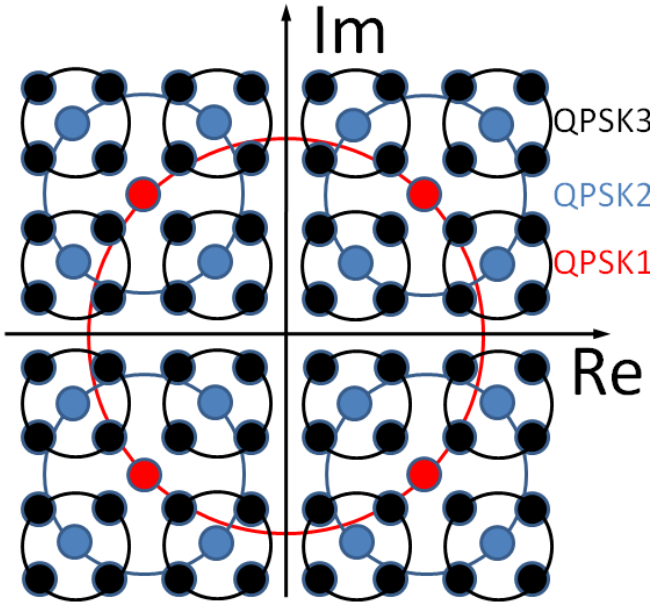

Figure 27: QAM64 signal generation using three QPSK signals with 6dB and 12dB difference between amplitude levels (blue and red points disappear during interference and are shown to help understand the generation process)

2.2.6 Literature review on advanced modulation formats

In the mid 2000's the interest in the OTDM technique diminished, mainly due to the revival of coherent detection following the advances in clock speed of silicon chips. This facilitated the use of complex modulation formats without OTDM to achieve the desired bit-rate. The simplest forms of modulation used with coherent detection are BPSK and QPSK (equivalent to DPSK and DQPSK, respectively, when differential direct detection is used). To further increase the capacity and spectral efficiency more complex modulation formats, such as QAM16 or QAM64, can be used. It is worth noting that advanced modulation formats have been extensively studied and successfully implemented in radio systems, however, their use in the optical domain is a very recent research trend.

The most widespread modulation format to date is QPSK with polarisation division multiplexing (PDM), where the data is transmitted on two polarisations simultaneously to yield 2 bits of information per transmitted symbol per polarisation. The first implementation of a QPSK signal generation from discrete components (MZMs) was shown in 2002 [65], and later in 2003 demonstrated as a photonic integrated circuit (PIC) [76]. A number of high-performance QPSK experiment have been carried out since then. This includes the highest capacity-distance product, arguably the most important single parameter defining the fidelity of an optical system, of 141 (Pbit/s • km) [15]. In this experiment 198 PDM RZ-QPSK wavelength channels were successfully transmitted over 6860km. Another experiment demonstrated a record spectral efficiency (SE)-distance product of 43 (Mm • bit/s/Hz) [77], surpassing the previous record of 33.7 (Mm • bit/s/Hz) [14]. This experiment was based on a PDM-QPSK configuration, with 3.6 bit/s/Hz of SE and the maximum transmission distance of 9360km.

An alternative to PDM-QPSK is polarisation switched (PS)-QPSK, where a symbol is transmitted only on one polarisation at a time, resulting in 3 bits per symbol. This means that PS-QPSK requires a higher symbol rate than PDM-QPSK to obtain the same overall bit-rate. The generation and transmission of PS-QPSK has been recently demonstrated in [78] [79] with the conclusions that PS-QSPK has a ~0.7dB advantage in the required OSNR compared to PDM-QPSK. The results in [79] showed that at 42.9Gbit/s this benefit in the required OSNR could translate into a 30% improvement in the maximum reach. PS-QPSK modulation format is expected to be an active topic of research in years to come, particularly for long-haul transoceanic applications.

The most promising solution to obtain bit-rates exceeding 100Gbit/s is by using more complex modulation formats, such as PSK8, QAM8, QAM16, QAM64 etc. The generation of both PSK8 and QAM8 signals requires an additional phase modulator [80] and both signals can transmit 3 bits/symbol per polarisation (i.e. 6 bits/symbol when PDM is used). PSK8 has a higher tolerance to nonlinearity than QAM8 due to its constant modulus, which reduces the peak-to-mean power. However, QAM8 can tolerate 1.5dB more ASE noise than PSK8 due to the more efficient allocation of constellation points on the complex plane [80]. The transmission of both PSK8 and QAM8 has been successfully demonstrated to achieve high capacity. In 2008, a transmission of 17Tbit/s PSK8 signal has been demonstrated in [81] – this was a record

achieved capacity within the C-band EDFA bandwidth at the time of the publication. The results in [82] have also showed the feasibility of achieve long-haul distances of up to 2800km (carried out for a 30Gbit/s RZ-PSK8 signal). The same authors from NEC Labs and AT&T Labs have later demonstrated transmission of a 32Tbit/s RZ-QAM8 signal over 580km [83], which was the highest overall capacity at the time of publication.

To further increase the capacity and spectral efficiency, QAM16 modulation can be used to transmit 4 bits/symbol per polarisation (8 bits/symbol for PDM), which also allows to obtain 200Gbit/s and potentially 400Gbit/s with a relatively modest electrical bandwidth. Over the last 2-3 years substantial progress has been achieved in generating QAM16 signals, which is a non-straightforward task (possible ways of generating QAM16 have been outlined in section 2.2.5). A number of QAM16 transmission experiments have been carried out for bit-rates of up to 448Gbit/s. The first notable 100Gbit/s transmission was carried out in [67], where a WDM QAM16 signal was transmitted over 315km. The same group from Bell Labs later increased the transmission distance to 1022km [84]. A further refinement of the process of QAM16 generation allowed to decrease the implementation penalty to 1.5dB (at the BER = $3x10^{-3}$) and increase the maximum transmission distance to 4320km - both values were achieved in the course of this research work and represent the best 112Gbit/s QAM16 performance reported to date.

The transmission of 200Gbit/s QAM16 has been also recently demonstrated in [10] [68] [69] [85]. The results in [68] show the feasibility of achieving 480km WDM QAM16 transmission using NRZ pulses and SMF link with EDFAs only. As shown in [69] the transmission distance could be further increased to 1500km when using RZ50 pulses, advanced fibre type and hybrid optical amplification. The lowest implementation penalty of 224Gbit/s QAM16 reported to date is 3.4dB (measured at the BER = $1x10^{-3}$); this work showed 2000km transmission in a single-channel experiment and 1200km in WDM – both achieved for NRZ pulses, advanced fibre type and Raman amplification. Finally, the experiments carried out as a part of this research work [10] show that the same 2000km reach could be achieved for a conventional SMF link with EDFAs only. This is an important consideration for a potential upgrade of existing links, many of which are based on SMF. The results presented in this research work also

represent the first experimental comparison of NRZ and RZ50 pulse shapes – both with and without the use of digital nonlinearity compensation (NLC) [9] [10].

The generation of 400Gbit/s per carrier using QAM16 modulation is also possible; however, it requires high-bandwidth components at the transmitter and receiver, which increases the complexity and cost to generate and detect such signals. To date, the only demonstration of 400Gbit/s QAM16 generation is reported in [5]; this work also demonstrated 1200km transmission. The highest detected data rate to date is 606-Gb/s [86], achieved using orthogonal frequency-division multiplexed (OFDM) signals with QAM32.

Parameter	**Value**	**Reference**	**Author/Group**
Capacity-Distance Product	141 Pbit/s x km	[15]	Cai J.-X./TE Subcom
Capacity	101.7Tbit/s	[16]	Qian D./NEC Labs
Spectral Efficiency	11bits/s/Hz	[16]	Qian D./NEC Labs
Spectral Efficiency-Distance Product	43 Mm x bit/s/Hz	[77]	Foursa D./TE Subcom
Longest reach (40G)	17900km	[77]	Foursa D./TE Subcom
Highest detected rate	606Gbit/s	[86]	Liu X./Bell Labs
Highest QAM order	QAM512	[87]	Okamoto S./Tohoku University

Table 2. Record experimental results for coherently detected advanced modulation formats

The generation and transmission of higher-order QAM signals has also been demonstrated in a number of experiments. Notable examples are [88] [89]. In [88] 64Tbit/s QAM36 was transmitted over 320km, while the results in [89] show the generation and 400km transmission of 400Gbit/s signal using QAM32 modulation and spectral efficiency of 8.37 bit/s/Hz. The most successful demonstrations of QAM64 generation are reported in [75], where two 8-level electrical signals were generated with a custom-built high-power DAC, and [90], where an AWG was used. Both also reported transmission distances of 400km for a 21.4Gbaud QAM64 [75] and 1280km for a 10Gbaud QAM64 [90], respectively. The experiment in [16] demonstrates the record total capacity of 101.7Tbit/s employing a QAM128 OFDM signal. This exceeded the previous record in the total capacity of 69.1Tbit/s achieved using a QAM16 modulation [91]. An experiment in [16] also demonstrated the highest SE of 11bits/s/Hz reported to date. The only demonstration of QAM512 generation and transmission at 54Gbit/s is reported in [87]. Table 2 highlights the record experimental results for coherently detected advanced modulation formats reported to date.

A promising way to obtain the bit-rates, potentially exceeding 1Tbit/s is by using a "super-channel" approach, which can be implemented either using Nyquist WDM or OFDM techniques. In both cases a "super-channel" is assembled from multiple lower-rate closely spaced subcarriers. The main advantages of OFDM include a well-define narrow optical spectrum, resulting in high achievable spectral efficiencies [92], and implicit parallelisation, which enables a slower signal processing speed [93]. The main disadvantages of OFDM technique include the requirement for the DAC at the transmitter, leading to an increase in the cost and complexity of the system, and the fact that an OFDM signal has a higher peak-to-mean ratio, which reduces its tolerance towards nonlinearity [92]. The Nyquist WDM approach relies on the generation of multiple closely-spaced WDM channels with tight spectral shaping (up to the baud-rate spacing), which are bundled together to create a "super-channel". Several "super-channels" can then be combined in a similar way as in the conventional WDM transmitter with a certain guard-band (e.g. on a 50GHz grid). The advantage of Nyquist WDM over OFDM is its reduced complexity, since no DAC at the transmitter is needed. The feasibility of long-haul transmission using Nyquist WDM was shown in [94] [95].

The experiments carried out in this research work do not aim to compete with the industrial research labs in terms of the achieved total capacity, since this would require a large number (200-400) of lasers at the transmitter to generate a WDM comb and a generous amount of human resource to maintain the stability of the WDM channels. The focus of this research work is to demonstrate ultra long-haul transmission distances for both QPSK and QAM16 signals, and investigate the linear and nonlinear transmission performance of these modulation formats at different bit-rates.

2.3 Digital coherent receiver

A coherent receiver maps an entire optical field into the digital domain, therefore, allowing detection of not only the amplitude of the signal but also its phase and the state of polarisation. The knowledge of the phase allows to invert a linear optical channel and digitally compensate for practically unlimited amount of chromatic dispersion and a large amount of PMD [96]. The absence of dispersion compensating fibre (DCF) also means an increased tolerance towards nonlinearity (due to the lower peak-to-mean ratio) and a faster signal propagation time. Coherent detection with digital signal processing (DSP) also facilitated the use of polarisation division multiplexing (PDM) to increase the overall bit rate by a factor of two, since two polarisations can be adaptively tracked and restored at the receiver.

Secondly, coherent reception is very effective in demodulating advanced spectrally efficient modulation formats, where the information is encoded not only on the signal amplitude, but also its phase. While the detection of such modulation formats like differential phase shift keying (DPSK) or differential quadrature phase shift keying (DQPSK) are feasible using differential direct detection, the use of such detection scheme would be impractical for higher-order modulation formats. The hardware part of the coherent receiver is almost independent on the complexity of modulation format - only DSP needs to be adapted, which is beneficial from a laboratory upgrade point of view.

Finally, a coherent receiver also brings the benefit of improved receiver sensitivity, which is a particularly important feature in unamplified links, such as those used in access networks. An improvement in the receiver sensitivity is due to the fact that the local oscillator (LO), set to operate at the power exceeding the signal power, amplifies the weak signal, thus achieving the shot-noise limited performance [24] [97]. A coherent receiver also performs the frequency selectivity function, which can be achieved by tuning a free-running LO to demultiplex a WDM channel of interest. This simplifies the design of the receiver hardware part, since no optical filters are required for filtering out the channel of interest.

An interesting aspect of a digital coherent receiver is that the combination of coherent detection, DSP and advanced spectrally efficient modulation formats represent

a truly symbiotic relationship (Figure **28**), as highlighted in [98]. Coherent detection allows both the phase and the state of polarisation of the received signal to be detected, but without the subsequent DSP it would be impossible to recover the data from the received signal, and without the use of spectrally efficient modulation formats the benefits of a coherent detection cannot be fully exploited.

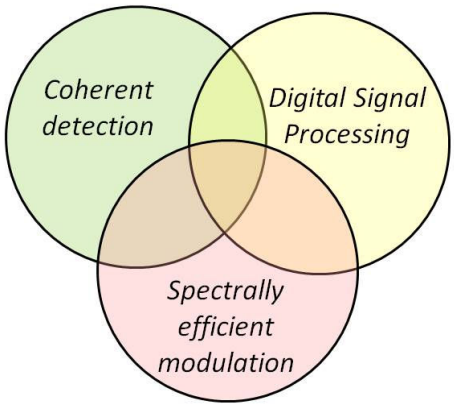

Figure 28: Three elements of a digital coherent receiver

2.3.1 Coherent receiver design

The schematic diagram of a coherent receiver is shown in Figure **29**. Both the incoming PDM signal and LO are split into two orthogonal polarisations using a polarisation beam splitter, after which the co-polarised signal and the local oscillator are mixed in two 90° optical hybrids to produce an in-phase and quadrature components for each polarisation. The four signals are then digitised by four ADCs after which DSP can be performed.

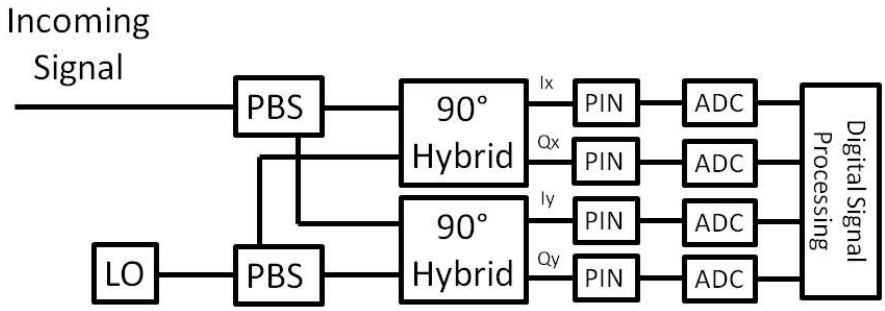

Figure 29: Schematic diagram of a digital coherent receiver

A 90° optical hybrid can be realised either in fibre-based or free-space optics configurations. For simplicity, let's consider the principle of operation of a fibre-based 90° hybrid. A key building block of such a hybrid is an 2x2 optical fibre coupler with its property of a 90° phase shift between its direct-pass and cross-coupling outputs. By combining such optical couplers into the configuration shown in Figure **30**, together with an additional 90° phase shift in one arm, a detection of real and imaginary parts can be achieved.

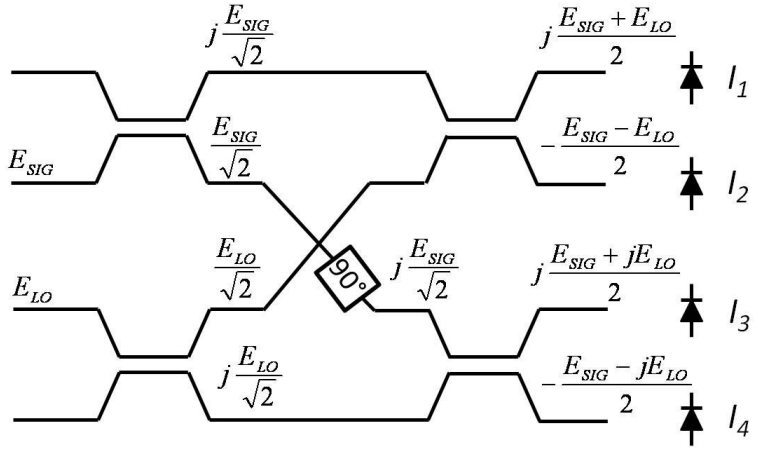

Figure 30: Schematics of a 90° optical hybrid

The four photocurrents generated by the photodetection process are then proportional to:

$$\boldsymbol{I_1 \sim |E_{SIG}|^2 + |E_{LO}|^2 + 2Re\{E_{SIG}E_{LO}^*\}} \quad \textbf{(2)}$$

$$\boldsymbol{I_2 \sim |E_{SIG}|^2 + |E_{LO}|^2 - 2Re\{E_{SIG}E_{LO}^*\}} \quad \textbf{(3)}$$

$$\boldsymbol{I_3 \sim |E_{SIG}|^2 + |E_{LO}|^2 + 2Im\{E_{SIG}E_{LO}^*\}} \quad \textbf{(4)}$$

$$\boldsymbol{I_4 \sim |E_{SIG}|^2 + |E_{LO}|^2 - 2Im\{E_{SIG}E_{LO}^*\}} \quad \textbf{(5)}$$

It is clear that directly detected terms, $|E_{SIG}|^2$ and $|E_{LO}|^2$, do not contain any information about the phase and can be removed using a direct current (DC) blocking capacitor. It is also apparent that the power of the real and imaginary parts (Eq. 2-5) could be enhanced by subtracting the two photocurrent pairs ($I_1 - I_2$ and $I_3 - I_4$) – this procedure could be implemented using balanced detection. For a phase- and polarisation-diverse coherent receiver, one optical 90° hybrid per polarisation must be used to produce real and imaginary parts per polarisation.

2.3.2 Digital signal processing (DSP)

DSP functionality can be illustrated by the following flow of steps. First, the four digitised signals (i.e. in-phase and quadrature components for each polarisation) are passed through the block for the compensation of front-end imperfections, and re-sampling from an asynchronous sampling rate of the ADC (e.g. 50GSamples/s) to 2Samples/symbol. The front-end imperfections might include timing skew between the four channels due to the difference in both optical and electrical path lengths within a coherent receiver. Other types of front-end imperfections can be the difference in output powers for four channels due to different responses of PINs in the receiver, and quadrature imbalance due the imperfect phase in the optical hybrid [99].

While compensating for the transmission impairments in optical fibre, it is important to note the different time scales of the dynamics of these impairments. While PMD typically varies on a millisecond scale, the chromatic dispersion can be considered constant on that scale. On the contrary, the Kerr effect is virtually instantaneous and varies on the 10^{-15}s scale. Because of such difference in the dynamics of these effects, it is important to split the equalisation of the received signal into two steps. First, static equalisation for chromatic dispersion compensation is performed on each polarisation separately, and then a fast adaptive equalisation is carried out jointly for two polarisations [100]. For QPSK signals the adaptive equalisation was performed using a constant modulus algorithm (CMA), which minimises the deviation of the amplitude of the equalised signal from a desired fixed value. For a QAM16 CMA alone is not sufficient due to the presence of three amplitude levels in a QAM16 constellation, and is typically used in combination with a multi-modulus algorithm (MMA), such as a radially directed equaliser (RDE) [98] [101] [102]. Then the frequency offset between the source laser and the local oscillator (LO) is estimated and removed to prevent the constellation rotation at the intradyne frequency. Finally, the carrier phase noise is estimated and removed from the modulated signal, which is then followed by symbol estimation and BER calculation. The diagrams showing the DSP flow are shown in Figure **31** for QPSK and Figure **32** for QAM16. Both the QPSK and QAM16 constellations show examples of the experimentally received signal after linear transmission over uncompensated SMF link with EDFAs only.

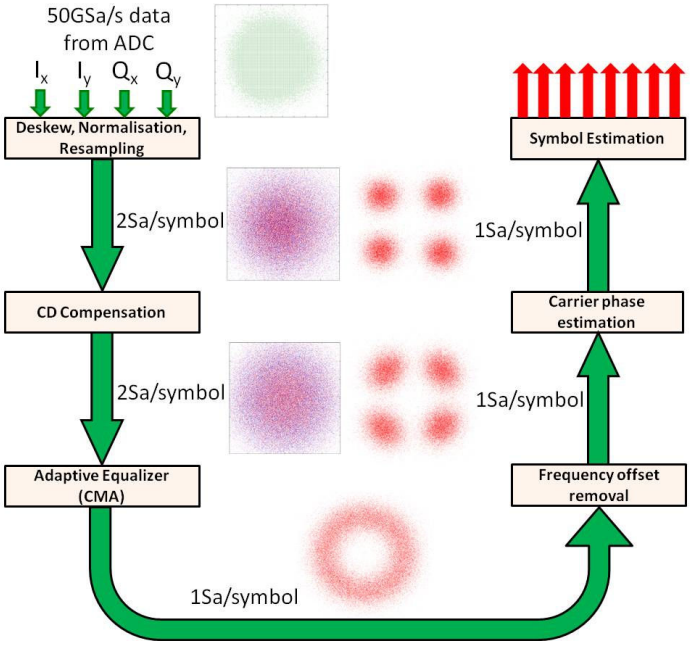

Figure 31: DSP flow for received 112Gbit/s PDM-QPSK signal after transmission

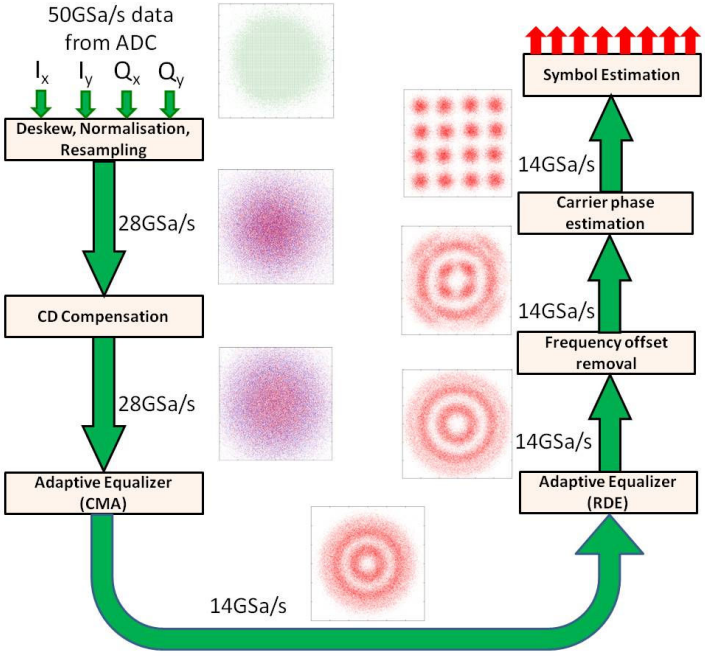

Figure 32: DSP flow for received 112Gbit/s PDM-QAM16 signal after transmission

2.3.2.1. Static equalisation

A static equaliser can be realised by assuming a linear channel (e.g. with an absence of fibre nonlinear impairments), for which the optical fibre transfer function is given by [96]:

$$\boldsymbol{G(z,\omega) = exp\left(-j\frac{D\lambda^2}{4\pi c}\omega^2\right)} \quad \textbf{(6)}$$

where z – signal propagation distance, ω – angular frequency, *D* – chromatic dispersion coefficient, λ – central wavelength. Thus the chromatic dispersion filter is given by an all-pass filter 1/G(z,ω). However, the design of such filter is often more practical in the time domain, therefore, one could obtain the impulse response of the fibre from G(z,ω) using an inverse Fourier transform:

$$\boldsymbol{g(z,t) = \sqrt{\frac{c}{jD\lambda^2 z}}exp\left(j\frac{\pi c}{D\lambda^2 z}t^2\right)} \quad \textbf{(7)}$$

By inverting the sign of chromatic dispersion to obtain the impulse function of a compensating filter and truncating the impulse response to a finite duration, a non-recursive finite impulse response (FIR) digital filter can be implemented. Such FIR filter can be realised using a tapped delay line with a filter length (number of taps) given by [96]

$$\boldsymbol{N = 2 \times \frac{|D|\lambda^2 z}{2cT^2} + 1} \quad \textbf{(8)}$$

The tap coefficients (weights) are then given by

$$\boldsymbol{a_k = \sqrt{\frac{jcT^2}{D\lambda^2 z}}exp\left(-j\frac{\pi cT^2}{D\lambda^2 z}k^2\right)} \quad \textbf{(9)}$$

where k – tap index.

2.3.2.2. Adaptive equalisation

After chromatic dispersion compensation a block of rapidly variable equalisation adaptively restores two rotating polarisations, compensates for time-varying PMD and recovers the sampling phase [84]. The signal processing at 2 samples/symbol yields an opportunity to recover the sampling phase; the information about the correct timing means that the subsequent signal processing can be done with only 1 sample/symbol in

the subsequent DSP blocks, and sampling points at the transition states can be discarded. An adaptive equalisation can be partitioned into three parts: the filter bank, an error estimator, and a device for updating the filter coefficient [100]. An adaptive equaliser is realised in a multiple input multiple output (MIMO) "butterfly" structure.

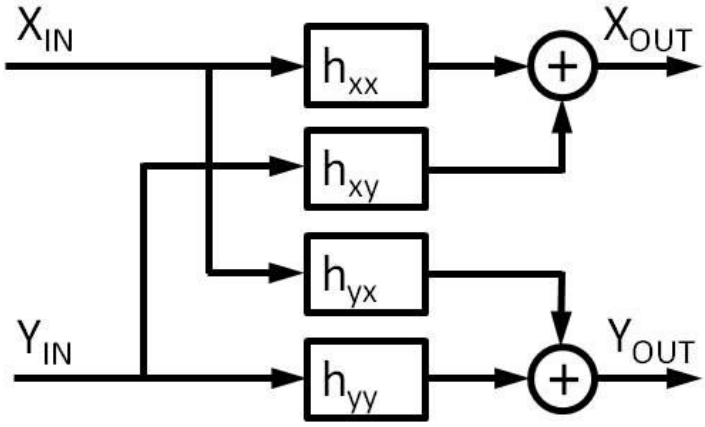

Figure 33: MIMO structure of an adaptive equaliser

The filter bank consists of four filters (h_{xx}, h_{xy}, h_{yx}, h_{yy}) with short filter response (15 taps were used for most of the experiments in this work) and fast tap coefficient adaptation speed (Figure **33**). The relationship between the input and output signals is given by

$$\boldsymbol{x_{OUT}(k) = h_{xx} \cdot x_p + h_{xy} \cdot y_p =}$$
$$\boldsymbol{= \sum_{m=0}^{M-1} h_{xx}(m) x_p(k-m) + h_{xy}(m) y_p(k-m)} \quad \textbf{(10)}$$
$$\boldsymbol{y_{OUT}(k) = h_{yx} \cdot x_p + h_{yy} \cdot y_p =}$$
$$\boldsymbol{= \sum_{m=0}^{M-1} h_{yx}(m) x_p(k-m) + h_{yy}(m) y_p(k-m)} \quad \textbf{(11)}$$

i.e. the two outputs of the adaptive equaliser are calculated per symbol *k* and the complexity of the equaliser depends on the number of taps *M*.

The error estimator part of an equaliser depends on the specific modulation format, as discussed previously. This involves CMA for QPSK signals, and CMA in combination with RDE for QAM16 signals. For QPSK signals the deviation from the desired value is represented by the error terms with a magnitude of $\varepsilon_x = 1 - |x_{OUT}|^2$ and $\varepsilon_y = 1 - |y_{OUT}|^2$, and the gradient of the error can be minimised by taking a partial derivative of the mean-squared error with respect to the filter coefficients (least-mean

square (LMS) algorithm). The gradient estimates are calculated from instantaneous measures of the error, and in each step the filter coefficients are updated by adding a small measure proportional to the negative gradient estimate given by

$$\boldsymbol{h_{xx} \rightarrow h_{xx} + \mu \varepsilon_x x_{OUT} \cdot x^*_{IN}} \quad \textbf{(12)}$$

$$\boldsymbol{h_{xy} \rightarrow h_{xy} + \mu \varepsilon_x x_{OUT} \cdot y^*_{IN}} \quad \textbf{(13)}$$

$$\boldsymbol{h_{yx} \rightarrow h_{yx} + \mu \varepsilon_y y_{OUT} \cdot x^*_{IN}} \quad \textbf{(14)}$$

$$\boldsymbol{h_{yy} \rightarrow h_{yy} + \mu \varepsilon_y y_{OUT} \cdot y^*_{IN}} \quad \textbf{(15)}$$

where μ is a convergence parameter used to control the adaptation speed and residual error of the adapted filter coefficients, and x^*_{IN}, y^*_{IN} - the complex conjugate of the input sequences.

The description of adaptive equalisation for QAM16 signals can be found in [102].

2.3.2.3. Carrier frequency offset removal and phase recovery

The output of the adaptive equalisation (as seen on a complex plane) appears as a circle in the case of a QPSK signal (Figure **31**) or three concentric circles in the case of a QAM16 signal (Figure **32**). The reason for not being able to determine the four distinct constellation points of the QPSK signal (16 constellation points in the case of QAM16) is due to the fact that the constellation is still spinning at the intradyne frequency – the residual frequency offset between the transmitter laser and the LO. To compensate for the frequency offset the complex symbols are raised to the 4th power to remove the modulation, and the offset is determined by finding the peak of the fast Fourier transform (FFT) of this signal [12] [103].

The received complex symbols contain not only the desired phase modulation but also the phase noise of the optical carrier (Figure **31** and Figure **32**). The variation of this noise is typically slower than the phase modulation (e.g. 10Gbaud) and is determined by the finite laser linewidth - 100kHz for ECLs to few MHz for DFB lasers. Therefore, by averaging the carrier phase over many symbol intervals, it is possible to obtain an accurate phase estimate. For a QPSK signal with four phase states, the received complex symbols are first raised to the 4th power to remove modulation and

make sure that only the phase noise is present. The k[th] symbol x(k) is then added to N predecessors and successors to average the estimated phase, which is given by

$$\boldsymbol{\varphi_k = \frac{1}{4} arg\left(\frac{1}{2N+1}\sum_{l=-N}^{N} x^4(k+l)\right)} \quad \textbf{(16)}$$

Because the phase varies over the range of 2π, the estimated phase will revert back to 0 if it reaches 2π, hence, creating a discontinuity. The estimated phase must, therefore, be "unwrapped" to provide a continuous and unambiguous estimation of phase. After the phase "unwrapping", the compensation of an estimated phase error is performed with respect to the received complex symbols (Figure **34**). To synchronise the two paths (input symbols and the corrected phase, a further delay (Z^{-1}) is used. The phase estimation process yields a QPSK constellation with four distinct phase states, after which the symbol estimation can be performed using rectangular decision boundaries. The received symbols are then cross-correlated with the known transmitted symbols to synchronise the two sequences, after which the symbol by symbol comparison can be performed to calculate the symbol error rate (SER) and the bit error rate (BER) on each polarisation [8].

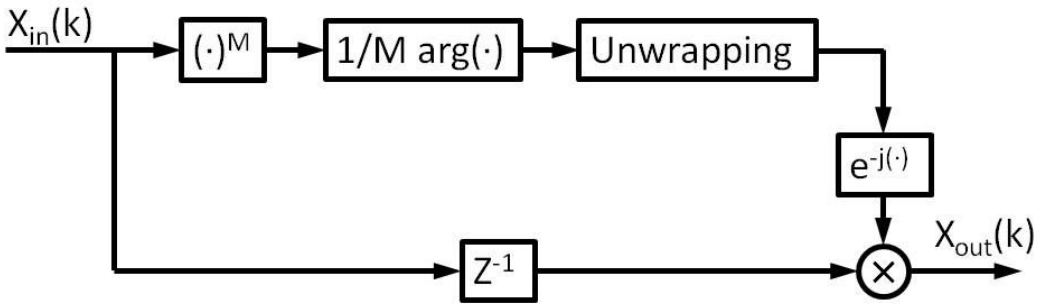

Figure 34: Carrier phase recovery using the M[th] power algorithm

The details on carrier phase recovery for QAM16 signals can be found in [103] [104].

2.3.2.4. Nonlinearity compensation (NLC)

While dispersion compensation can be considered as a reversal of a linear optical channel, the partial reversal of a non-linear optical channel is also possible, and means that the nonlinearity can be digitally mitigated. If a signal is known at the transmitter

side, the signal after transmission over the fibre can be obtained by using the split step method (SSM) to solve the Manakov equation, given by [105]:

$$\frac{\partial A_x}{\partial z} = -\frac{\alpha}{2}A_x + \frac{j\beta_2}{2}\frac{\partial^2 A_x}{\partial t^2} + \frac{8j\gamma}{9}\left(|A_x|^2 + |A_y|^2\right)A_x \qquad (17)$$

$$\frac{\partial A_y}{\partial z} = -\frac{\alpha}{2}A_y + \frac{j\beta_2}{2}\frac{\partial^2 A_y}{\partial t^2} + \frac{8j\gamma}{9}\left(|A_y|^2 + |A_x|^2\right)A_y \qquad (18)$$

Such an approach is a very useful simulation technique and allows modelling of the transmission behaviour of optical fibre systems. The same procedure can be applied in the backward direction to obtain the signal at the transmitter provided that an output signal can be measured at the receiver with adequate fidelity [105]. The block diagram of solving the Manakov equation backwards using SSM is shown in Figure **35**. In the first step the FFT translates the signal into the frequency domain where chromatic dispersion of 1 span is compensated. The signal is then translated into the time domain, where the instantaneous nonlinear phase shift is applied. The amount of nonlinear phase shift is determined by solving the Manakov equation, ignoring the chromatic dispersion term. The process is repeated *N* times, where *N* is the number of fibre spans. Although the granularity of step *N* can be both increased or decreased, the experiments carried out in this research work showed that 1 nonlinear step per span is a good trade-off between the complexity of the algorithm and the amount of nonlinearity that can be mitigated. Further details on complexity vs. performance can be found in [106].

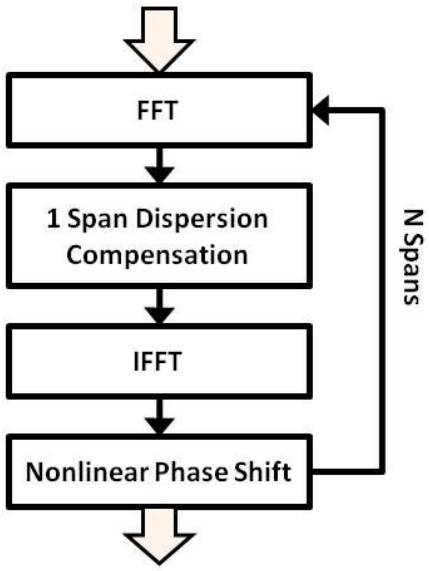

Figure 35: A block diagram of solving Manakov equation using digital back-propagation technique (DBP)

The digital back-propagation (DBP) technique for digital nonlinearity compensation (NLC) is currently an active topic of research. It should be noted, however, that DBP can only compensate for deterministic nonlinearities (SPM, potentially XPM) and cannot undo nonlinear phase noise due to its stochastic nature. The theoretical analysis of DBP was described in detail in [107] and experimentally demonstrated in [10] [11] [12] [105], including the results of this research work. The results in [106] analysed the impact of the number of nonlinear steps per span on the efficiency of DBP – 1 step per span was found to be an optimum trade-off between the DBP efficiency and the computational complexity involved. The main conclusion is that DBP can significantly increase the maximum reach (by up to 70%) for single-channel transmission; however, its benefit is reduced in the WDM transmission [10] [108]. This is due to the fact that the effective compensation of cross-phase-modulation (XPM), the dominant source of nonlinearity in the WDM systems, would require a simultaneous detection of multiple channels and, hence, impractically large receiver bandwidth (>200GHz, assuming DWDM with 50GHz spacing). The efficient compensation of inter-channel nonlinear effects via DBP is currently an active topic of research [105] [109] [110].

2.3.2.5. Symbol estimation

The result of the carrier phase recovery is a set of distinct constellation points. To calculate the symbol error rate (and BER) the four received symbol sequences (in-phase and quadrature for each polarisation) are first cross-correlated with the known transmitted PRBS sequences to align both transmitted and received patterns, and recover the delay between the two. The transmitted QPSK symbols are also inherently Gray coded, because the change of state of one of the MZMs is equal to the change of only one information bit. The transmitted QAM16 symbols, however, are not necessarily Gray coded, and the actual bit coding depends on the QAM16 generation technique. The method to provide the Gray coding for the QAM16 signal, generated using the technique used in this research work, is shown in section 5.2.1.

Rectangular decision boundaries can then be used to carry out symbol estimation for both QPSK and QAM16 signals. In this case each received symbol is compared with the pre-defined rectangular boundaries to assess whether an error is present (Figure **36**). For a QPSK signal these boundaries should coincide with the horizontal and vertical axes of

the complex plane. For a QAM16 signal the boundaries are set using *a priori* knowledge of the location of the complex mean of all 16 transmitted symbols.

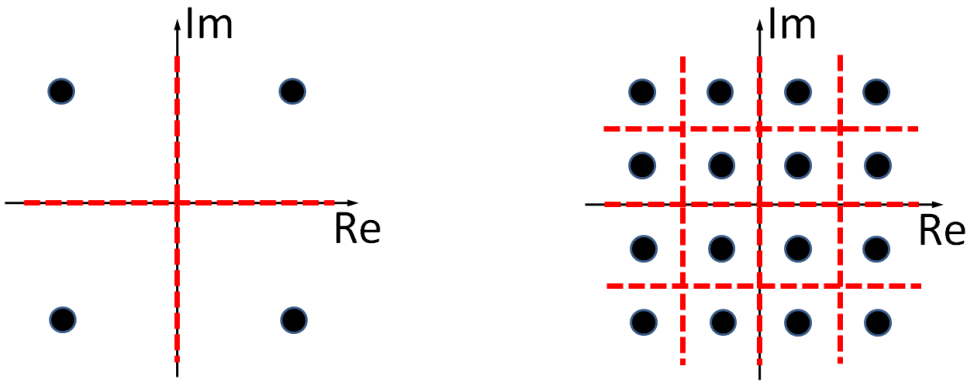

(a) (b)

Figure 36: Rectangular decision boundaries for (a) QPSK and (b) QAM16 symbol estimation

Whilst this method is easy to implement, in the presence of modulation distortions (particularly relevant to multilevel formats like QAM16 and higher [70]) the symbol estimation based on rectangular decision boundaries can cause additional errors. Since tuning a QAM16 transmitter to obtain a perfectly square QAM16 constellation is not always possible, the symbol estimation using minimum Euclidian decision boundaries can be more effective than rectangular decision boundaries. The idea behind this symbol estimation technique is as follows: the received symbols are first compared to the complex mean of each of the 16 transmitted symbols per polarisation, and the decision is made based on the minimum distance between each of the received symbols and the complex mean of the transmitted symbols. Figure **37** shows a deliberately distorted QAM16 constellation used to illustrate the benefit using minimum Euclidian distance decision boundaries; in this particular case the BER is reduced from 5.3×10^{-4} to 2.1×10^{-4} [103].

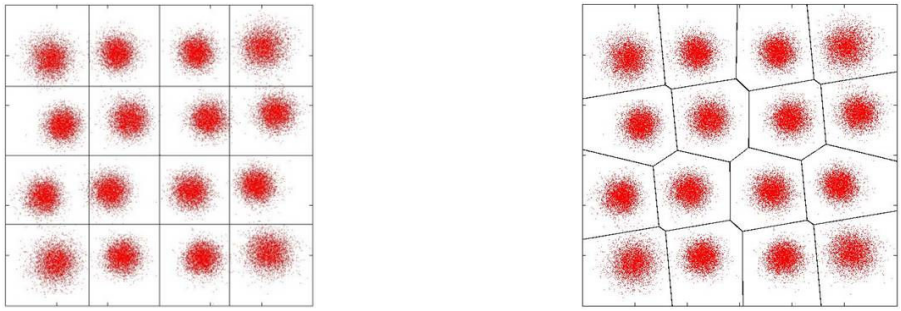

(a) (b)

Figure 37: QAM16 symbol estimation using (a) rectangular decision boundaries, BER = 5.3×10^{-4} (b) minimum Euclidian distance decision boundaries, BER=2.1×10^{-4}.

2.4. Sources of Transmission Impairments

Transmission in optical fibres is limited by two main factors: linear, namely amplified-spontaneous-emission (ASE) noise when launch powers into the fibre are low, and nonlinearities when launch powers are high. This means that it is possible to find an optimum launch power for which the best trade-off between ASE and nonlinearity can be achieved, resulting in the longest transmission distance. The exact value of launch power depends on the specific system and link parameters, such as modulation format, bit rate, fibre type, amplifier noise figure etc.

The ASE noise arises from the spontaneous emission in the optical amplification process, and increases with the number of amplifiers (hence, transmission distance) along the transmission link. Due to its stochastic nature, ASE noise is a fundamental impairment and cannot be removed from the system. One of the ways to offset an impact of ASE noise is to use lower-noise amplifiers, such as Raman amplifiers instead of EDFAs, and lower-loss fibres, such as pure-silica core fibres (PSCFs) instead of SMF; however, this also increases the cost of the system. Another way is to increase the signal power into the fibre, which also increases the OSNR and allows longer distances. However, for very high signal powers an optical fibre ceases to be a linear medium due to the Kerr effect and triggers nonlinear impairments, distorting the signal.

From the system design point of view there are two types of nonlinearity: intra-channel (occurring when only one wavelength channel is present) and inter-channel (occurring in the presence of multiple WDM channels). The most common and widely-known type of intra-channel nonlinearity is self-phase modulation (SPM), which arises from the Kerr effect – the dependence of the refractive index on the peak power in the fibre. The variations in the refractive index caused by pulse propagation in the fibre changes the light propagation speed in the fibre. This produces a phase shift in the pulse, resulting in a change of the pulse frequency spectrum and producing chirp [111]. The induced chirp symmetrically broadens the signal spectrum, and during the propagation over dispersion channel converts frequency distortions into time distortions. SPM is the dominant source of nonlinearity for 10Gbaud systems (Figure **38**).

For WDM systems cross-phase modulation (XPM) becomes the dominant source of nonlinearity, although the deleterious effect of SPM might still be present. This XPM effect is similar to the SPM with the difference that the phase (and frequency) of a pulse is affected by neighbouring WDM channels rather than within the channel itself. XPM causes a timing jitter and intensity distortions after propagation through a dispersive medium [112].

At higher symbol rates, however, the effects of intra-channel cross-phase modulation (IXPM) and intra-channel four-wave-mixing (IFWM) become dominant sources of intra-channel nonlinearity (Figure **38**). This is because the broadening due to chromatic dispersion increases quadratically with the symbol rate, that is, at 40Gbaud the spectrum broadening due to dispersion is 16 times higher than at 10Gbaud. Because more pulses overlap in the time domain during the propagation over a dispersive medium, the efficiency of IFWM and IXPM also increases. As shown in Figure **38** the effect of IFWM and IXPM is less pronounced for nonzero dispersion shifted fibre (NZ-DSF) than SMF; this is because the lower dispersion in NZ-DSF decreases the amount of pulse overlap and, hence, the efficiency of IFWM and IXPM.

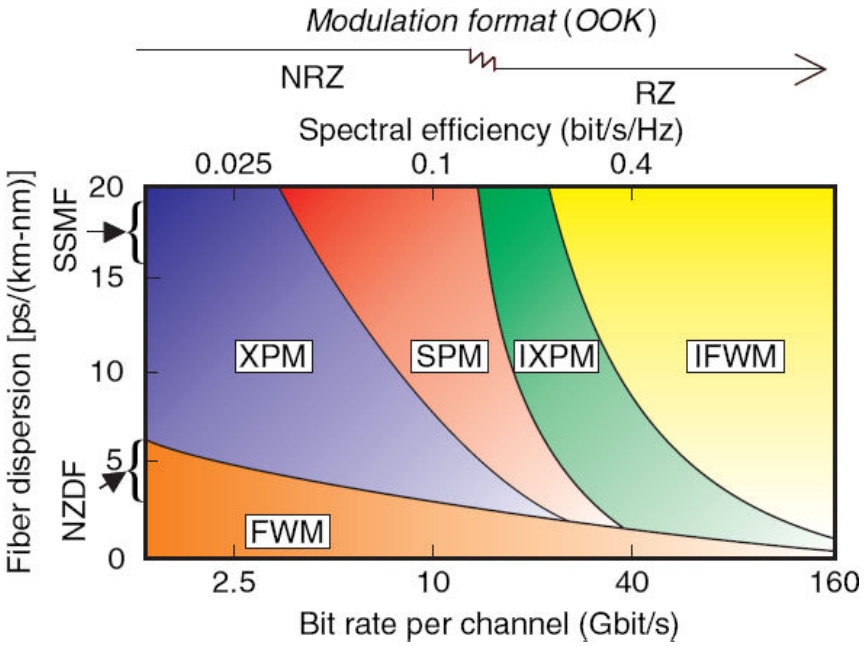

Figure 38: Dominant sources of nonlinearity at various bit rates and fibre types **[24]**

The seed for both IXPM and IFWM is the fact that the lower frequencies of the trailing pulse travel faster that the higher frequencies of the leading pulse, and the different frequencies of two or more pulses “collide” in the middle between two pulses. The IFWM generates a “ghost” pulse if the collision occurs in the middle of an empty time slot and amplitude jitter in the case when collision occurs in the middle of the slot where the optical pulse is present. The IXPM induces a frequency shift on interacting pulses during propagation in dispersive medium, which is then converted to timing jitter when the signal is dispersion compensated [112] [113].

While chromatic dispersion (CD) also affects the signal shape during transmission, in the linear transmission regime dispersion can be fully compensated and, therefore, does not directly pose transmission limitation in modern optical fibre systems. In such system CD can be compensated either using dispersion compensating fibre (DCF) or using a digital filter when coherent detection is used. A more serious implication of the CD is its interplay with nonlinearity, which converts the spectral broadening induced by SPM into the temporal distortions. PMD, a limiting factor for an upgrade of some optical networks [114], can also be compensated digitally in systems with coherent detection [98].

3. OTDM 80Gbit/s Transmission Experiments

At the beginning of this research work in January 2007, OTDM was considered a practical technology used to investigate the transmission performance at >40Gbaud for systems employing direct detection. Over the next years, however, the interest in the OTDM technique has diminished, mainly due to the advances in the coherent detection and the benefits associated with this, as described in section 2.3. While early research efforts of this work were focused on the technique to optimise of 80Gbit/s OTDM transmission to increase the maximum transmission distances (and a long-term idea to increase the OTDM bit-rate to 160Gbit/s and beyond), since late-2008 the experimental activities of this research work have switched towards the investigation of advanced modulation with coherent detection (described in chapters 4, 5).

An initial aim of the 80Gbit/s OTDM experiment carried out in this research work was to investigate the impact of a wide and continuously variable range of phase values between the adjacent OTDM channels on the transmission performance, and finding an optimum phase value to achieve the longest transmission distance for a given system configuration.

Some investigation of optimum phase relationships between adjacent data pulses has been previously carried out by other research groups at 40Gbit/s, albeit, sometimes with contradictory conclusions. In fact, it has been mathematically shown that at 40Gbit/s the maximum suppression of ghost pulses and amplitude jitter due to IFWM is achieved using $\pi/2$ phase difference between adjacent pulses [115] [116]. On the other hand, it was suggested in [117] that amplitude distortion due to phase-to-intensity conversion is higher in the case of $\pi/2$ phase modulation, and the overall performance is better in the case of π [117] [118]. This, however, contradicts the experiments in [119] where more than a 2dB improvement in Q-factor was shown for $\pi/2$ compared with π. At a higher OTDM bit-rate of 160Gbit/s, the Q-factor has been simulated as a function of the phase difference between adjacent OTDM channels, and an optimum performance was found in the case of $\pi/2$-RZ [115] [120].

It should be noted, however, that the transmission at various bit-rates might be limited by different types of nonlinearities, as shown in section 2.4. In addition the optimum phase difference strongly depends on the duty cycle, as described in [30] [121]. In the experiments carried out in this research work the transmission was performed at 80Gbit/s under condition of partial overlap of adjacent pulse tails. To create an overlap between the pulses, an 8ps data pulse train was generated (the bit period at 80Gbit/s is 12.5ps). The investigation of such "wider than normal" pulses is interesting from a practical point of view, since such pulses are easier and less expensive to generate.

3.1. Short Pulse Generation

The transmitter setup to generate a 39.8Gbit/s RZ-OOK signal is shown in Figure **39**. First, the 7dBm output of an external cavity laser (ECL) was modulated by an EAM with a 3dB-bandwidth of around 40GHz. This EAM had a negligible polarisation dependent loss (PDL) of ~0.1dB, therefore, no polarisation controller at the input was used. The RF part was provided by a 39.8Gbit/s PPG with a data output of $3V_{p-p}$ and a pattern length of 2^7-1 – such a pattern was used due to the limitation in the clock recovery operation with longer patterns at the time this experiment was carried out. The output signal was then amplified with an EDFA to overcome the insertion loss of the EAM and subsequently attenuated to obtain an appropriate launch power for the next EAM, which operated as a pulse carver. The polarisation before the pulse-carving EAM was manually adjusted with a polarization controller (PC) in order to minimise the impact of PDL (~1dB) of the EAM. The 39.8GHz clock output of the same PPG was amplified using a 40GHz narrow-band RF amplifier to $7V_{p-p}$, which was found to be the optimum driving voltage for this particular EAM. Due to the fact that the PPG used in this experiment had a fixed output power, additional attenuators before and after the RF amplifier were used to obtain the value of $7V_{p-p}$. The clock signal was also time-adjusted with respect to the data using a PPG in-built delay line to guarantee that the pulse carving occurs in the middle of the symbol period.

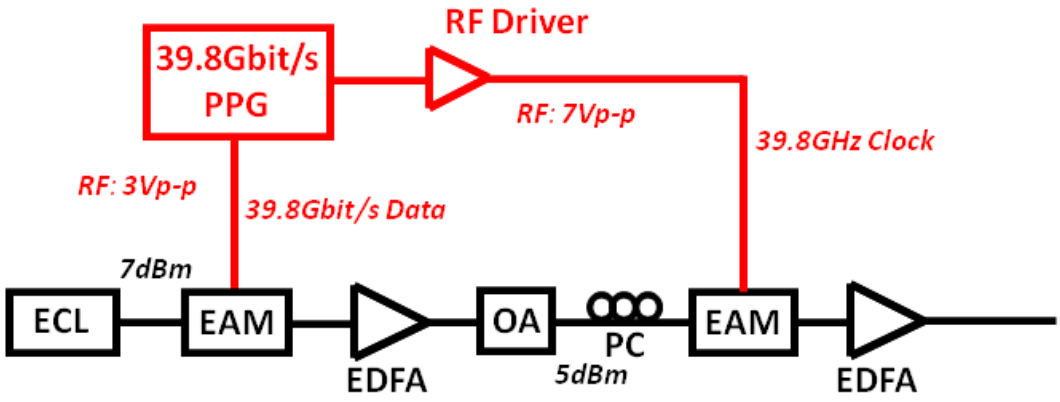

Figure 39: Generation of short data pulses using EAMs

3.2. Bit-wise OTDM Multiplexer with Phase Control

The motivation for a bit-wise OTDM multiplexer with phase control was explained in Section 2.1.2 - fixed phase difference between the adjacent OTDM channels could yield a better back-to-back and transmission performance. In the course of this work, a novel, simple and low-cost bit-wise OTDM transmitter was designed to generate a 79.6Gbit/s signal from an incoming 39.8Gbit/s. The set-up was assembled in the interferometric structure from fibre-coupled commercially available components, and is shown in Figure **40**.

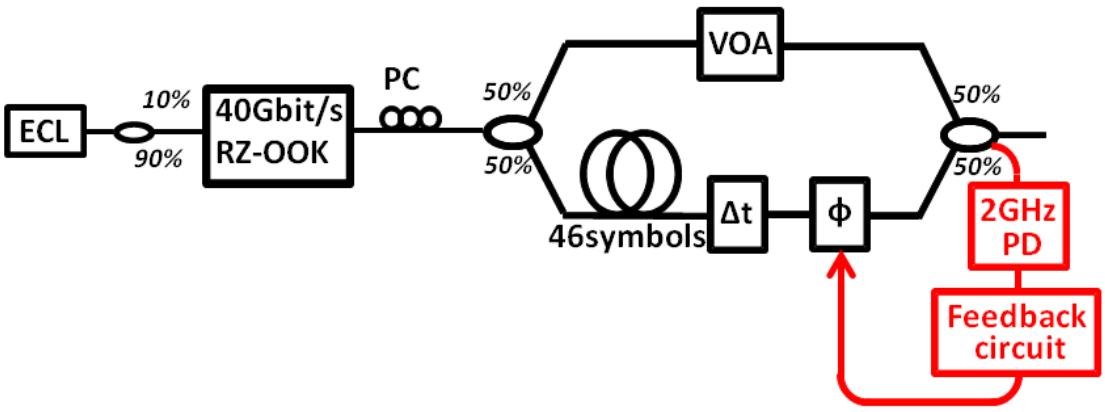

Figure 40: Experimental set-up to generate 79.6Gbit/s OTDM signal with a controllable phase between the adjacent tributaries. Δt – delay line, Φ – phase shifter (piezoelectric fibre stretcher)

The OTDM multiplexer design is based on the interferometric approach described in Section 2.1.2. The incoming 39.8Gbit/s RZ-OOK signal was split into two replicas, time-delayed by half a symbol period and re-combined to yield a 79.6Gbit/s OTDM signal. Any power mismatch between the two arms of the interferometer was compensated using a variable optical attenuator (VOA). A short segment of fibre was also placed in one of the arms to decorrelate the data pattern in the upper arm from the data pattern in the lower arm (the choice of the length of the decorrelation fibre is explained later). In order to control the phase between the adjacent OTDM channels, the

two arms of the interferometer have to coherently interfere, which is only possible when the coherence length of the laser source is larger than the difference in two path lengths within the interferometer [18]. The coherence length L_C of the laser source was found using the following formula [122]:

$$\boldsymbol{L_C = \frac{\lambda^2}{n \cdot \Delta\lambda} = \frac{c}{n \cdot \Delta f}} \quad \textbf{(19)}$$

where λ is the laser source central wavelength, n – refractive index of the fibre, c – speed of light in vacuum, $\Delta\lambda$ – laser spectral width, Δf – laser source linewidth. In the OTDM experiment carried out in this work, a laser source with a measured 700kHz linewidth was used, which corresponds to the laser coherence length of 184 meters. This means that the length of the decorrelation fibre must be less than 184m to enable the coherent interference. To satisfy this criterion the decorrelation length of ΔL = 25cm was used in this work, which yielded a decorrelation in time equal to 1214ps according to:

$$\boldsymbol{\Delta t = \frac{\Delta L}{c \cdot n}} \quad \textbf{(20)}$$

The time period at 39.8Gbit/s is equal to ~25.1ps, which means that at this bit-rate two OTDM tributaries are decorrelated by 46 symbols. Since the transmission experiments were carried out with a 2^7-1 pattern length, 46 symbols provide nearly a half-pattern decorrelation.

It is important to note, that due to the temperature fluctuations and the source laser wavelength drift, a conventional multiplexer is not capable of maintaining a fixed phase difference between the adjacent OTDM channels. In the OTDM multiplexer designed in this work temperature fluctuations were mitigated by placing the multiplexer in a confined temperature-controlled environment. The laser wavelength drift, however, is more complicated to deal with. The wavelength drift upsets the phase stability of the interferometer due to the narrow free-spectral range (FSR) of the OTDM interferometer with various optical paths, which are inevitable due to the presence of decorrelation fibre. In fact, the free spectral range is inversely proportional to the decorrelation length of the fibre and can be calculated according to [122]:

$$\Delta\lambda = \frac{\lambda^2}{n \cdot \Delta L} \quad (21)$$

$$\Delta f = \frac{c \cdot \Delta\lambda}{\lambda^2} \quad (22)$$

where $\Delta\lambda$ is an wavelength FSR, Δf – frequency FSR. For the OTDM multiplexer used in this work with 1214ps of decorrelation, its FSR range is 6.5picometers or 542MHz. Such a narrow FSR means that sub-picometer laser wavelength change could cause a change in phase as large as 50°.

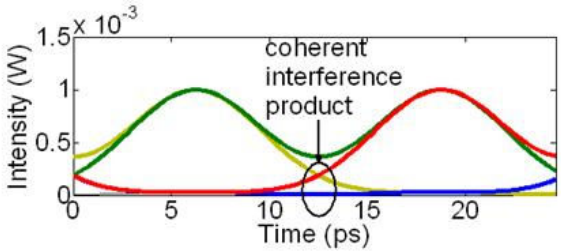

Figure 41: Optical OTDM signal before slow p-i-n photodiode

To minimise the wavelength drift, a stable external cavity laser (ECL) with a frequency drift of less than ±100MHz/hour was used in the experiment carried out in this work. In order to set a specific phase difference between the adjacent OTDM channels and maintain it over a long number of hours, a dedicated feedback circuit was used, as shown in Figure **40**. This circuit is a ditherless bias controller and is commercially available (YYLabs, 0103). When the two OTDM channels propagate in the two different arms, they should not interfere since they are located at different time slots. In practice, however, the 8ps pulses are sufficiently wide to make the tails of adjacent pulses partially overlap and interfere with each other (Figure **41**). The degree of overlap and the interference product, determined by the relative phase shift, are detected by a low-speed photo-detector (~2GHz of bandwidth) and used as an input signal to the feedback circuit. The stronger the pulse overlap, the larger $V_{p\text{-}p}$ (V_{max} – V_{min}) in Figure **42** and the more stable the feedback circuit operation.

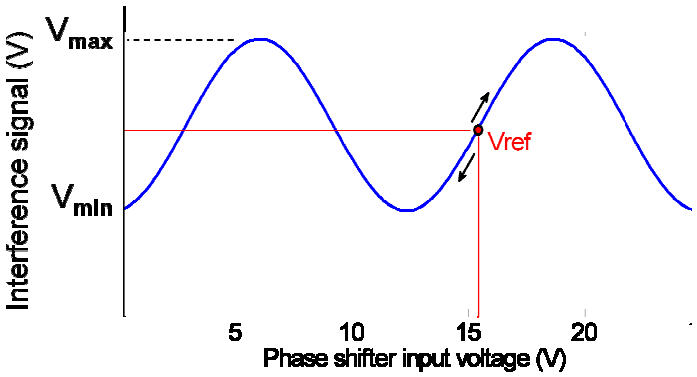

Figure 42: Electrical signal after slow p-i-n photodiode

The phase shifter requires a DC input voltage in the range of 0 - 140V, therefore, the output of the feedback circuit (0 – 5V) was amplified by a voltage converter (General Photonics, MPD-001/PCD-M02) to obtain the required voltage range for the phase shifter operation. The principle of the feedback circuit operation can be described as follows: first, the reference voltage (V_{ref}) is manually set to a particular value to define an operational point at the transfer function of the OTDM interferometer and, hence, the phase. A constantly changing phase between the OTDM channels also varies the power of the interference signal. The feedback circuit then constantly tracks the difference between the known reference signal and the interference signal, and applies an appropriate change to its output voltage, as shown in Figure **42**.

The setup shown in Figure **40** was subsequently refined to provide a steady operating condition for arbitrary pulse widths. It is clear that in the case of very short duty cycles (50% and less, corresponding to <6.25ps pulses for a 79.6Gbit/s OTDM signal), the interference signal between adjacent OTDM channels becomes negligible. This means that alternative information about the phase dynamics within the interferometer must be fed to the phase shifter. In this case phase control was obtained by counter-propagating a part of the ECL unmodulated light with respect to the signal Figure **43**. Because of the bidirectional nature of propagation, a presence of the feedback signal does not adversely affect the data signal, and the feedback signal will interfere only with its own replica in the interferometer. This interference product is detected and processed in exactly the same way as previously discussed. Since the feedback signal is CW light, the operation of such a setup is independent of the data pulse width.

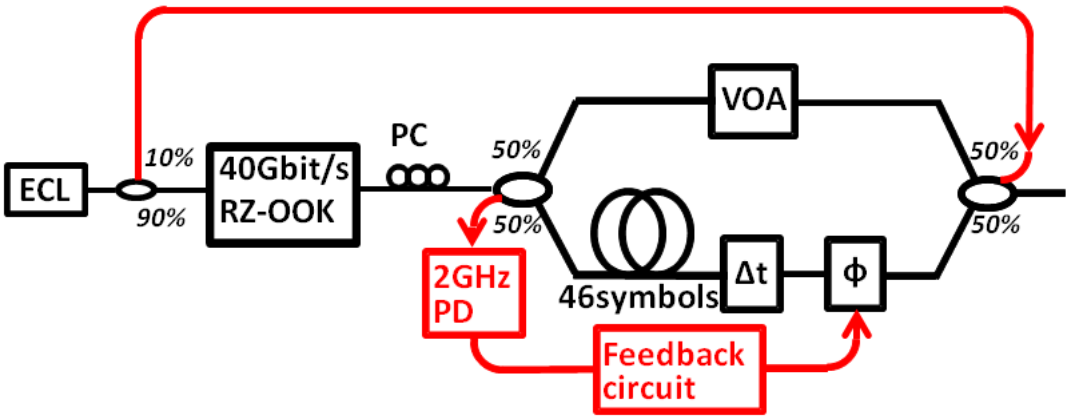

Figure 43: The designed experimental set-up to generate 80Gbit/s OTDM signal with a controllable phase between the adjacent tributaries. Δt – delay line, Φ – phase shifter

In practice, the range of phase values that could be obtained is less than [0°, 180°]. This is because precise phase shifts of 0° and 180° cannot be maintained due to ambiguity in the feedback circuit operation at peak values. This can be best illustrated by assuming the V_{REF} is set at the minimum transmittance point on the nonlinear transfer function in Figure **42**. From now on, the interference voltage can only increase, but the feedback circuit will not be able to detect whether it should increase or decrease the voltage to the phase shifter, and will immediately lose its phase stabilisation ability.

A phase-stabilised fibre interferometer is a versatile tool; its application is not only limited to OTDM but could also be used to optically synthesise advanced modulation formats, such as QAM16 and QAM64. A detailed description of QAM16 generation using the optical interferometric technique is given in Section 4.2.1.

3.3. OTDM Demultiplexer, Clock Recovery and Direct-Detection Receiver

As mentioned previously, an OTDM demultiplexer is essential to downconvert a high bit-rate OTDM signal to an original lower bit-rate rate by extracting a base rate signal from the OTDM stream. For the transmission experiments in this work simultaneous demultiplexing and clock recovery using a single EAM was performed (Figure **44**). The clock recovery was needed to provide timing for the demultiplexer to synchronise it with the incoming data, and error detector to perform sampling at the correct instant in time to determine the BER.

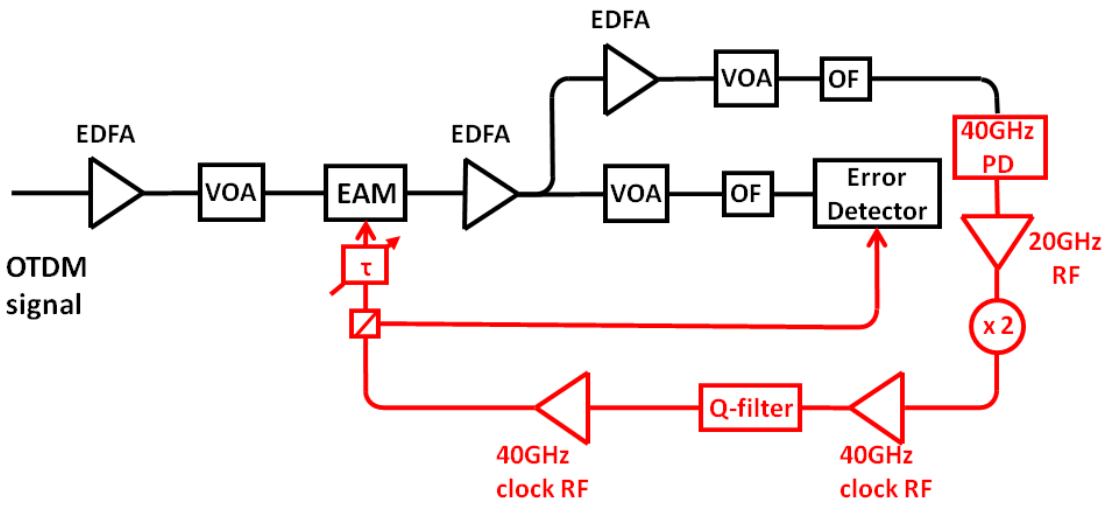

Figure 44: OTDM receiver end with simultaneous demultiplexing to the base rate and clock recovery (clock recovery electrical part is shown in red).

The transmitted OTDM signal was first amplified to provide sufficient optical power at the input of the EAM. After the EAM the signal was split into two parts: a high power output for data recovery and a low power output to form a closed loop with the EAM for the clock recovery operation. In a closed loop path the signal was further amplified and then passed through the wavelength-tunable flat-top optical filter (OF) with 100GHz 0.5dB bandwidth (a similar OF was used at the receiver). The input power to the 40GHz photo-detector (PD) was set to be 1dBm. The idea behind this clock

recovery is to use a high-Q filter to directly carve a clock signal from the incoming data, which can then be fed to the EAM and error detector. An important feature of this clock recovery is its ability to operate when no data is entering the closed loop, e.g. in the presence of long sequences of 'zeros' when long patterns are used. Due to the fact that the amplifiers in the closed loop create a positive feedback, such absence of data could cause the EAM to modulate the noise at 39.8GHz. This will essentially create an "incorrect" clock component and the clock recovery will not be able to lock back when the actual data arrives.

To prevent noise build-up when there is no data entering the loop, a broadband 20GHz RF amplifier was used to cut-off a 39.8GHz component and to block any positive feedback. The frequency doubler then re-creates the frequency components up to 39.8GHz, and the signal is amplified using a narrowband (~4.3GHz) amplifier with a central frequency of ~40GHz. Following this the frequency multiplied signal was passed through the high-Q filter with a central frequency of 39.8 GHz for clock component extraction.

The clock recovery unit was also designed for use with the recirculating loop, where the optical signal must be analysed during the propagation time through a single loop span denoted by τ_{LOOP} (equal to 500μs for a 100km span). This means that the time to recover the clock must be significantly smaller than 500μs to have enough time to analyse the transmitted signal with the error detector or digital sampling scope [123]. Compared to the voltage-controlled oscillator (VCO)-based clock recovery design, where the clock restoration time depends on the strength of the phase locked loop, the restoration time of the high-Q filter clock recovery solely depends on the bandwidth of the filter and can be evaluated according to the following equation [123]:

$$\boldsymbol{\tau_R = \frac{1}{0.35\Delta f}} \qquad \textbf{(23)}$$

where Δf is the 3dB bandwidth of the filter. In this work a Q-filter with a bandwidth of 68MHz (Q = 585) was used, which corresponds to the clock restoration time of 0.042 μs. A further narrowband 40GHz RF amplifier was used to provide the required power to the EAM. A tunable delay line before the EAM allowed to separate a particular OTDM tributary. At the time the experiment was carried out the operation of the clock recovery was limited to short patterns of up 2^9-1, which was later corrected by

optimising RF powers in the clock recovery unit to allow the operation for the patterns up to 2^{31}-1. The OTDM receiver comprised a p-i-n photodiode with 65GHz bandwidth, broadband 45GHz amplifier and an error detector with broadband front-end electronics.

Other implementations of high-speed OTDM clock recovery have been also reported in the literature, although many of them are complex. The most prominent involve taking advantage of the nonlinearity in an RF doubler to prevent noise build-up [124] or using bi-directionally operated EAM as a phase comparator [125]. The advantage of the clock recovery used in this research work is its simplicity in the design, fast restoration time and an ability to work with long PRBS (up to 2^{31}-1).

3.4. OTDM Transmission Results at 80Gbit/s

As mentioned in section 3.1 the aim of this experiment was to quantify the impact of the phase difference between the adjacent OTDM channels on the intra-channel four-wave mixing (IFWM) in the presence of significant pulse overlap. Figure **45** shows the experimental setup developed in the course of this work. A 39.8Gbit/s RZ-OOK signal was generated by modulating the output of an ECL at 1545nm with two EAMs. One EAM was used for data encoding with a 2^7-1 PRBS pattern, while the second EAM was used for pulse carving, generating RZ pulses with 8ps FWHM, 38dB OSNR and 15dB extinction ratio. The 39.8Gbit/s signal was multiplexed to 79.6Gbit/s OTDM signal using a phase-stabilised interferometer, as described in section 3.3. The resultant 79.6Gbit/s signal was then launched into a single-span recirculating loop, consisting of a 100km SMF link, whose chromatic dispersion was fully compensated using an inline dispersion compensating fibre (DCF) and amplified with an EDFA (noise figure ~4.5dB). The description of the recirculating loop used in the experiments is given in Appendix A. A flat-top optical filter (OF) with 100GHz bandwidth (specified at 0.5dB) was placed in the loop to reject the out-band ASE noise at every recirculation. After transmission, a 79.6Gbit/s OTDM signal was downconverted back to the base rate of 39.8Gbit/s using an EAM-based demultiplexer and clock recovery, as described in the previous section. An error detector was gated by a signal from the signal generator, which was also used to provide timing for acousto-optical modulators (AOMs) in the recirculating loop.

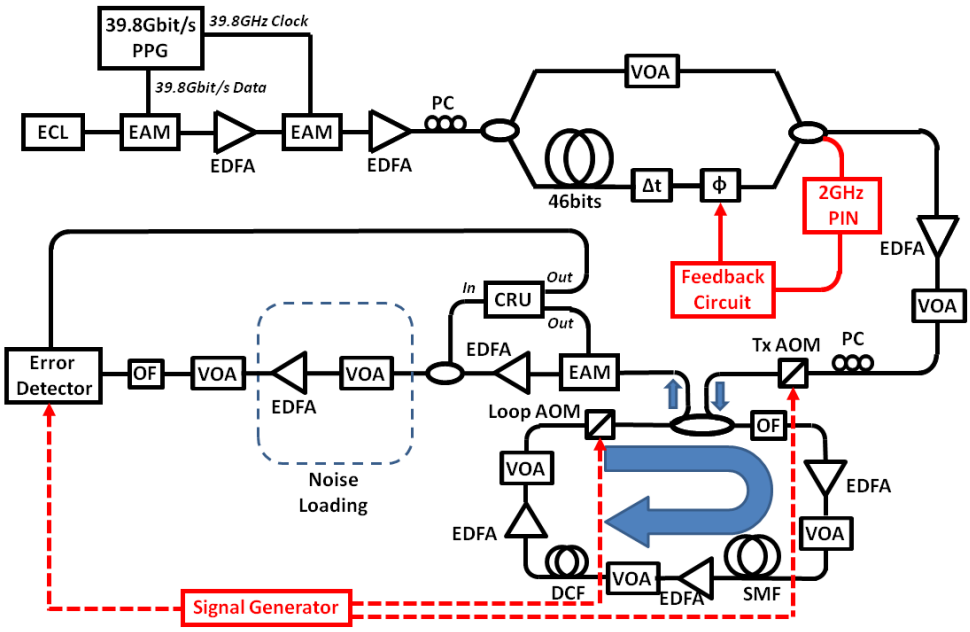

Figure 45: Experimental set-up for 79.6Gbit/s OTDM signal transmission

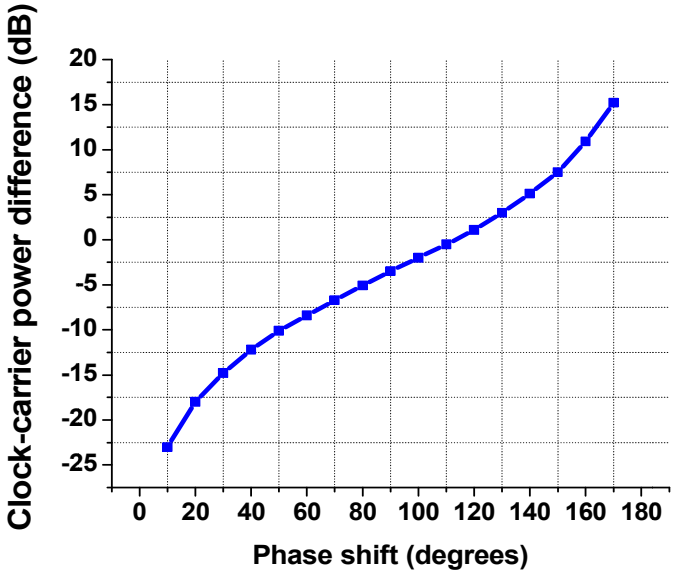

Figure 46: Clock-carrier power difference (CCPD) dependance on phase shift between adjacent OTDM channels

First, a method to accurately set the phase values was devised. The variation in the phase shift between OTDM channels introduces a power change in the carrier and the 39.8GHz clock components. Figure **46** shows the ratio between the carrier and 39.8GHz spectral components (clock-carrier power difference - CCPD) calculated numerically as a function of phase shift between the OTDM channels. This result leads to two

considerations; first, experimentally measured CCPD (Figure **47(a)** and Figure **47(b)**) can be related to the results in Figure **46** and can be used to set the desired phase shift values in the coherent OTDM multiplexer. Secondly, different phase modulated OTDM formats will have different optimum optical filter bandwidth due to associated spectral reshaping [126]. The optimum filtering is a trade-off between reduction of noise during the detection process and partial rejection of the spectral components. Phase values corresponding to CCPD = -14, -12, -8, -4, 0 and 4dB were set during the experiment. Figure **47** shows the optical spectra of optical signals with two extreme values of measured CCPD. Pure RZ and CS-RZ (0° and 180° of phase shift between adjacent OTDM channels, respectively) were outside the operating range of the feedback circuit and, therefore, were not implemented during the experiments.

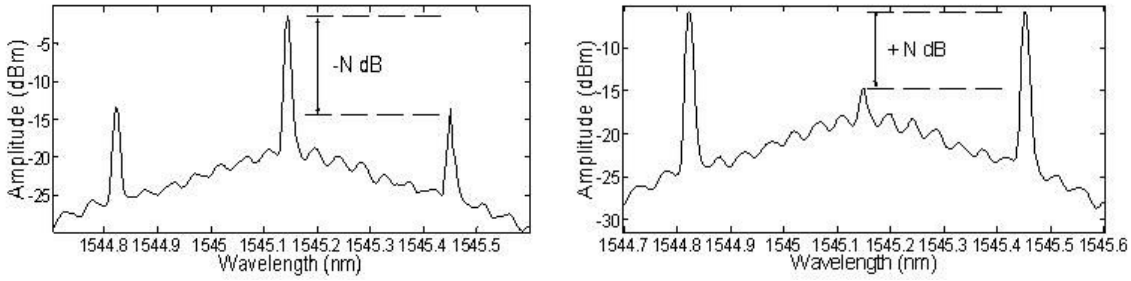

(a) (b)

Figure 47: Measured OTDM spectrum before transmission with (a) clock component weaker than carrier by N dB; CCPD = -N; (b) clock component stronger than carrier by N dB; CCPD = +N

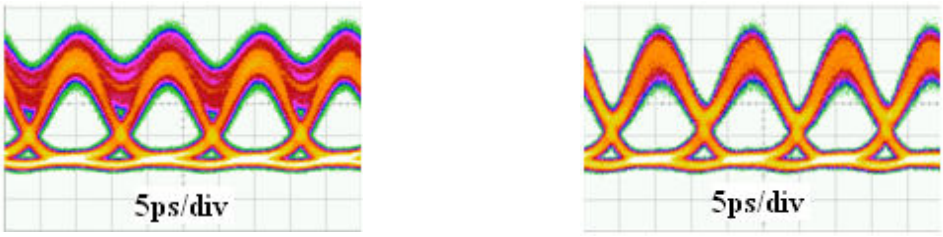

(a) (b)

Figure 48: Optical signal eye-diagrams before transmission for (a) 32°-RZ (CCPD = -14 dB) (b) 135°-RZ

In back-to-back 80Gbit/s measurements, a 4dB improvement in receiver sensitivity at a BER of 10^{-9} was measured when increasing the phase difference from 32°-RZ towards 135°-RZ. This improvement can be attributed to the reduced inter-symbol interference

(ISI) between the adjacent pulses modulated with orthogonal phase values. In fact, the simulations showed that the 4dB back-to-back penalty disappears when shorter pulses are used (e.g. 2ps) due to reduced pulse overlap and ISI (Figure **48**).

The maximum transmission distance (assuming the BER = 3×10^{-3}) was measured as a function of the phase difference between the adjacent OTDM channels (Figure **49**). As is well known, the optical launch power to the fibre is limited by two factors: accumulated ASE for low input powers due to the multiple EDFAs used in transmission and nonlinearity for high input powers. Therefore, it is possible to find an optimum launch power, at which the transmission distance is maximised. In the experiments the launch power into the SMF was optimised for each modulation format and was in the range of -1 to 1.5dBm; constant launch power into the DCF (0dBm) was maintained during the experiment.

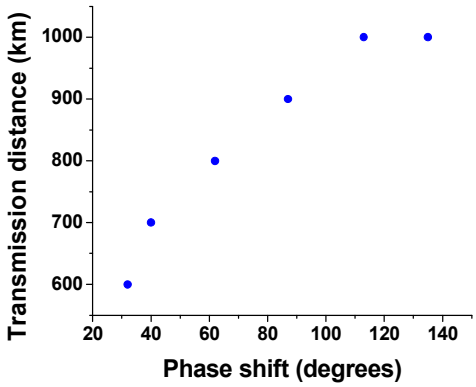

Figure 49: Experimentally measured maximum transmission distance as a function of the phase shift between the adjacent OTDM channels at BER=3x10^{-3}

A differential phase modulation of 120° between the adjacent data pulses (120º-RZ) yielded the longest transmission, which can be attributed to a combination of two factors: increased tolerance to IFWM and increased receiver sensitivity (compared with RZ or 90°-RZ) due to decreased ISI. In fact, IFWM is a phase sensitive effect determining the strength of the "ghost" pulses and amplitude jitter effects between interacting channels. A limited extinction ratio (15dB) also impacts the modulation format tolerance to IFWM, as residual power in 'zeros' will also contribute to IFWM generation dynamics [127]. It should be noted that transmission was limited by nonlinearity both in SMF and DCF. To quantify the strength of nonlinear effects, a set of numerical simulations at 79.6Gbit/s was performed and the results were compared with those experimentally obtained, as described in the next section.

3.5. Supporting Simulations for Bit-Wise OTDM Transmission

Numerical results were obtained in Matlab by simulating the link used in the experiment at 79.6Gbit/s. During the simulations a span loss of 20dB, chromatic dispersion of 17 ps/nm/km and nonlinearity coefficient (γ) of 1.3 1/W/km. A flat-top 2^{nd}-order Gaussian filter at the receiver with variable bandwidth was used in numerical simulations to enhance the rejection of the out-of-band noise without sacrificing the signal spectral profile. Figure **50** shows the comparison of experimental and numerical results. Both results show a similar trend in terms of the phase shift; however, optimising the filter shape and bandwidth yielded an increased transmission distance, compared with experimental results where fixed-bandwidth filter was used.

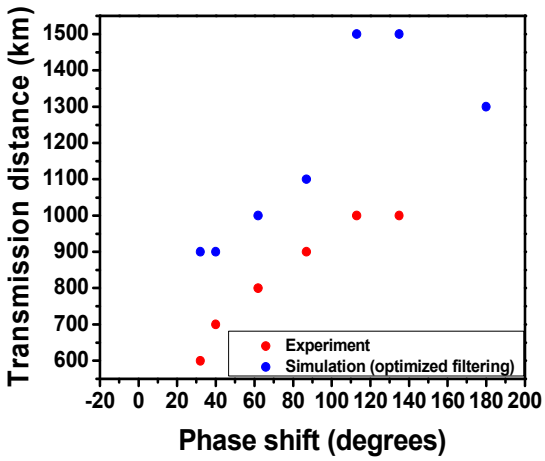

Figure 50: Comparison of the experimentally measured and simulated maximum transmission distance as a function of the phase shift between adjacent OTDM channels at BER=$3x10^{-3}$

Figure **51** shows power in 'zero' bit slots (this is due to the generation of "ghost" pulses, limited extinction ratio and ISI) and amplitude jitter of 2056 bits of a 2^{31}-1 PRBS pattern after 100km for 8ps and 2ps FWHM pulse widths, calculated as a function of phase shift between the adjacent channels.

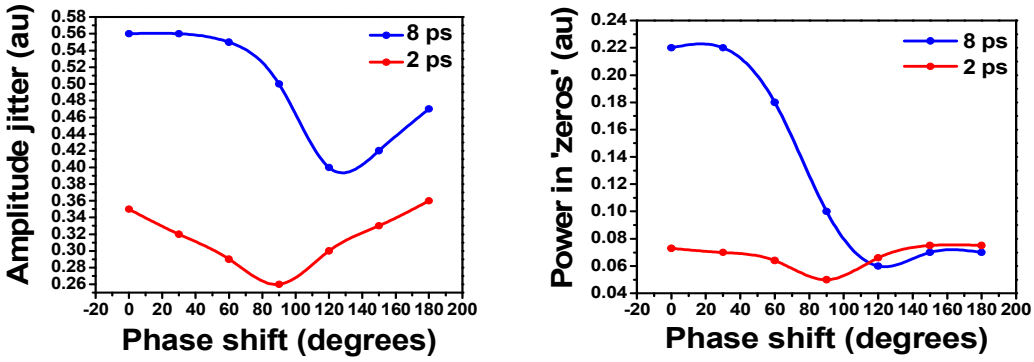

(a) (b)

Figure 51: (a) Amplitude jitter and (b) power in 'zero' bit slots in 79.6Gbit/s transmission, simulated as a function of the phase shift between adjacent OTDM channels for 2 and 8ps pulse widths

In these simulations noise from EDFA was neglected, and a 13dBm input launch power was used to investigate signal distortion only due to intra-channel nonlinearities. A single span transmission with a high input launch power was selected (as opposed to real transmission with multiple spans) in order to obtain intra-channel nonlinear effects within a reasonable computational time. Both pulse power within 'zeros' and amplitude jitter in 'ones' were minimized for 120º-RZ and 8ps pulses (Fig. 51). It was also found that for phase differences lower than ~40º, the power in 'zeros' and amplitude jitter remained nearly constant; this is in good agreement with the numerically obtained curve in Figure **50**, where low phase shift values yielded the same transmission distance. However, when the pulse width was decreased to 2ps, 90º-RZ resulted in maximum suppression of IFWM effects, with symmetrical curves for amplitude jitter and power in 'zeros'. In the case of 8ps pulses, however, initially overlapping pulses needed higher phase separation to cause destructive interference of the IFWM components [117]. In addition, 8ps pulse tails spread over adjacent bits, causing ISI, which contributes to the total power in 'zeros'. Examples of RZ and CS-RZ 8ps data pulse traces are shown in Figure **52**.

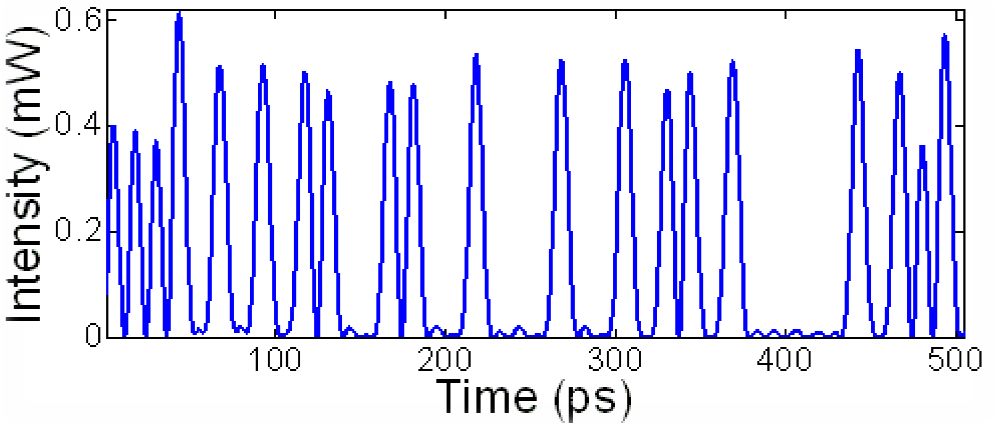

(a)

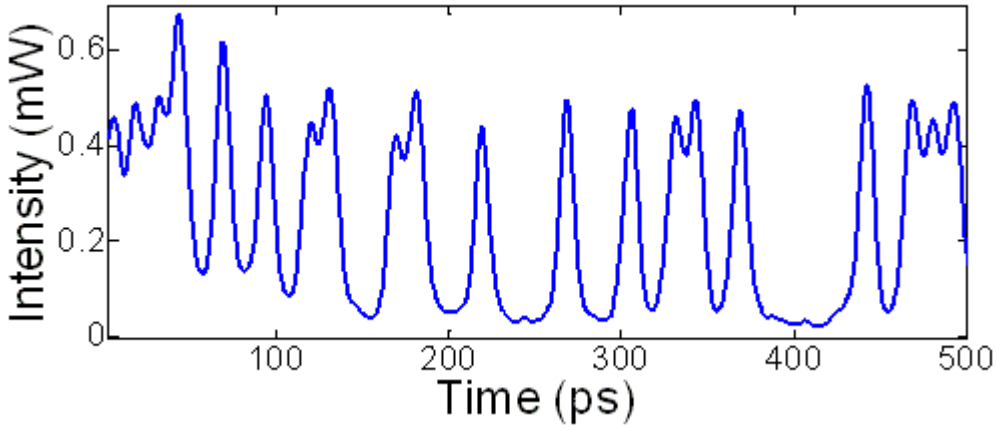

(b)

Figure 52: (a) CS-RZ and (b) RZ simulated signal traces

To further investigate the impact of the phase modulation and the pulse width on the transmission distance at 79.6Gbit/s, a set of simulations was carried out to obtain the maximum transmission distance as a function of both the applied phase shift and FWHM pulse width (Figure **53**). Simulations showed that the π/2-RZ modulation format is optimal with 2ps pulses (in agreement with [120]); however, the optimum phase difference increases for larger pulse width (Figure **53(a)** and Figure **53(b)**). Therefore, it can be concluded that the optimum phase relationship for maximum transmission distance depends on the OTDM duty cycle. This is due to a combination of an increase in receiver sensitivity for out-of-phase formats and the dependence of the phase shift on tolerance to IFWM when changing the pulse width. This consideration is particularly important as, at high bit rates, low duty cycles become unfeasible with

EAM (cascading many EAMs will inevitably lead to OSNR degradation due to the additional EDFAs required). Thus, it is important to assess the modulation formats performance with the pulse width that can be practically generated by EAMs.

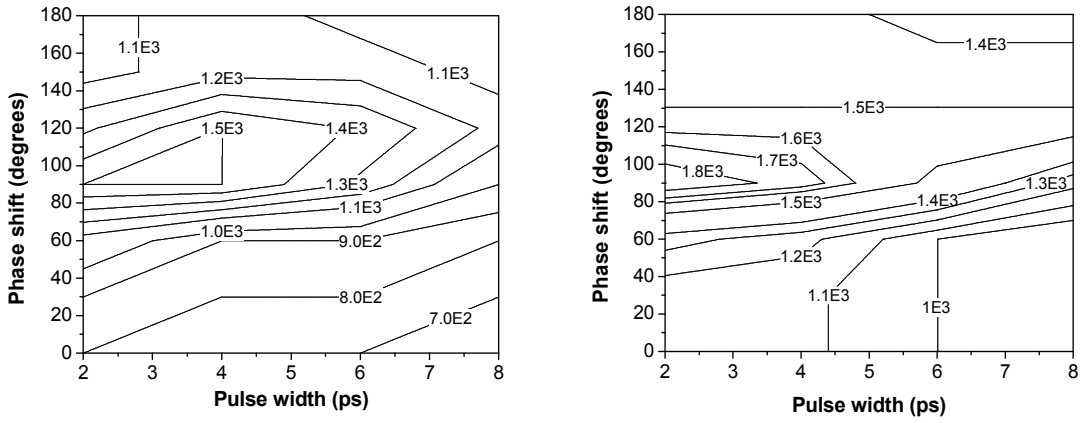

(a) (b)

Figure 53: Simulated maximum transmission distance (km) at 80 Gbit/s for BER=3x10^{-3} as a function of pulse width and phase shift between OTDM channels. (a) fixed-bandwidth filter as in an experiment; (b) optimised filter

To understand the effect of the optical filter bandwidth on the performance of phase modulation formats, the variation in transmission distance as a function of pulse width and phase shift, when optimised optical filtering for each modulation format is applied, was investigated. In the simulations, a 2nd-order optical Gaussian filter bandwidth at the receiver was varied from 130 - 200 GHz (specified as FWHM) to ensure longest transmission distance for a particular modulation format at BER=3×10^{-3}, and the results are shown in Figure **53(b)**). As was previously mentioned, the optimum filtering is a trade-off between reduction of detected noise and partial rejection of the spectral components; therefore, by careful adjustment of filter bandwidth it was possible to boost transmission performance.

3.7 Summary

The results in this section investigated the performance of 80Gbit/s bit-wise OTDM transmission in terms of the maximum reach, and quantified the impact of intra-channel four-wave mixing (IFWM). To generate a bit-wise OTDM signals with fixed phase relationships between the adjacent channels a novel phase-stabilised interferometer was assembled from commercially available components.

For the SMF dispersion-compensated link studied in this experiment the maximum reach was found to be 1000km, and was obtained when using ~120º phase difference between the channels. When the phase difference between the adjacent channels was not optimised (e.g. 30º) the maximum reach was reduced to as little as 600km. This is due to the reduced tolerance towards IFWM for low phase values and a larger cross-talk when the adjacent channels are in-phase.

To further support the experimentally obtained results, Matlab computer simulations were carried out. Simulations showed the possibility of increasing the maximum reach further to 1500km when an optimised filter bandwidth is used at the receiver. Next, the impact of IFWM, which manifests itself as amplitude jitter and the appearance of the "ghost" pulses, was calculated. When 8ps pulses were used at the transmitter (in line with the experiments), both the amplitude jitter and power in "zeros" have minimum values at 120º, which verifies the experimentally obtained results in terms of transmission performance. The reduction of the pulse width to 2ps resulted in a lower optimum phase difference (90º) between the adjacent channels. This is due to the reduced initial pulse overlap for 2ps pulses. The optimum transmitter configuration was found to be for 2ps pulses and 90º of phase shift, for which 1800km of transmission distance was achieved.

The aim of this work on OTDM was not to produce record transmission distances but to investigate and quantify the transmission improvement by using different phase relationships between the adjacent OTDM channels. By comparing the maximum reach of 1000km (achieved experimentally in this research work) with previously reported OTDM results at the bit-rate exceeding 40Gbit/s, that the maximum reach can be further increased by employing shorter pulses, phase modulation formats, advanced fibre type and advanced amplification techniques. The results in [45] and [49] show the feasibility

to achieved 2000km and 4000km, respectively. Both experiments were carried out at 160Gbit/s.

The research work carried out in this chapter also allowed to clarify further direction of the work - advanced modulation formats with coherent detection. The rationale for this is that advanced modulation formats (QPSK and QAM16) allow to obtain the equivalent bit-rates using only a fraction of spectral bandwidth needed for OTDM. The coherent detection significantly simplifies the detection of advanced modulation formats and facilitates the use of DSP to mitigate transmission impairments.

4. Single-Channel Transmission of QPSK and QAM16 Signals

As explained in Chapter 1, future commercial optical transport systems are likely to use advanced modulation formats with coherent detection. It is, therefore, important to understand the transmission performance and limitations of these formats. The benefit of advanced modulation formats and coherent detection can be seen not only for long-haul applications where both capacity and reach need to be maximised, but also for unrepeated access networks for which receiver sensitivity is an important parameter.

The main aim of the research work on advanced modulation formats was to systematically study the performance of two modulation formats (QPSK and QAM16) at various bit rates to understand their linear and nonlinear limits. A particular focus of this work was to explore the techniques that could enable to further increase the maximum reach of QPSK-based systems over transoceanic distances (>6000km). The studied techniques involve the use of RZ pulses instead of NRZ to increase the tolerance towards nonlinearity, and digital back-propagation for nonlinearity compensation (NLC). The same techniques were also investigated for QAM16 signals, but for shorter transmission distances (up to 4000km). The work in this thesis represents one of the first demonstration of these techniques in coherent transmission and quantification of their benefits.

This chapter begins with single-channel transmission experiments to establish the upper-bound limit on the achievable transmission, i.e. in the absence of inter-channel nonlinearities present in practical WDM systems. The WDM transmission results are described in Chapter 5.

4.1. QPSK

The investigation of transmission limits of QPSK-modulated signals and the techniques to maximise the transmission distance will benefit system designers and network operators, since the first generation of coherent systems to be deployed will be based on the QPSK modulation format. The first commercial QPSK optical transport solutions based on coherent detection and DSP were introduced in 2008 [128], and the first deployment of a 100Gbit/s QPSK coherent solution was performed by Verizon in Europe in 2009 [129]. Verizon has also committed to deploy 100Gbit/s technology on selected segments of its U.S. backbone network by the end of the second quarter of 2011 [130].

The results of the research carried out in this thesis showed the first comprehensive experimental study of QPSK transmission at 42.7, 85.4 and 112Gbit/s to understand the linear and nonlinear limits at each bit rate, and the maximum achievable reach at each bit-rate. The results were also extended to experimentally quantify the benefits of using NLC at the receiver [12], and RZ pulses instead of NRZ at the transmitter at 112Gbit/s [9]; this was the first comparison of the two pulse shapes in terms of maximum reach. The bit rate of 112Gbit/s was chosen to match the speed of the next generation optical networks.

The main quantities measured in these QPSK single-channel experiments are back-to-back performance (BER vs. OSNR) and the dependence of maximum reach on the launch power into the fibre for the NRZ- and RZ50-QPSK signals, measured at 42.7, 85.4 and 112Gbit/s. Both the implementation penalty (in the back-to-back) and maximum reach data points are measured assuming the BER = $3\text{x}10^{-3}$, which is less than the current limit of $3.8\text{x}10^{-3}$ on hard-decision FEC [131].

4.1.1. Transmission performance at 42.7 and 85.4Gbit/s

4.1.1.1.Experimental setup

The experimental setup designed and built to generate and transmit QPSK signals at various bit rates is shown in Figure **54**. First, a 42.7Gbit/s Yokogawa pulse pattern generator (PPG) was pre-programmed by doubling or quadrupling each consecutive bit in an original 42.7Gbit/s binary pattern to create PRBS sequences at 21.3 or 10.66Gbit/s, respectively. The PRBS sequences with the length of 2^{12}-1 were chosen to facilitate data processing in a realistic time frame. Two $3V_{p-p}$ outputs of the PPG, inverted with respect to each other, were then decorrelated by 1.4ns using RF cables with different lengths and amplified to $7V_{p-p}$ using SHF803P 45GHz broadband amplifiers (drivers), the value for $2V_{\pi}$ for the specific I-Q modulator used in this experiment. As mentioned in section 2.2.3., driving an I-Q modulator over $2V_{\pi}$ is desirable, as it allows for the maximum modulation depth and the suppression of noise transfer from the electrical driving signal into the optical domain. The bias points of the two inner Mach-Zehnder modulators were then set to the null transmittance points; these were found by minimising the output power of the I-Q modulator with no RF signal present. After the correct bias points were found, the RF signals were switched on and the phase between two BPSK signals was tuned to 90º by looking at the QPSK signal eye diagram on a digital communication analyser. A distributed-feedback (DFB) laser with a linewidth of 2MHz (measured using a self-heterodyne technique) and operating at a wavelength of 1554nm was used as the transmitter light source.

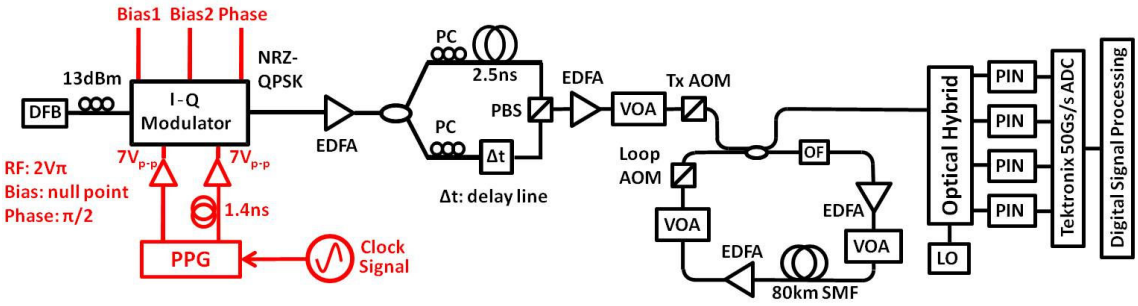

Figure 54: Experimental setup for 42.7 and 85.4Gbit/s PDM-QPSK transmission.

The QSPK signal was then equally split into two paths, in which the two QPSK

signal replicas were decorrelated by 2.5ns, with the polarisations adjusted to be orthogonal using manual polarisation controllers (PCs), and recombined with a polarisation beam splitter (PBS) to obtain a PDM-QPSK signal. The decorrelation lengths of 1.4ns at the transmitter and 2.5ns at the polarisation multiplexer, respectively, were sufficient to create an equal distribution of symbol transitions in the QPSK signal. The signals on the two polarisations were aligned in time with respect to each other; the measured eye diagrams of the PDM-QPSK signals at 42.7Gbit/s and 85.4Gbit/s are shown in Figure **55**. As mentioned in section 2.2.3., the presence of transitions in the eye diagram is due to the finite rise and fall times in the electrical driving signals. The number of transition states is increased from 3 states for a single-polarisation QPSK signal to 5 states for a PDM-QPSK signal.

The resulting signal was then launched into a recirculating fibre loop consisting of an 80.2km single-mode fibre (SMF) span with an overall chromatic dispersion (CD) of 1347ps/nm and loss of 15.4dB. The transmission link did not contain any dispersion compensating fibre (DCF), and the CD was compensated digitally at the receiver. The noise figure of the amplifiers used in the loop was 4.5-5dB. An optical filter (OF) with 100GHz bandwidth (specified at 0.5dB) was placed to reject the ASE. The operating principle of the recirculating loop used in all transmission experiments throughout this research is described in Appendix A. After the desired number of recirculations the signal was sent to a polarisation- and phase-diverse coherent receiver to detect the in-phase and quadrature components of each polarisation.

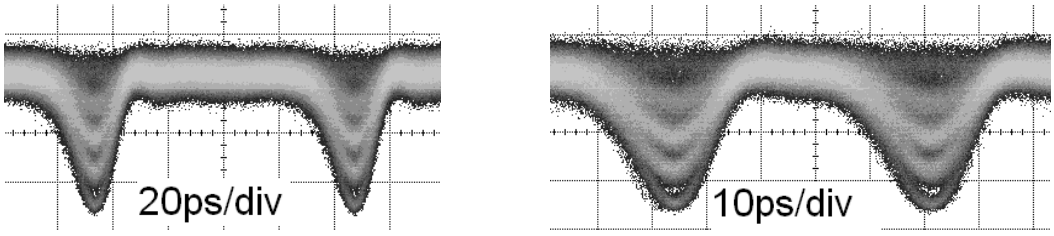

(a) (b)

Figure 55: Eye diagrams of PDM-QPSK signal at (a) 42.7Gbit/s and (b) 85.4Gbit/s

The first block of a coherent receiver consisted of a PBS to split the incoming PDM-QPSK signal with -13dBm of power into the two orthogonal polarisations. A 100kHz-linewidth ECL (also measured using the self-heterodyne technique), operating as the

LO, was set to its maximum output power of 7dBm and split into two outputs using an optical coupler. Such signal and LO power values were chosen to provide 20dB difference between the two, in accordance with [96]. The polarisation controllers at each output were used to align the state of the polarisation of the LO with respect to the signal. The co-polarised signal and local oscillator were then coupled in the 90° optical hybrid, assembled from two asymmetric 3x3 fibre couplers, to downconvert the incoming signal to an intradyne frequency and produce in-phase and quadrature components for each polarisation: Re(E_x), Im(E_x), Re(E_y), Im(E_y) [96]. The detected signals were digitised using a Tektronix real-time scope at 50GSamples/s and processed offline using Matlab. A photograph of the laboratory receiver rack is shown in Figure **56**.

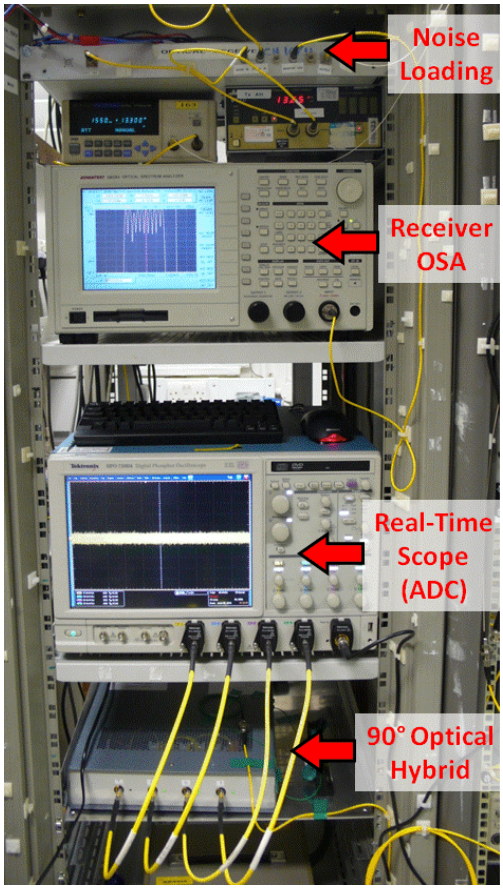

Figure 56: Receiver rack photo

4.1.1.2.Back-to-back and OSNR measurements: results and discussion

To characterise the PDM-QPSK signals at 42.7Gbit/s and 85.4Gbit/s, the back-to-back BER was measured as a function of OSNR, and the results are presented in Figure

57. At BER = $3x10^{-3}$ the implementation penalty (that is, the difference between the theoretical and measured OSNR) was found to be 1dB at 42.7Gbit/s and 1.5dB at 85.4Gbit/s. However, without any noise loading the PDM-QPSK constellation at 42.7 and 85.4Gbit/s, measured over 2^{19} symbols, was determined to be error free.

The characterisation of the receiver sensitivity requires the knowledge of OSNR, which is defined as [132]:

$$\boldsymbol{OSNR = 10log\left(\frac{S}{N}\right) + 10log\left(\frac{B_{MEAS}}{B_{REF}}\right)} \quad \textbf{(24)}$$

where S – signal power, N – noise power, B_{MEAS} – resolution bandwidth of the measurement, B_{REF} – reference optical bandwidth of 0.1nm. B_{MEAS} was chosen to be 0.5nm (62.5GHz) to ensure that all frequency components of 10.7 and 21.4Gbaud signals are measured, so as not to underestimate the signal power. An incorrect measurement of the signal power will result in the incorrect value of OSNR. The second term of Eq. 25 is used to ensure that the OSNR value is independent of the instrument's resolution bandwidth B_{MEAS} for the measurement, so that results obtained with different instruments can be compared [132].

Recalling that $10log\left(\frac{S}{N}\right) = 10log(S) - 10log(N)$, the value of OSNR in dB can simply be measured by subtracting the readings of the OSA noise power in dB from the signal power in dB and adding the second term from Eq. 25. It is important to note, however, that any attempt to measure the signal power will inevitably result in measuring the combination of both signal and noise powers, that is $\frac{S+N}{N} = \frac{S}{N} + 1$ instead of $\frac{S}{N}$. The measured difference D(dB) between the two OSA readings must, therefore, be converted to the linear units, followed by the subtraction of 1: $D_{LIN} = 10^{\frac{D}{10}} - 1$; D_{LIN} can then be used in Eq. 25 instead of $\frac{S}{N}$ to calculate the true value of the OSNR. During the measurements the OSNR values were varied with a step of 1dB.

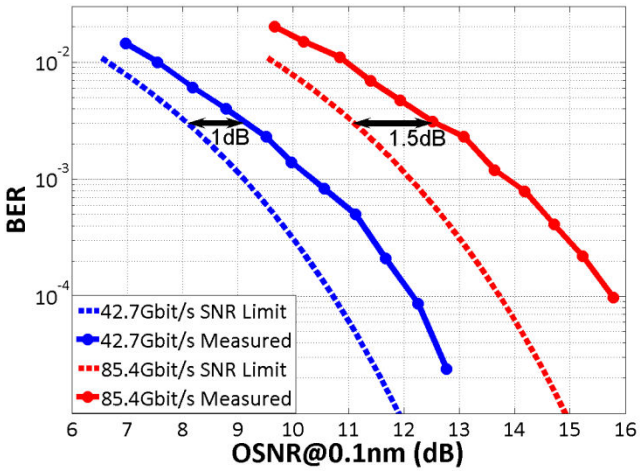

Figure 57: Measured receiver sensitivity for 42.7Gbit/s and 85.4Gbit/s PDM-QPSK signals

4.1.1.3.Maximum reach measurements: results and discussion

To characterise the linear and nonlinear limits for QPSK transmission, the maximum reach was measured as a function of the power launched into the fibre at 42.7Gbit/s and 85.4Gbit/s (Figure **58**), assuming the BER = $3x10^{-3}$. Two cases were considered: one in which only linear impairments were compensated (such as CD and PMD), and the other in which digital back-propagation was applied to perform nonlinear compensation (NLC) of intra-channel effects. The NLC was performed using one nonlinear step per span, as described in section 2.3.2. For the ASE limited region (up to -10dBm of launch power for 42.7Gbit/s and -7dBm for 85.4Gbit/s) both curves are identical, since digital back-propagation cannot undo the accumulated ASE noise. However, as the launch power was increased and the impact of self-phase modulation became more pronounced, the use of the digital back-propagation allowed improvement of the nonlinear threshold, therefore, increasing the optimum launch and the maximum reach. At 42.7Gbit/s the optimum launch power was increased from -6dBm in the case with dispersion compensation only to -3dBm in the case when NLC was used. This increase by 3dB corresponded to a 72% increase in the maximum reach, that is, from 7760km (97spans) to 13600km (170 spans). At 7760km the use of NLC yielded an increase in the Q-factor of 0.94dB.

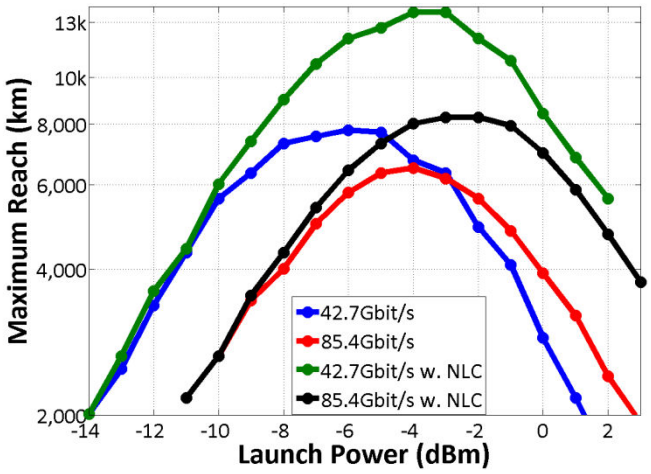

Figure 58: Measured maximum reach of PDM-QPSK transmission at 42.7Gbit/s and 85.4Gbit/s with linear and nonlinear compensation

For 85.4Gbit/s PDM-QPSK transmission the launch power had to be increased by ~3dB to achieve the same distances in the linear transmission regime as at 42.7Gbit/s. This is because the in-band noise power scales linearly with the symbol rate due to the associated spectral broadening. The optimum launch power at 85.4Gbit/s was found to be -4dBm, corresponding to a maximum reach of 6080km. The use of NLC increased the optimum launch power to -2dBm, corresponding to a maximum reach of 8080km (increase by 33%). For 85.4Gbit/s the relative increase in reach is smaller than for 42.7Gbit/s; this is due to the low-bandwidth photodiodes (11GHz at 6dB) used at the receiver at the time these experiments were carried out. At 85.4Gbit/s and high launch powers, self-phase modulation broadens the spectrum by introducing chirp, which produces new frequency components outside the receiver photodiodes bandwidth. For 112Gbit/s QPSK experiments, as described later in the section, the balanced photodiodes with the bandwidth of 30GHz were used to ensure that most of signal frequency components are detected. The performance was then limited by the 16GHz bandwidth of a real-time scope, which was used in all experiments.

An interesting observation when comparing the 42.7Gbit/s and 85.4Gbit/s maximum reach curves, obtained with dispersion compensation only, is that for launch powers higher than -2.5dBm, the 85.4Gbit/s PDM-QPSK signal can be transmitted further than a 42.7Gbit/s signal (Figure **58**). This may lead to a wrong conclusion that an 85.4Gbit/s PDM-QPSK signal is more tolerant towards intra-channel nonlinearity than a 42.7Gbit/s signal. The reason for this superior performance at 85.4Gbit/s at high launch powers is solely due to the fact that the whole transmission curve is shifted up by 3dB due to the

extra in-band noise, which increases the OSNR penalty, as discussed previously. In order to quantify the difference in nonlinear tolerance at various symbol rates, power spectral density (PSD) rather than absolute power should be used to take into account that the signal power is distributed over a certain bandwidth (the PSD measurement unit is W/Hz). Such characterisation was carried out in [133] with the conclusion that for a single-channel PDM-QSPK transmission the tolerance towards intra-channel nonlinearity decreases with an increase of the symbol rate.

The experimentally obtained constellations of a 42.7Gbit/s PDM-QPSK signal after transmission over 7760km (maximum reach when no NLC was used) are shown in Figure **59**.

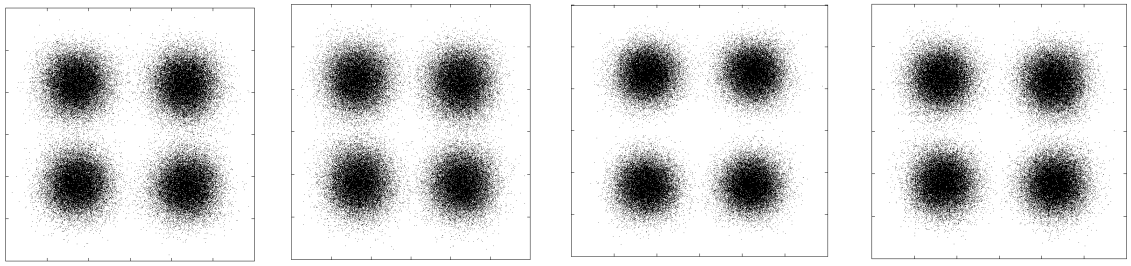

(a) (b) (c) (d)

Figure 59: Recovered constellations of a 42Gbit/s PDM-QPSK signal after 97 spans (7760km) and -6dBm launch power. (a) X-polarisation with no NLC; (b) Y-polarisation with no NLC; (c) X-polarisation with NLC; (d) Y-polarisation with NLC.

4.1.2. Transmission performance at 112Gbit/s

4.1.2.1.Experimental setup

The experimental set-up used for 112Gbit/s QPSK generation and transmission is similar to the one shown in **Figure 54**. Due to the fact that a different PPG (with the capability of operation at 28Gbaud), larger-bandwidth photodiodes (30GHz, as mentioned previously), and a different $LiNbO_3$ I-Q modulator were used in this experiment (compared to 42.7 and 85.4Gbit/s experiments), the 112Gbit/s transmission results were not included in **Figure 57** and **Figure 58**, and are plotted separately. The new modulator had the same $2V_\pi$ of $7V_{p\text{-}p}$, as the one used in the previous experiment, but the lower loss of 8.5dB and the higher launch power (of up to 20dBm) at its input. Therefore, a maximum achievable optical power of 17dBm was launched into the I-Q

modulator directly from the output of the EDFA. This higher launch power into the modulator also allowed to achieve a higher output power, which improved the noise characteristics of the following EDFA and the quality of the generated QPSK signal. An external cavity laser (ECL) with a measured linewidth of 100kHz was used in this and all subsequent experiments, instead of the previously used DFB laser. Such low linewidth is required for the blind carrier phase recovery of higher-order modulation formats, such as QAM16 [104].

4.1.2.2. Back-to-back measurements: results and discussion

Figure 60 shows the receiver sensitivity curve for 112Gbit/s PDM-QPSK signal, where the measured BER is plotted as a function of OSNR; the green curve shows the results obtained when 30GHz single-ended photodiodes were used, while the red curve was measured using balanced photodiodes with the same 30GHz bandwidth. The results highlight that both balanced and single-ended detection perform identically when 20dB difference between signal and LO powers is maintained. The implementation penalty, measured as a difference in theoretical SNR limit [66] and measured BER vs. OSNR curve, was determined to be 1.1dB at the BER = $3x10^{-3}$. This is an improvement in the performance compared with 85.4Gbaud PDM-QPSK signal, and occurs due to the combination of higher bandwidth receiver, lower loss I-Q modulator and a lower-noise PPG used for the 112Gbit/s experiments.

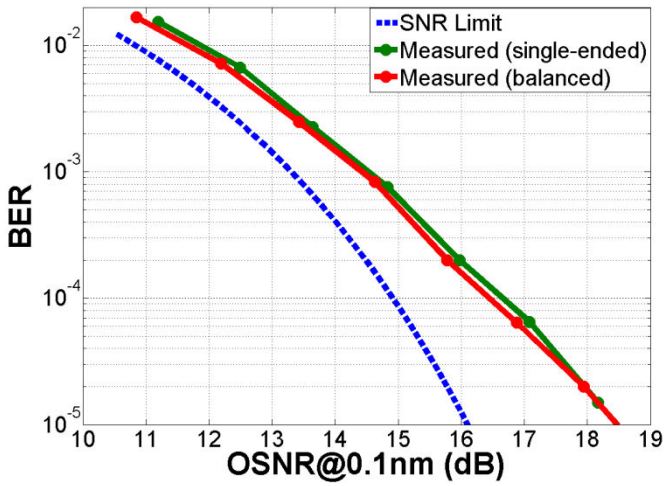

Figure 60: Receiver sensitivity for 112Gbit/s PDM-QPSK when single-ended and balanced photodiodes were used

4.1.2.3.Maximum reach measurements: results and discussion

In 112Gbit/s PDM-QPSK transmission, a maximum reach of 6560km (measured at the BER=$3x10^{-3}$) was achieved (**Figure 61**). This is an improvement compared to the maximum reach at 85.4Gbit/s, which occurs due to an improved implementation penalty at 112Gbit/s, as discussed previously. The use of NLC allowed an increase in the optimum launch power from -3.3dBm to 0dBm, resulting in an increase in maximum reach to 9600km (corresponding to 46%). These results show that 112Gbit/s PDM-QPSK can be used for long-haul, and potentially transatlantic (in the case of linear DSP) or trans-pacific (in the case when NLC was used) transmission.

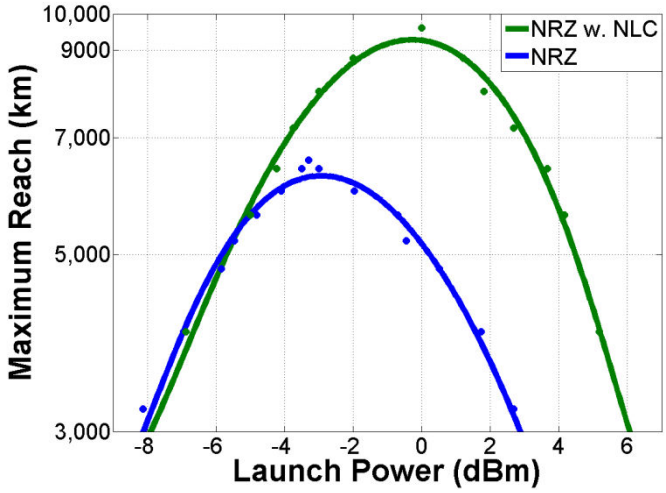

Figure 61: Measured maximum reach of PDM-QPSK transmission at 112Gbit/s with linear (blue line) and nonlinear (green line) compensation

The disadvantage of the NLC technique is that it is more computationally intensive than the conventional DSP for linear compensation only, which may present a problem for practical transponder design where speed and energy consumption are important. In addition, it is not clear whether NLC brings a significant benefit to systems operating in the WDM regime. This is further discussed in Chapter 5, which looks at the functionality of NLC in WDM transmission, comparing the achievable benefits. To maximise the benefit from NLC in WDM systems would require the receiver bandwidth to cover not only the channel of interest but also to extend over several adjacent channels (equivalent to few hundred GHz of bandwidth). This would allow to compensate not only for self-phase-modulation (SPM) but also for the cross-phase-modulation (XPM) – the limiting nonlinear transmission impairments in WDM systems.

The detailed analysis of the number of channels required to be detected to maximise the efficiency of NLC, and the usefulness of NLC in compensating inter-channel nonlinear effects was outside the scope of the research covered in this thesis. This, however, is currently an active topic of research amongst other research groups, e.g. [109].

4.1.3. Comparison of NRZ and RZ pulse shapes

The rationale behind using RZ instead of NRZ pulses at the transmitter is to increase the tolerance towards nonlinearity, which ultimately results in an increase in the maximum reach and the launch power margin for a fixed transmission distance. Such increased tolerance is due to the wider spectrum of an RZ signal, which reduces phase-matching between the adjacent frequency components during propagation through dispersive media [62]. This effect has been shown in [60], where for a fixed transmission distance of 1600km over a dispersion-managed link the use of WDM RZ-QPSK did not affect the maximum *Q*-factor, but improved the *Q*-factor margin. For a single-channel, the results in [61] demonstrated that RZ-QPSK with interleaved polarisations performed better than NRZ-QPSK with aligned polarisations for a fixed distance of 1200km over dispersion-managed link with low dispersion fibre. Despite the potential disadvantages associated with a wider spectrum of RZ signal, i.e. reduced spectral efficiency, increased linear WDM crosstalk and the need for higher-bandwidth ADCs at the receiver, its use is justified by a significant (as will be shown in a later section) increase in the maximum reach. In the experiments carried out in this research work, RZ pulses with 50% duty cycle (RZ50) were studied.

4.1.3.1.Experimental setup

The experimental setup for 112Gbit/s RZ50-QPSK transmission is similar to the one in **Figure 54**, with the exception of a pulse carver to generate an RZ50 data pulses from the incoming NRZ pulses (**Figure 62**). For pulse carving the Mach-Zehnder modulator (MZM) was driven from the same clock generator as the PPG; the MZM was driven by a full clock rate of 28GHz, whilst the PPG – at the half clock rate of 14GHz. The driving conditions were $5V_{p\text{-}p}$ (V_π of the modulator) with the bias point set in the middle

point (in terms of amplitude) of the modulator transfer function, as shown in **Figure 16** in section 2.2.3. An electrical delay line was used to align the carving window with the symbol duration. The polarisation multiplexing stage and the design of the recirculating loop were identical to the 112Gbit/s NRZ-QPSK experimental set-up.

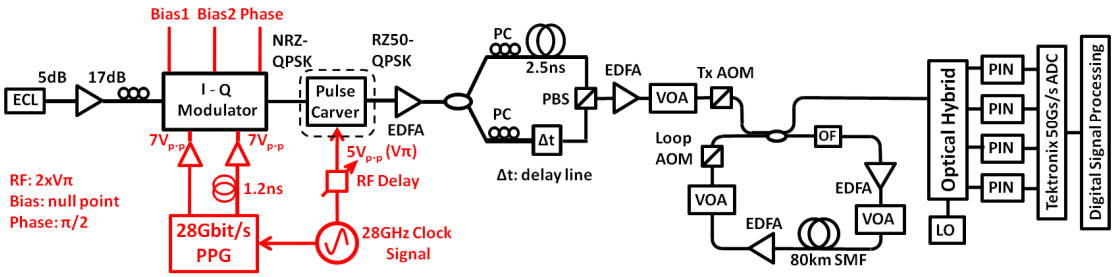

Figure 62: Experimental setup for 112Gbit/s PDM-RZ50-QPSK transmission

4.1.3.2. Back-to-back measurements: results and discussion

An optical spectrum broadening when using RZ50 pulse shape instead of NRZ was measured using an OSA and is shown in **Figure 63**. The eye diagrams of 28Gbaud NRZ-QPSK and RZ50-QPSK signals are also shown in **Figure 64(a)** and **Figure 64(b)**, respectively. Because the carving signal is aligned with the symbol duration, the transitions from one signal state to another are removed in the process of pulse shaping.

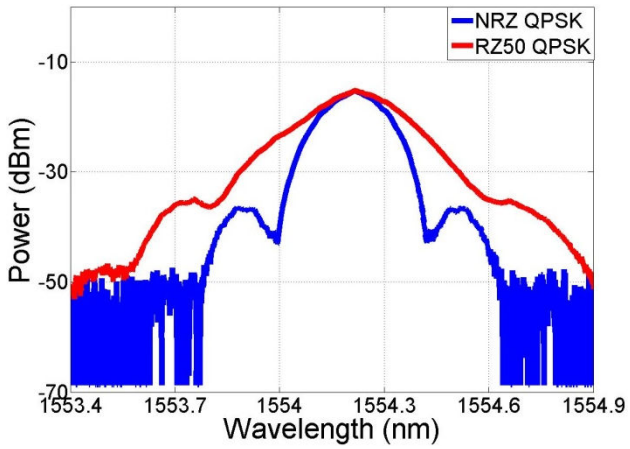

Figure 63: Optical spectra of 112Gbit/s PDM-QPSK NRZ and RZ50 signals

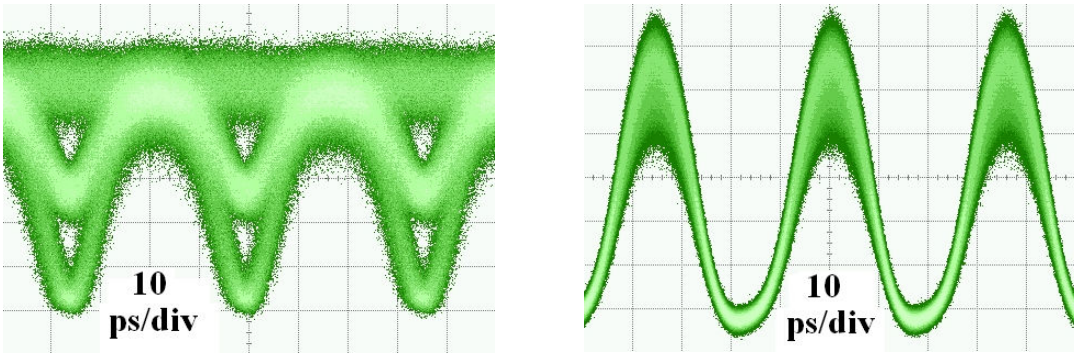

(a) (b)

Figure 64: Eye diagrams of 28Gbaud QPSK signal; (a) NRZ (b) RZ50

When comparing the receiver sensitivity of 112Gbit/s NRZ-QPSK versus RZ50-QPSK, the use of an RZ50 pulse shape increased the implementation penalty by additional 0.6dB to overall value of 1.7dB (**Figure 65**). This can be attributed to the limited bandwidth (16GHz) of the analogue-to-digital converters (ADCs), which for an RZ50 signal with wider spectrum yields larger cut-off in its frequency contents. At the time this experiment was carried out, these were the state-of-the-art commercially available ADCs and it was, therefore, not possible to increase the overall receiver bandwidth. However, similarly to NRZ, the 112Gbit/s RZ50-QPSK signal performed error-free without the noise loading (also measured over 2^{19} symbols).

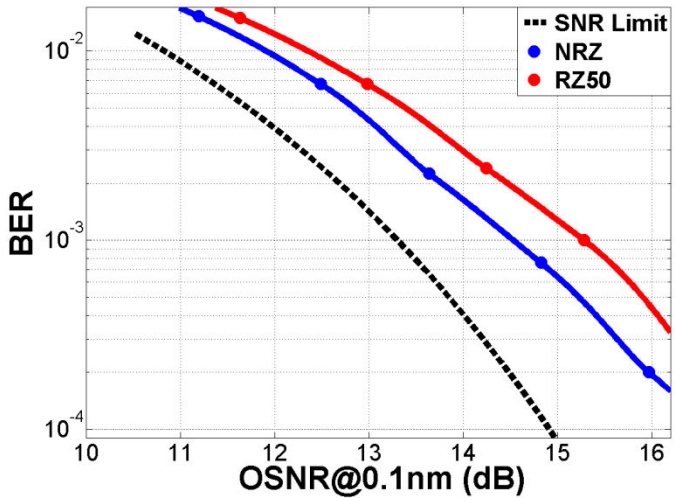

Figure 65: Measured and theoretical receiver sensitivity for a single-channel 112Gbit/s PDM-QPSK with NRZ and RZ50 pulse shapes

4.1.3.3.Maximum reach measurements

Next, the maximum reach was measured as a function of the launch power into the fibre (with a step between 0.5-1.5dB), and the results are shown in **Figure 66**. These results allow the comparison of NRZ- and RZ50-QPSK transmission at 112Gbit/s, both with and without NLC. It can be seen that at the low input launch powers of up to -5dBm the performance for all four configurations was practically identical, as expected (since NLC cannot undo the ASE noise accumulation); RZ50 performed slightly worse (~0.5dB) than NRZ due to the OSNR penalty shown in **Figure 65**. Because of the higher tolerance towards intra-channel nonlinearity, the use of RZ50 allowed an increase in optimum launch power from -3.3dBm to -2.3dBm. This also resulted in an increase in the maximum reach from 6560km to 7760km (18% improvement) and an increase in the launch power margin for high powers by ~1.5dB. The use of NLC for RZ50-QPSK transmission resulted in a further increase in the optimum launch power from -2.3dBm to -0.5dBm, and in the maximum reach from 7760km to 10160km (31% improvement). The launch power margin was increased by up to 3dB, depending on the transmission distance. It should be noted that the improvement when NLC was used for RZ50-QPSK was reduced compared to NRZ-QPSK (31% instead of 46%). This means that in the case when NLC was used, RZ50-QPSK yielded only a marginal increase in the maximum reach, and the two curves almost overlap, as shown in **Figure 66**. This is due to the fact that in the nonlinear transmission regime (launch powers >1dBm) the new frequency components are introduced in the RZ50 signal spectrum, which is already broader than NRZ signal as shown in **Figure 63**. This means that in the nonlinear transmission regime the limited analogue bandwidth of the ADCs at the receiver further filters the RZ50 signal frequency components.

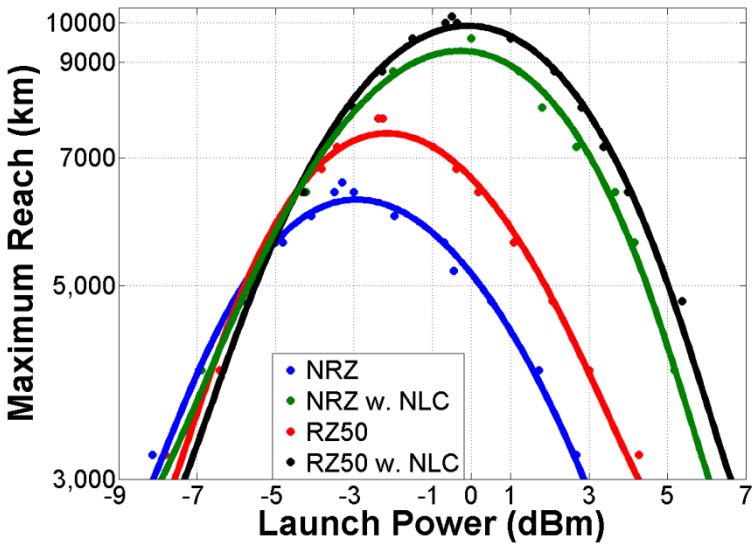

Figure 66: Measured maximum reach of single-channel NRZ- and RZ50-QPSK transmission at 112Gbit/s with linear (blue and red lines) and nonlinear (green and black lines) compensation

It can, therefore, be concluded that the use of RZ50 pulses instead of NRZ significantly improves the transmission performance. While RZ-QSPK with linear DSP underperforms NRZ-QPSK with NLC by 24% in terms of the maximum reach, the complexity of the digital receiver is also reduced in the case of RZ-QPSK with linear DSP. In the next sections of the thesis the performance of RZ50 pulses vs. NRZ is compared for QAM16 signals (section 4.2) and also for WDM configurations (Chapter 5).

4.2 QAM16

As described in section 4.1.2, the bit-rate of 100Gbit/s can be achieved using a PDM-QPSK signal operating at 28Gbaud (for the overall bit rate of 112Gbit/s including FEC). Indeed, such a configuration can yield ultra-long distances, potentially sufficient to cover trans-oceanic routes, as shown in Figure **66**. The QPSK signal has a lower required OSNR than higher-order modulation formats both for the equivalent symbol- and bit-rates. It also benefits from the single amplitude (constant modulus), which makes the DSP at the receiver easier and increases the tolerance to nonlinearity compared to multi-level modulation formats.

The benefit of generating 112Gbit/s signals using QAM16, however, is due to the lower symbol rate of 14Gbaud required (lower by a factor of two compared to QPSK). A lower symbol rate relaxes the requirements on the bandwidth of the electronics at the transmitter and the receiver, reducing the cost of the electrical and optoelectronic components used. QAM16 can also increase the spectral efficiency in WDM transmission, as the spacing between the WDM channels can be reduced.

Another advantage of QAM16 over QPSK signals is that at higher bit-rates (e.g. 224Gbit/s), it becomes impractical to use a QPSK signal since this would require a symbol rate of 56Gbaud for which electronics at the transmitter and receiver is not easily available. Therefore, a 28Gbaud PDM-QAM16 could be a more effective solution to obtain a 224Gbit/s overall bit-rate. To date, 28Gbaud PDM-QAM16 transmission has been carried out by only 4 research groups, including the present research work at University College London. Table 3 compares several possible configurations for 224Gbit/s QAM16 transmission: advanced fibre vs. SMF, EDFAs vs. hybrid amplification, RZ50 vs. NRZ, and linear impairments compensation vs. NLC. The importance of the 224Gbit/s QAM16 transmission results, carried out as part of this research work, is that the feasibility of long-haul transmission was demonstrated for standard SMF links with EDFAs only. In particular, a transmission distance of 2000km can be achieved by only upgrading the transmitter (from NRZ to RZ pulses) and the receiver (to include NLC); this is in contrast with another demonstration of 2000km transmission using an advanced fibre type and Raman amplification [85].

Group	Link	No. of Channels	Pulse Shape	NLC	Maximum Reach
Bell Labs *(JLT2011)*	100km ULAF / Raman	1 / 10	NRZ	No	2000km / 1200km
HHI *(ECOC2010)*	80km SMF / EDFAs	8	NRZ	No	480km
TUE-COBRA / NSN *(ECOC2010)*	100km LLF+PSCF / Hybrid Amp	11	RZ50	No	1500km
UCL *(OFC2011)*	**80km SMF / EDFAs**	**1 / 3**	**RZ50**	**Yes**	**2000km / 1520km**

Table 3. Comparison of previous work on 200Gbit/s QAM16 transmission and the results of the present research work

QAM16 is also a promising candidate to generate 400Gbit/s – the likely bit-rate of the 2nd generation future optical transport systems. Indeed, the feasibility to generate and transmit a 448Gbit/s (56Gbaud and PDM) QAM16 signal over 1200km was studied in [5]. Although custom built components were used for QAM16 generation and detection, with the further developments in the transmitter and receiver technology, it is likely that a 400Gbit/s solution based on QAM16 modulation format will be a viable one.

The aim of this set of experiments was to design a technique for the generation of QAM16 modulation format and investigate its transmission performance at 100 and 200Gbit/s. Similarly to the QPSK transmission, this research work shows the first comprehensive experimental study of QAM16 transmission at 112 and 224Gbit/s in terms of the maximum reach [10] [11]. The results also show the first direct comparison of NRZ and RZ pulse shapes at both 112 and 224Gbit/s, and the first demonstration of NLC at such bit-rates. Finally, this research work shows the longest 224Gbit/s QAM16 transmission distance for SMF links with EDFAs only.

Similar to the QPSK experiments carried out in the last section, the main quantities measured in the QAM16 single-channel experiments are back-to-back performance (BER vs. OSNR) and the dependence of maximum reach on the launch power into the fibre of the NRZ- and RZ50-QPSK signals, measured at 112Gbit/s and 224Gbit/s.

4.2.1 Optical synthesis of a QAM16 signal

It was shown in Section 2.2.5 that it is highly desirable to use binary rather than multilevel electrical signals to drive the I-Q modulators. With this is mind, a new approach was proposed for a QAM16 transmitter, which can be assembled from inexpensive, off-the-shelf fibre-coupled components, and represents a valuable research tool for the investigation of high-speed transmission performance.

The QAM16 generation mechanism is based on the modified version of the phase-stabilised OTDM multiplexer, as described in section 3.2. First, a QPSK signal was generated as described in section 2.2.4, using an I-Q modulator driven with two binary signals. The QPSK signal was then launched into a phase-stabilised fibre interferometer, similar to the one used in the bit-wise OTDM transmission experiment. Similarly, phase stabilisation was achieved by counter-propagating part of the CW light of the source laser in the interferometer, detecting the interference product between the two arms with a low-bandwidth (2GHz) photodiode and processing an electrical interference product with a feedback circuit to provide a control signal for the phase shifter (**Figure 67**). The feedback circuit used in the experiment was a commercially available ditherless bias controller from YYLabs, and had the option to set the desired operating point (hence, the phase) and to track the phase variations in the interferometer, as described in section 3.2.

Within the fibre interferometer, signals in the two arms were decorrelated by 1214ps (corresponding to 17 and 34 symbols for 14Gbaud and 28Gbaud QAM16 signals, respectively), time aligned and attenuated by 6dB with respect to each other. Note, that this is different to the OTDM multiplexer in section 3.2, where two signals with equal amplitudes were interleaved by ½ the bit period. In the QAM16 generation process a large-amplitude QPSK signal determines the quadrant to which the QAM16 symbol is mapped, while the small-amplitude QPSK signal determines the phase within each quadrant (**Figure 68**). The large amplitude constellation points, shown in red, disappear during the interference. This QAM16 generation technique allowed for simple design, suppressed electrical noise transfer into the optical domain and the ability to use the RF components suited for binary signals.

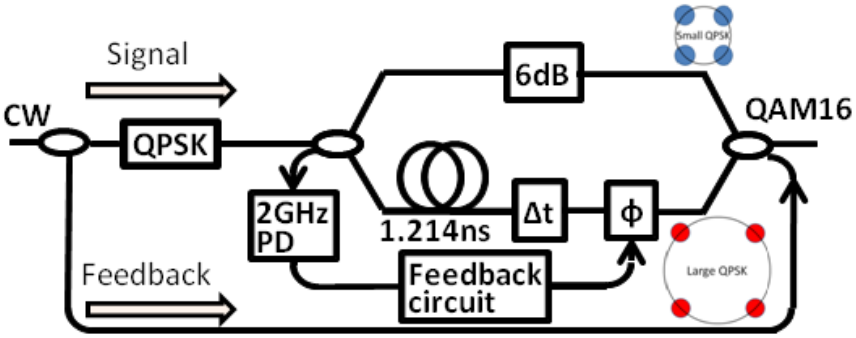

Figure 67: Experimental set-up for optical generation of QAM16

It is important to note that the phase difference between the two arms of the interferometer must be set to 0° or 90° due to the symmetry of the original QPSK signal to obtain a perfect QAM16 signal with three intensity levels (**Figure 68(a)**). Intermediate phase values will distort the QAM16 constellation, e.g. 45° will result in a signal with only 2 intensity levels (**Figure 68(b)**).

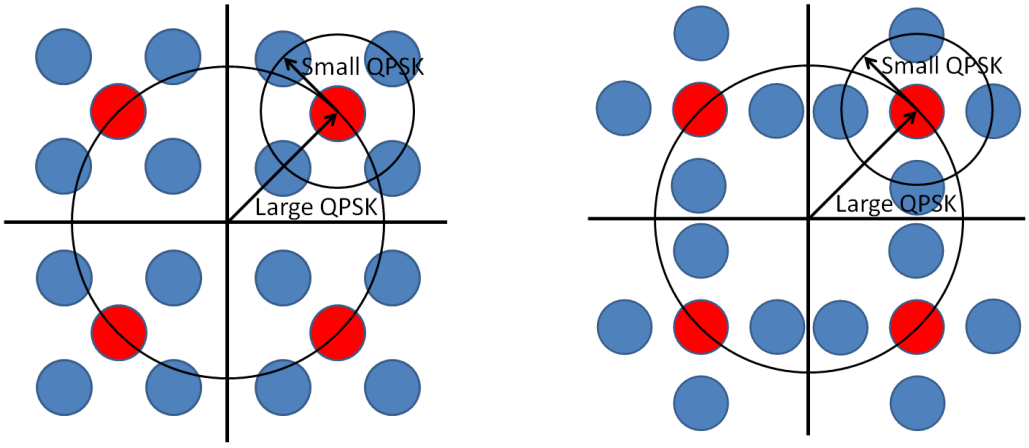

(a) (b)

Figure 68: The generation principle of QAM16 signal. Red constellation points disappear during the generation process and are simply shown to help understand the generation process (a) Perfect phase alignment in the interferometer (0° or 90°); (b) Phase misalignment (45°)

While the QPSK bits at the transmitter are inherently Gray coded, as discussed previously in Section 2.3.4, the QAM16 bit mapping is not necessarily Gray coded. This means that one symbol error can result in more than one bit error, which is undesirable. For the QAM16 generation used in this research work (Figure **67** and Figure **68**), an

initial bit mapping [A, B, C, D] is shown in Figure **69(a)**. To obtain a Gray mapping [I_0, Q_0, I_1, Q_1] on the QAM16 bits the following procedure must be performed [8] (Figure **69(b)**):

$$\boldsymbol{I_0 = A} \quad \textbf{(25)}$$

$$\boldsymbol{Q_0 = B} \quad \textbf{(26)}$$

$$\mathbf{I_1} = \boldsymbol{A}\ \textbf{XOR}\ \boldsymbol{C} \quad \textbf{(27)}$$

$$\mathbf{Q_1} = \boldsymbol{B}\ \textbf{XOR}\ \boldsymbol{D} \quad \textbf{(28)}$$

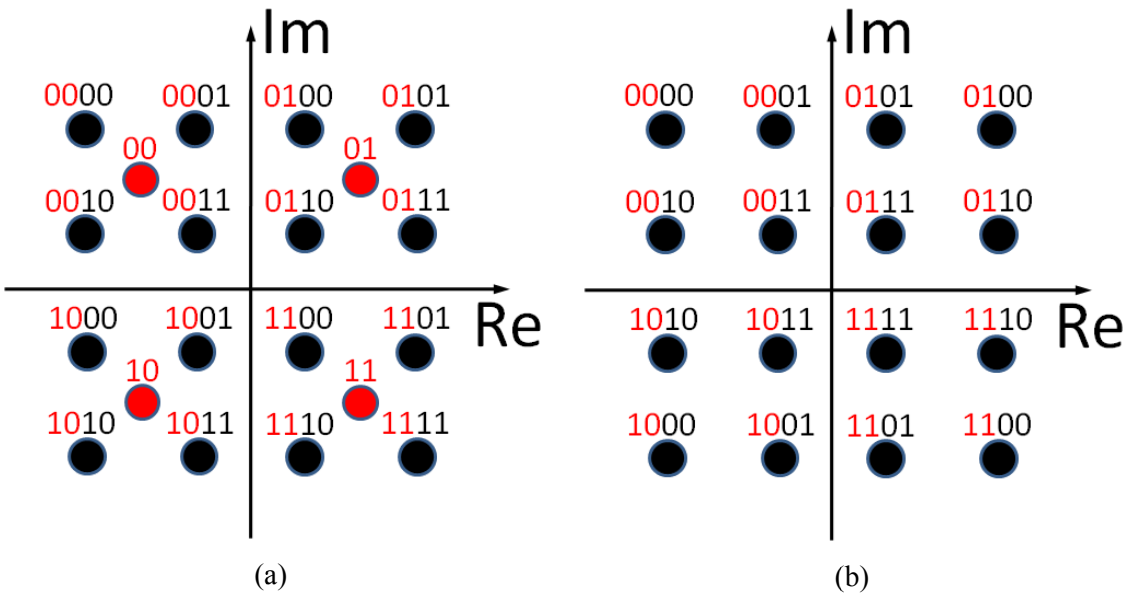

Figure 69: (a) Initial QAM16 bit mapping at the transmitter (b) QAM16 bit mapping after Gray coding

It must be noted that the proposed setup emulates a realistic optical QAM16 transmitter, which would consist of two I-Q modulators, separately driven in each MZI arm. To date, a real QAM16 transmitter using an optical interferometric arrangement has been realised in a PLC-based MZI configuration with two I-Q modulators – one in each waveguide path [70].

4.2.2. Transmission performance at 112Gbit/s and 224Gbit/s

4.2.2.1.Experimental setup

To generate a 14/28Gbaud QAM16 signal, a 14/28Gbaud QPSK signal was first generated using the technique, previously described in section 2.2.4. In the case of 14Gbit/s, the PPG had a capability of using two PRBS binary patterns, decorrelated by ½ pattern length with respect to each other. The half pattern decorrelation was not available at 28Gbit/s due to an additional 2:1 electrical multiplexer used to generate binary PRBS at higher than 14Gbit/s, therefore, the bits used for I and Q modulation were decorrelated with respect to each other using different length RF cables (by ~500ps) (Figure **70**). A QAM16 signal was then optically synthesised from the two QPSK signals with different amplitude levels, as described in Section 5.2.1. Within the polarisation multiplexing stage, the two polarisations were decorrelated by 32 symbols and 64 symbols for 14Gbaud and 28Gbaud QAM16 signals, respectively. The recirculating loop and the coherent receiver were identical to the previous experiment.

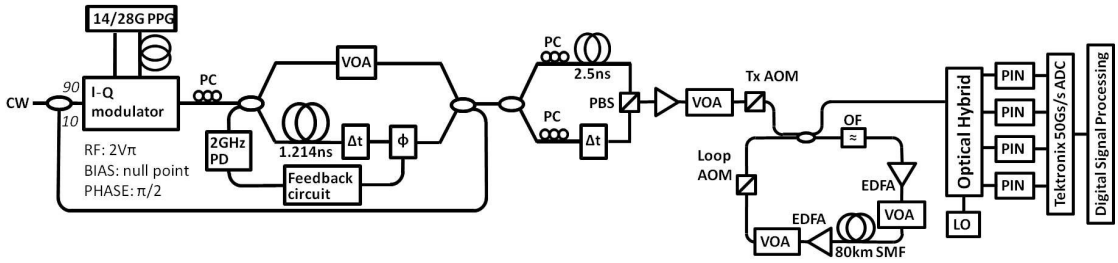

Figure 70: Experimental setup for 112 and 224Gbit/s PDM-QAM16 transmission

4.2.2.2.Back-to-back measurements: results and discussion

The eye diagrams of the generated QAM16 signal at 14 and 28Gbaud were measured using a digital communication analyser (DCA), and are shown in Figure **71**. No major degradation can be observed from the eye diagrams with the increase in the symbol rate, which means that the 28Gbaud signal is not subject to bandwidth limitation at the transmitter.

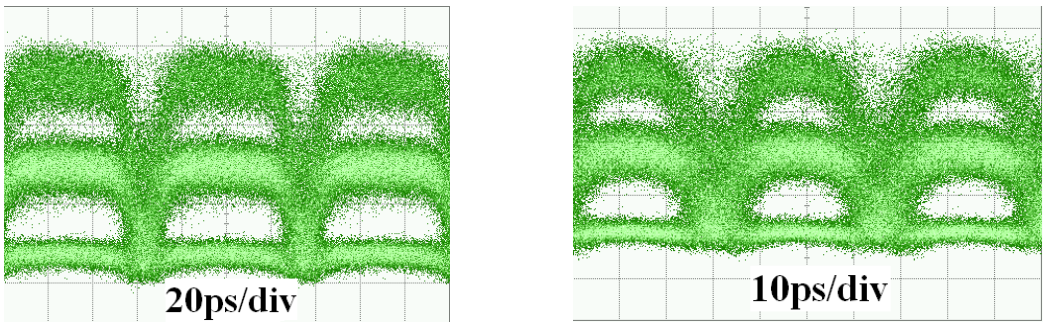

(a) (b)

Figure 71: Measured eye diagrams of (a) 14Gbaud and (b) 28Gbaud QAM16 signal

In the back-to-back measurements, 1.7dB of implementation penalty was measured for 112Gbit/s PDM-QAM16 signal (Figure **72**). This penalty increased to 3.3dB for 224Gbit/s PDM-QAM16 signal. Both penalty values were measured at BER = $3x10^{-3}$. As before, an increase in symbol rate by a factor of two resulted in an additional 3dB OSNR penalty due to the doubling of the bandwidth.

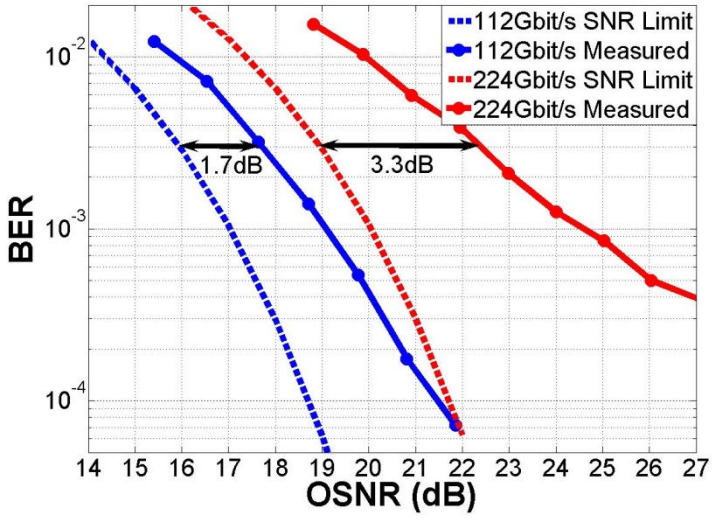

Figure 72: Measured and theoretical receiver sensitivity for 112Gbit/s (blue) and 224Gbit/s (red) PDM-QAM16 signals

Figure **73** shows an equalised back-to-back QAM16 constellation before (Figure **73(a,c)**) and after carrier frequency/phase estimation (Figure **73(b,d)**). In the case of 112Gbit/s the signal was found to be error free over 2^{19} symbols. At 224Gbit/s the error floor was found to be at $8x10^{-5}$.

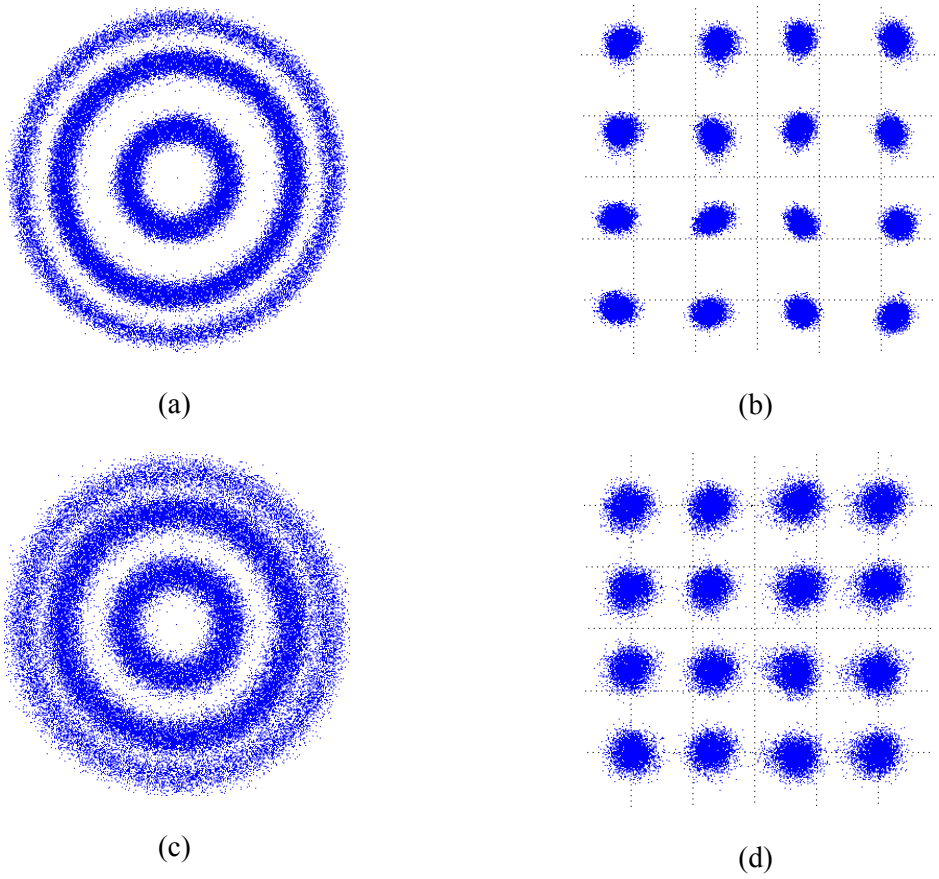

Figure 73: Received QAM16 signal in a complex plane at (a,b) 14Gbaud and (c,d) 28Gbaud. Figures (a) and (c) show the QAM16 signal after digital equalisation, while Fig. (b) and (d) show the recovered QAM16 constellation

4.2.2.3.Maximum reach measurements: results and discussion

To characterise the transmission performance of QAM16 signals, the maximum reach curves were measured as a function of launch power into the fibre (at BER = $3x10^{-3}$) and are shown in Figure **74**. In the case of 112Gbit/s the optimum launch power was found to be -3dBm, corresponding to the maximum reach of 2400km. When using NLC the optimum launch power increased to -0.5dBm, with a subsequent increase in reach to 3920km. This 63% increase in the maximum reach is comparable to a 72% increase in the case of 112Gbit/s QPSK transmission. At 224Gbit/s QAM16 transmission the optimum launch power was found to be -1dBm, corresponding to a maximum reach of 1280km. When using NLC the optimum launch power and maximum reach were increased to 0dBm and 1600km, respectively. The smaller relative increase (25%) in the maximum reach at 28Gbaud for QAM16 signals is due to the same reason as for QPSK: the rejection of spectral components due to the limited bandwidth of the ADCs at the receiver. The difference between the linear part of the

reach curves at 14 and 28Gbaud is 4.8dB (at 800km). This can be explained by the 3dB theoretical OSNR penalty at 28Gbaud and an additional difference in the implementation penalty, as shown in Figure **72**. The fact that at 800km and high launch powers to the fibre 224Gbit/s QAM16 slightly outperforms 112Gbit/s QAM16 (as shown in Figure **74(a)**), does not mean that 224Gbit/s is more tolerant towards nonlinearity. Similarly to the QPSK transmission results at different symbol rates, this is due to the fact that the absolute launch power plotted on the X-axis does not take into account the 3dB OSNR penalty at 224Gbit/s due the twice wider spectrum. The quantification of the tolerance towards nonlinearity using a power spectral density instead of an absolute launch power, was reported in [133]. Comparing the 112Gbit/s QPSK and QAM16 transmission (Figure **74(a)** and Figure **74(b)**) it is evident that the advantages of QAM16 modulation (increased spectral efficiency, lower bandwidth electronics) comes at the expense of reduced maximum reach. QPSK outperforms QAM16 by a factor of 2.7 when linear DSP was used and a factor of 2.45 when NLC was used. The comparison of QPSK and QAM16 transmission at 224Gbit/s was not performed, since the generation of 224Gbit/s PDM-QPSK signals would require the symbol rate of 56Gbit/s, currently unavailable in UCL research laboratory.

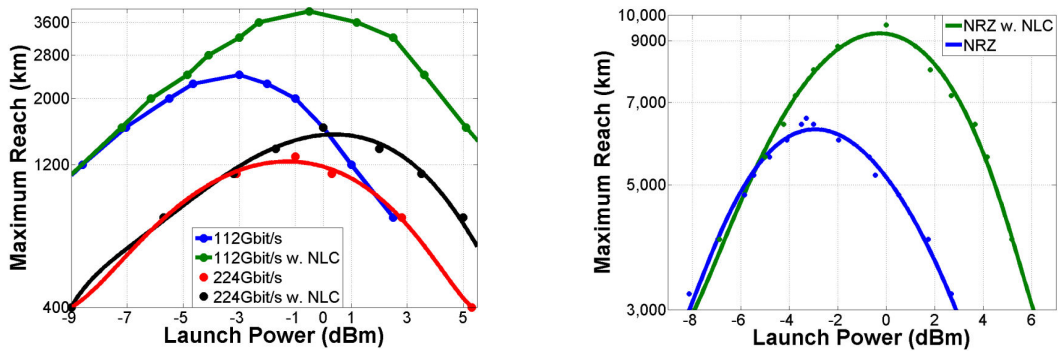

(a) (b)

Figure 74: Comparison of maximum reach of (a) PDM-QAM16 transmission at 112/224Gbit/s and (b) PDM-QPSK at 112Gbit/s with linear and nonlinear compensation.

4.2.3 Comparison of NRZ and RZ50 pulse shapes in transmission

4.2.3.1. Experimental set-up

To generate an RZ50-QAM16 signal the original QAM16 generation setup was modified to include a pulse carver, driven by 14GHz or 28GHz to generate a 14Gbaud or 28Gbaud RZ50-QAM16 signal, respectively (Figure **75**). The rest of the set-up, including the components used in the recirculating loop (optical filter, EDFAs etc.), is the same as in Figure **70**, described in section 4.2.2.1.

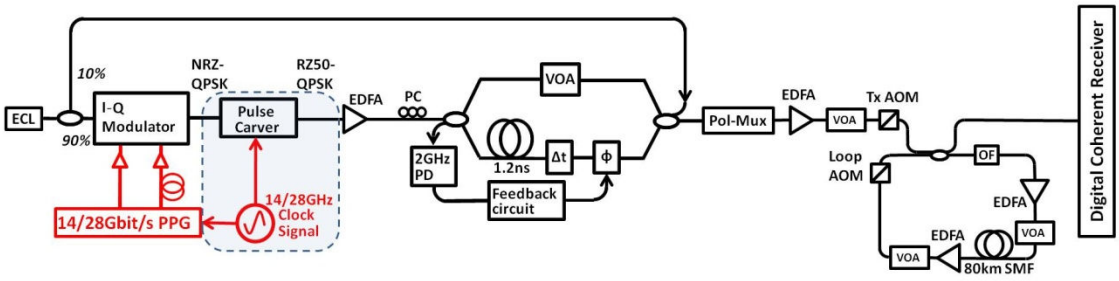

Figure 75: Experimental set-up for NRZ- and RZ50-QAM16 transmission at 112 and 224Gbit/s

4.2.3.2. Back-to-back measurements: results and discussion

The eye diagrams of the generated 14 and 28Gbaud QAM16 signals are shown in Figure **76**. Similar to the previously shown NRZ eye diagrams, there is apparently no difference between the RZ50 eye diagrams at two different symbol rates. However, the received back-to-back RZ50-QAM16 constellations exhibited different performance at 112 and 224Gbit/s due to the pronounced effect of limited bandwidth of the ADCs on the 224Gbit/s (28Gbaud) signals (Figure **77**). The back-to-back RZ50-QAM16 signal was determined to be error free at 112Gbit/s, and had an error floor of $1x10^{-5}$ at 224Gbit/s (both measured over 2^{19} symbols, as in the previous experiments).

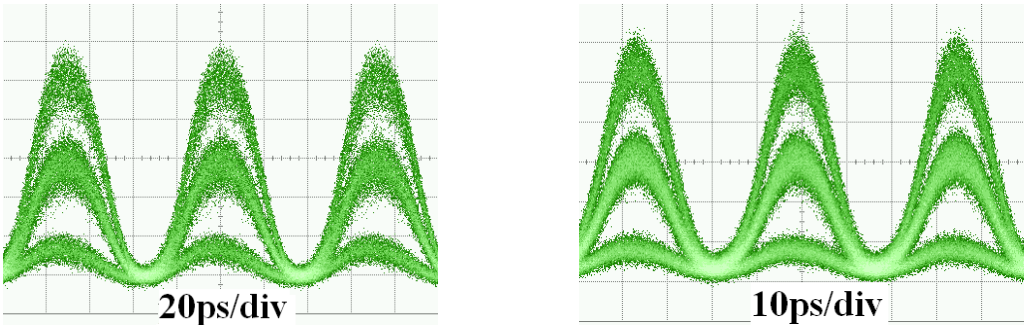

(a) (b)

Figure 76: Eye diagrams of (a) 14Gbaud and (b) 28Gbaud RZ50-QAM16 signal

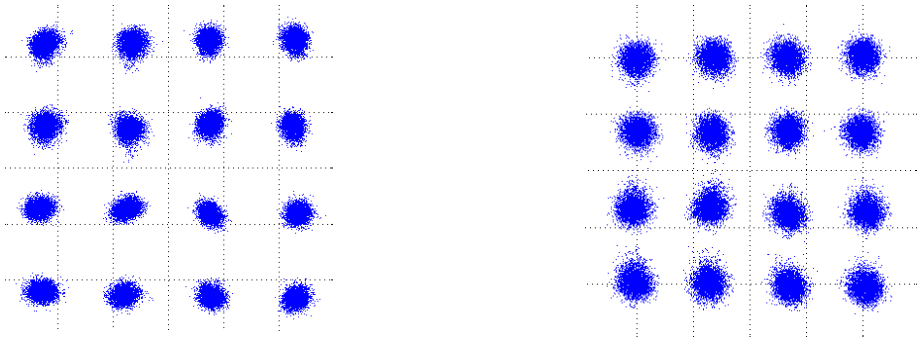

(a) (b)

Figure 77: RZ50-QAM16 constellation diagrams at (a) 112Gbit/s and (b) 224Gbit/s

To further compare the back-to-back performances of NRZ- and RZ50-QAM16 at 112 and 224Gbit/s, the receiver sensitivity was measured at each bit-rate (Figure **78**). Overall, NRZ and RZ50 show a similar performance in the receiver sensitivity at both bit-rates, however, RZ50 has a slightly better implementation penalty of 1.5dB at 112Gbit/s (measured at the BER=3x10-3). This is the lowest implementation penalty for 112Gbit/s QAM16 signal reported to date. In addition, at 224Gbit/s RZ50 starts to outperform NRZ for the BERs<$1x10^{-3}$. The back-to-back measurements were also carried out for the configuration with the interleaver at the transmitter – the use of an interleaver did not affect the shape of the BER vs. OSNR curves for all cases apart from RZ50 at 224Gbit/s, which is indicated in Figure **78(b)**.

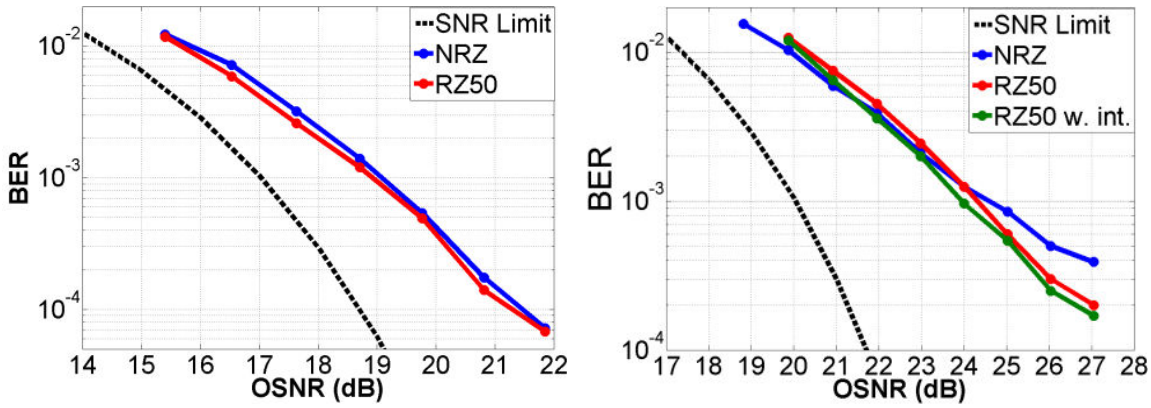

(a) (b)

Figure 78: Comparison of the back-to-back performances for NRZ- and RZ50-QAM16 signals at (a) 112Gbit/s; (b) 224Gbit/s

4.2.3.3.Maximum reach measurements: results and discussion

The similarity of the back-to-back performance of NRZ and RZ50 pulse shapes is also translated in the linear transmission regime where comparable distances are achieved for both pulse shapes, and the four curves overlap (Figure **79**). At 112Gbit/s the optimum launch power was found to be -3dBm for NRZ-QAM16, increased to -2dBm for RZ50-QAM16, and up to 0dBm when digital nonlinearity compensation (NLC) was used. Similarly to QPSK, such increased optimum launch power is due to an increased tolerance towards nonlinearity when RZ50 pulses were used and the fact that NLC can mitigate for nonlinearity, so the highest optimum launch power of 0dBm was obtained when both RZ50 and NLC were used. Overall, the use of RZ pulses instead of NRZ led to an increase in the maximum reach from 2400km to 2800km (17% increase). The use of NLC for NRZ pulses, however, allowed for an increase in the maximum reach from 2400km to 3920km (63% increase), compared with the configuration when no NLC was used. This means that for a single-channel transmission and when the symbol rate is such that there is no bandwidth limitation at the receiver, the use of NLC yields a higher benefit that the use of RZ50 pulses in terms of an improvement in the maximum reach. When applying both RZ50 pulses and NLC the maximum reach was increased to 4240km, i.e. by 77% compared when NRZ without NLC.

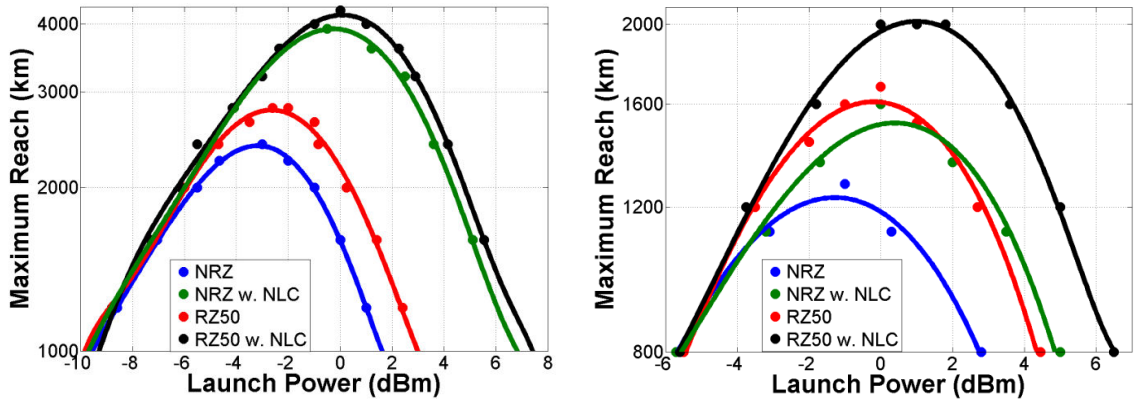

(a) (b)

Figure 79: Maximum reach of PDM-QAM16 transmission with NRZ and RZ50 pulse shapes, and linear and nonlinear compensation at (a) 112Gbit/s (b) 224Gbit/s

It can also be seen that at 224Gbit/s RZ50-QAM16 outperformed NRZ-QAM16 with NLC by 80km in terms of the maximum achievable transmission distance. This is because the use of NLC is less efficient at higher symbol rates due to an associated bandwidth limitation at the receiver ADCs, and therefore an upgrade from NRZ to RZ50 (1280km to 1680km; 31%) is more desirable compared to an upgrade from NRZ to NRZ with NLC (1280km to 1600km; 25%) from the performance and design simplicity point of view. When both RZ50 and NLC were used, the maximum reach was increased to 2000km, i.e. 56% improvement compared to NRZ without NLC. This result represents the longest transmission distance for SMF links with EDFAs only.

The results of this part of the research work represent the lowest implementation penalty (1.5dB) of the 112Gbit/s QAM16 generated signal and the longest 112Gbit/s QAM16 transmission (4240km) reported to date. At 224Gbit/s the achieved transmission distance of 2000km is currently the longest distance reported for SMF link with EDFAs only. The 224Gbit/s QAM16 transmission was also simulated in Matlab, and the results shown in section 5.2 represent an excellent agreement between experiments and simulations for both NRZ and RZ50 pulses.

4.2.4 Generation of QAM16 signals up to 42Gbaud

While 224Gbit/s (28Gbaud) QAM16 transmission has been demonstrated by research groups (including UCL) over the last 15 months, the generation and transmission of QAM16 signals with higher symbol rates still represents a challenge. The generation of a 400Gbit/s data rates per single carrier would be highly desirable for future optical networks; however, this would require 50Gbaud (+ FEC overhead) QAM16 symbol rates.

In this research work the lower QAM16 symbol rates of 34 to 42Gbaud were investigated as an interim step towards 50Gbaud symbol rates. For each symbol rate the back-to-back Q-factor was measured. Figure **80(a)** shows the single-polarisation QAM16 eye diagram at 35Gbaud, where 3 amplitude levels of the QAM16 signal are clearly visible. The corresponding constellation is shown in Figure **80(b)**, for which the calculated Q-factor was found to be 10.25dB (BER = 5.7×10^{-4}). When the symbol rate was increased to 42Gbaud the bandwidth limitation at the transmitter became apparent, and severely distorted the optical eye (Figure **81(a)**). The additional bandwidth limitation at the receiver (predominantly from the ADCs at the receiver) even further distorted the signal; the back-to-back Q-factor was measured to be only 6.25dB (BER = 1.58×10^{-2}) (Figure **81(a)**).

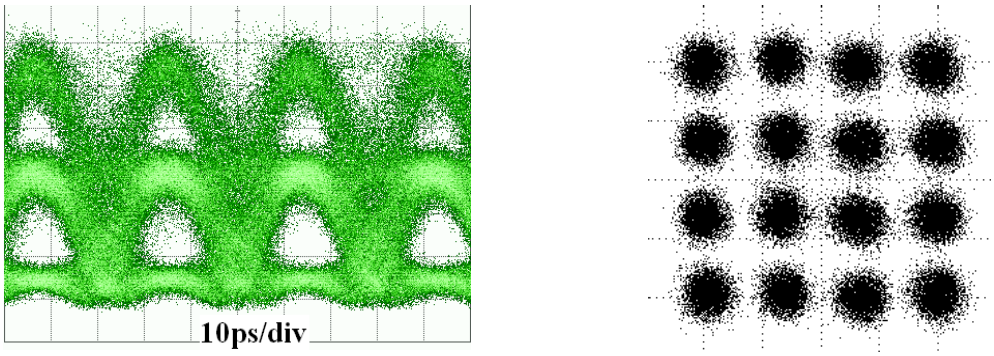

(a) (b)

Figure 80: (a) Measured eye diagram and (b) constellation diagram of a 35Gbaud single-polarisation QAM16 signal

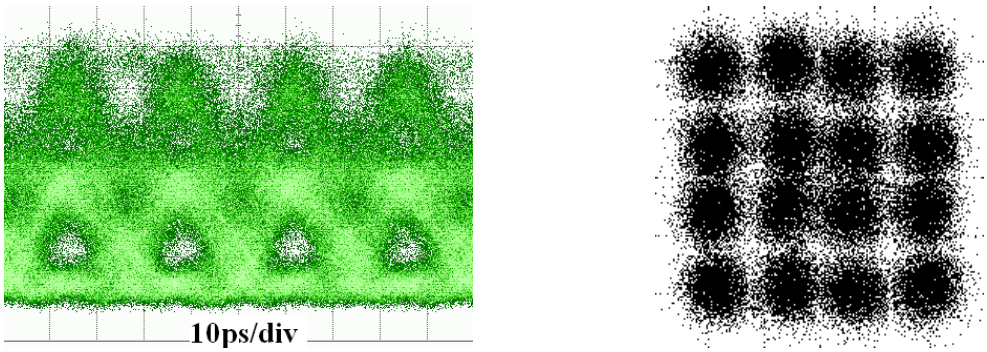

(a) (b)

Figure 81: (a) Measured eye diagram and (b) constellation diagram of a 42Gbaud single-polarisation QAM16 signal

Overall, it was found that the BER of 3.8×10^{-3} (the maximum allowable BER assuming conventional 7% FEC) was reached at approximately 39Gbaud (Figure **82**). To illustrate transmission at symbol rates higher than 28Gbaud, in a preliminary experiment, a 35Gbaud single-polarisation QAM16 signal was successfully sent over 320km, with a measured BER of 3.4×10^{-3}, although the detailed investigation of this was beyond the scope of this thesis due to time constraints. At the time this experiment was carried out this was the highest QAM16 symbol rate reported; however, by late 2010 the work by Bell Labs demonstrated 56Gbaud PDM-QAM16 generation and transmission using custom-built components and two synchronised 2-channel 80-GSamples/s ADCs with analogue bandwidth of 32.5GHz [5].

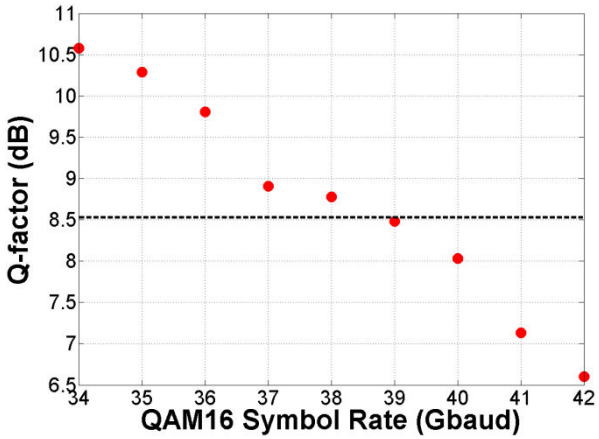

Figure 82: Measured back-to-back dependence of the Q-factor on QAM16 symbol rate

4.3 Summary

The performance of QPSK and QAM16 signals in single-channel transmission was described in this chapter. While QPSK modulation is most suitable for the optical transport networks with the bit rates of 40 and 100Gbit/s, the bit rates of 200Gbit/s and higher would most likely require the modulation formats with higher spectral efficiency, such as QAM16. The advantage of QAM16 over QPSK is the lower symbol rate (by a factor of two) required to achieve an equivalent bit-rate, which results in the higher spectral efficiency, and yields the potential of generating the bit-rate of 200Gbit/s and higher using the electronics with a modest bandwidth. The overall conclusion is that QPSK format is more suitable for transoceanic transmission, where distances exceeding 6000km are required, while QAM16 - for shorter (~1000-2000km) terrestrial links but at a higher bit-rate. The investigation of higher-order QAM signals was outside the scope of this research work.

At both 40 and 100Gbit/s the results of this research work show the feasibility of achieving transatlantic distances of >6000km (all measurements taken assuming BER = $3x10^{-3}$). At 42.7Gbit/s (40Gbit/s + FEC overhead) the maximum transmission distance of 7760km (transatlantic) was achieved and was further increased to 13600km (transpacific) when digital nonlinearity compensation (NLC) is used (i.e. 75% increase in reach). It is this long transmission distance that makes a 40Gbit/s QPSK coherent solution very attractive for submarine and long-haul applications.

At 112Gbit/s (100Gbit/s + FEC overhead) various transmission configurations employing a 28Gbaud polarisation-division-multiplexed (PDM) QPSK signals were tested in this research work. In the simplest one, employing NRZ pulses and no NLC, a maximum transmission distance of 6560km was achieved. In a more advanced scenario (RZ pulses with NLC) the transmission distance was increased to 10160km (i.e. 55% increase in reach), exceeding the transpacific distance. The main conclusion is that an upgrade at the receiver (from NRZ to NRZ with NLC) is the preferred solution to an upgrade at the transmitter (from NRZ to RZ50); the former solution yields the transmission distance of 9600km while the latter – 7760km (i.e. 24% difference). It must be noted that this improvement comes at the expense of digital coherent receiver complexity, since digital NLC is more computationally intensive, hence, less energy

efficient compared to the standard DSP algorithms. In the course of this research work it was determined that the use of NLC can increase the computational time by as much as 200%, compared to the case with linear DSP.

An alternative way to obtain a 112Gbit/s signal is by using a PDM-QAM16 modulation format at a lower symbol rate of 14Gbaud, which means that only half the bandwidth of a 28Gbaud QPSK signal is required to obtain the same overall bit rate. However, this increase in spectral efficiency comes at the expense of reduced transmission distance. The maximum reach of QAM16 signals at 112Gbit/s was found to be 4240km, which is lower than 10160km obtained for 112Gbit/s QPSK transmission. Although the difference in reach is substantial, this is still the longest transmission distance of 112Gbit/s QAM16 reported to date. In its simplest form (i.e. NRZ and no NLC) the maximum transmission distance was reduced down to 2400km. Similar to the QPSK transmission experiments, an upgrade at the receiver is a preferred solution to an upgrade at the transmitter in terms of the maximum achievable reach; the former allowed to achieve 3920km, while the latter only 2800km. This corresponds to a 40% difference in the obtained values for maximum reach.

At 224Gbit/s (28Gbaud) the maximum reach of QAM16 was found to be 2000km and was obtained when using RZ50 pulses and NLC, as previously. Out of the four configurations investigated, the worst performance was when using NRZ pulses and no NLC, as expected. Perhaps an interesting conclusion is that the configuration employing RZ pulses without NLC slightly outperforms the one with NRZ pulses and NLC in terms of the maximum reach (1680km vs. 1600km). The effectiveness of NLC also decreases in WDM experiments, as will be shown in the following chapter; hence, the use of RZ50 pulses becomes a preferred solution to the use of NLC.

Investigation of QAM16 signals at higher data rates (34-42Gbaud) was also carried out, and the maximum detected symbol rate was determined to be 39Gbaud (achieved BER 3.8×10^{-3}). To illustrate transmission at symbol rates higher than 28Gbaud, in a preliminary experiment, a 35Gbaud QAM16 signal was successfully sent over 320km. Further investigation of high-rate QAM16 signals would require higher bandwidth of components at the transmitter and the receiver, or the use of optical signal processing, such as OTDM.

5. WDM Transmission of QPSK and QAM16 Signals

While single-channel transmission experiments described in chapter 4 were used to establish an upper-bound on the transmission performance, all practical optical fibre transport systems are based on wavelength division multiplexing (WDM) (see chapters 1, 2). WDM allows the optical infrastructure to be shared amongst many channels, thus reducing the cost per transmitted information bit in a fully loaded system [134]. WDM also allows unprecedented capacities by using tens of channels, typically packed close to each other for ultimate spectral efficiencies (11bit/s/Hz is the highest reported to date [16]). In these operating regimes linear coherent cross-talk, manifesting itself in signal distortions during the detection process, and inter-channel XPM nonlinearity become important sources of impairments. Because of these additional impairments, it is clear that single-channel transmission alone can underestimate the performance of WDM systems with several tens of wavelength channels [3].

In transmission laboratories it is not always possible to generate and transmit such large number of channels due to the associated setup complexity and cost. The general consensus in the literature is, however, that a much lower number of channels is sufficient to reliably investigate the transmission performance of the central channel under test. This is due to the fact that most of the XPM and FWM on the central channel under test comes from the immediate WDM neighbours. While the exact required minimum number of channels is still a matter for debate and depends on the channel spacing, 9-11 WDM channels is generally considered to be adequate [135] [136] [137]. In fact, as shown later in this chapter (in section 5.2), as few as 5 WDM channels can be sufficient to reliably assess the transmission performance of the central channel.

The aim of the research work described in this chapter was to investigate the performance of QPSK and QAM16 signals in the presence of adjacent WDM channels. The studied data rates are: 112Gbit/s for QPSK, and 112 and 224Gbit/s in the case of QAM16. Similarly to the single-channel experiments in chapter 4, the benefit of using RZ pulses and digital nonlinearity compensation (NLC) was investigated.

5.1. WDM QPSK Transmission at 112Gbit/s

5.1.1. Experimental set-up

As described in section 4.1.2 RZ50 pulses exhibit higher tolerance towards nonlinearity compared to NRZ pulses, which results in higher launch powers into the fibre and longer transmission distances. To demonstrate the benefit of using RZ pulses over NRZ in the WDM configuration, the original setup in Figure **62** was modified to include the additional 9 channels (for which DFB lasers with 2MHz linewidth were used), as well as an extra I-Q modulator, pulse carver, optical interleaver and equalising filters in the recirculating loop. The modified setup for WDM transmission is shown in Figure **83**.

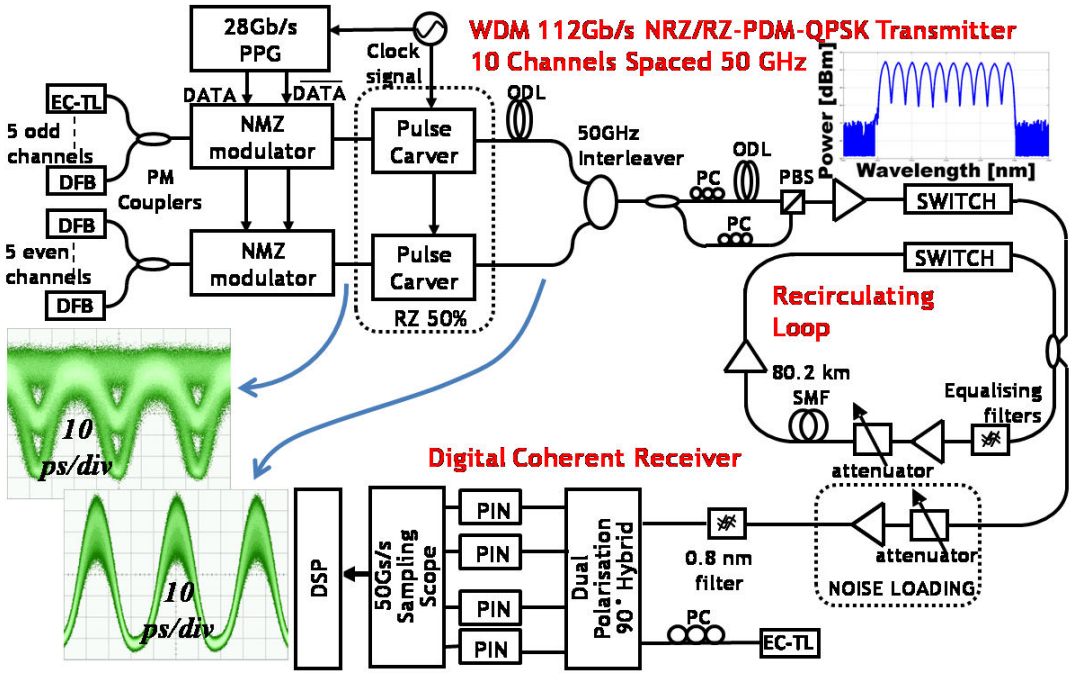

Figure 83: Experimental setup for 10 WDM channel PDM-QPSK transmission at 112Gbit/s to compare NRZ and RZ50 pulse shapes. Insets: 28Gbaud NRZ- and RZ50-QPSK eye diagrams, optical spectrum of 10 modulated WDM channels

The 10 transmitter lasers were divided into two groups of channels, referred to as odd and even channels, and each group was independently modulated for data decorrelation between the adjacent WDM channels. A photograph of the WDM-QPSK transmitter is

shown in Figure **84**. The modulated odd and even channels (NRZ or RZ50) were then combined using a flat-top optical interleaver with a 3dB bandwidth of 40GHz, designed to operate on a 50GHz WDM grid (Figure **85**). An amplitude-wavelength profile of the interleaver was measured using an optical spectrum analyser (OSA) in the case when an interleaver was placed after an ASE noise source. To equalise for the gain profile of the EDFA in the recirculating loop, a cascade of two Mach-Zehnder (MZ) filters was used. These MZ filters were MZ interferometers with a tunable extinction ratio and a tunable coupling ratio of the MZI. The free-spectral ranges of the two MZ filters was 9.6 and 24nm. In all WDM experiments carried out in this work an optical filter at receiver with 100GHz bandwidth (specified at 0.5dB) was used to limit the optical power at the input of the PINs.

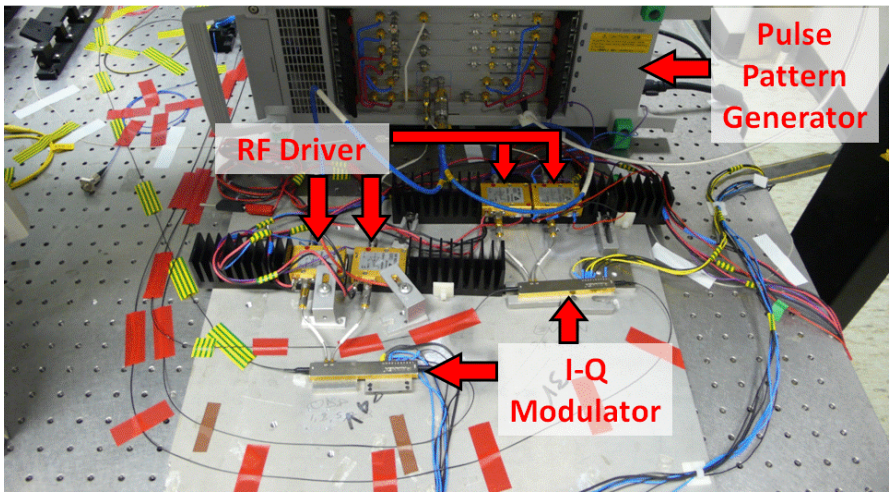

Figure 84: Experimental set-up for the WDM-QPSK transmitter

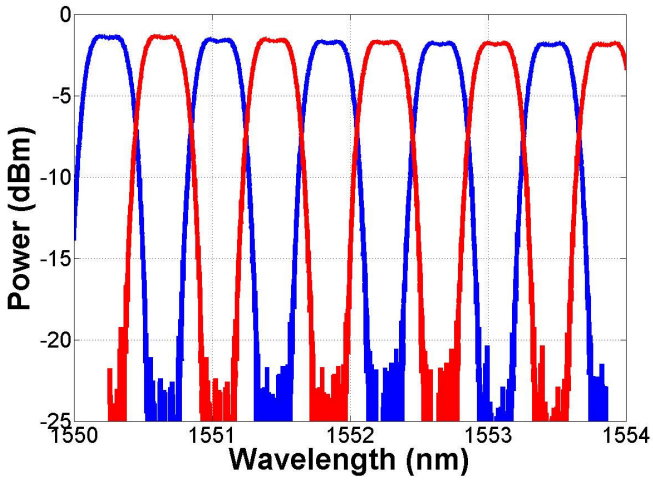

Figure 85: Measured transfer function of an optical interleaver used to combine odd (shown in red) and even (shown in blue) channels

5.1.2. Back-to-back measurements: results and discussion

Figure **86** shows the receiver sensitivity, measured for the central WDM channel, for both NRZ and RZ50 pulse shapes. The implementation penalty (at the BER = $3x10^{-3}$) was measured to have similar values for both pulse shapes: 1.6dB for RZ50-QPSK and 1.8dB for NRZ-QPSK. Similar to the single-channel QPSK experiments, both NRZ- and RZ50-QPSK signals were determined to be error free in the case of WDM, when no noise loading was applied.

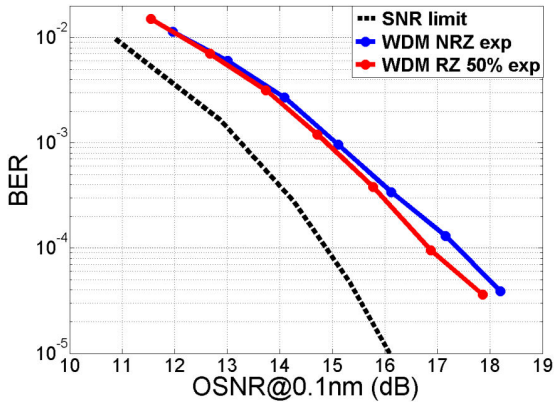

Figure 86: Measured receiver sensitivity for a WDM 112Gbit/s PDM-QPSK with NRZ and RZ50 pulse shapes.

To illustrate this concept the spectra of NRZ and RZ50 signals, both with and without the interleaver, were measured and plotted in Figure **87**. The spectral components of the NRZ-QPSK signal were all located within the interleaver bandwidth; therefore, it was concluded that the interleaver profile did not affect the spectrum of the NRZ signal. Since RZ50-QPSK has a broader spectrum than NRZ-QPSK, some spectral components of RZ50 are located outside the interleaver bandwidth. Therefore, the tight filtering performed by the interleaver reshapes the RZ50-QPSK signal. These considerations were also confirmed in [64] with the conclusion that to achieve the lowest required OSNR the RZ signals require slightly narrower optical bandwidth compared to NRZ. Interestingly, the RZ format also performs better than NRZ in the narrower filter regime where optical filter bandwidth approaches the baud rate. This is due to the fact that such narrow filtering essentially converts an RZ signal into a high-quality NRZ signal with less inter-symbol interference (ISI) compared with a conventional NRZ signal subject to narrow optical filtering [64].

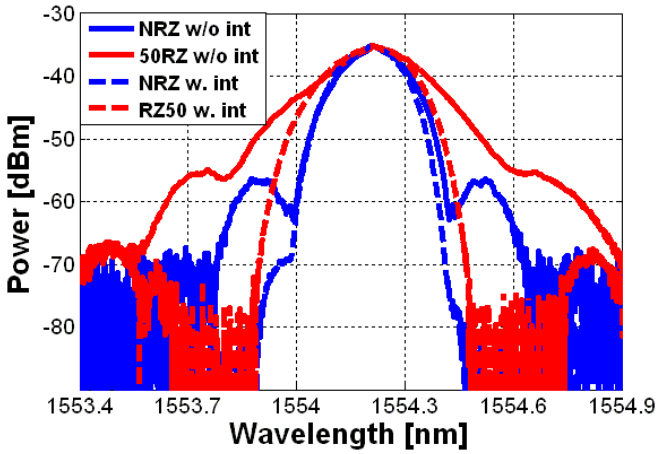

Figure 87: Measured optical spectra of 112Gbit/s NRZ- and RZ50-QPSK signals: solid lines show the configuration without an interleaver, dashed lines – with interleaver

5.1.3. Maximum reach measurements: results and discussion

To characterise the transmission performance of 112Gbit/s WDM-QPSK signals, the maximum transmission distance was measured (at BER = $3x10^{-3}$) as a function of the input launch power into the fibre (Figure **88**). In the same way as in back-to-back measurements, the transmission measurements were performed for a central WDM channel (channel 6), since the central channel experiences the maximum amount of inter-channel nonlinearity. This yields the worst-case scenario and, hence, the lower bound in the transmission performance. However, for the case of NRZ-QPSK transmission the BER of each WDM channel was measured to verify an overall performance, and was found to be $3x10^{-3}$ or less. For low launch powers (e.g. -10dBm) WDM-QPSK performed slightly better than QPSK in a single-channel configuration. This is due to the different optical filters used in the recirculating loop to reject the ASE noise, i.e. flat-top filter with fixed 100GHz bandwidth for single-channel experiments and gain-flattening filter with tight bandwidth for WDM experiments. The optimum launch power for both pulse shapes was found to be -2dBm; however, similar to the single-channel transmission RZ50-QPSK has a higher nonlinear threshold, which results in longer transmission distances.

Overall, the use of RZ50 pulse shape versus NRZ allowed the maximum reach to be increased from 5920km to 7360km (an increase of 24%). This is comparable with 18% increase in the maximum reach in single-channel transmission. This means that the benefit of using RZ pulses is also maintained in the case of WDM transmission. When using digital nonlinearity compensation (NLC) on the QPSK signal, the maximum reach

was increased by only 15% for NRZ-QPSK and 11% for RZ50-QPSK, respectively. This is due to the fact that the WDM systems are affected not only by intra-channel nonlinearity, for which NLC is most effective, but also by inter-channel XPM. The compensation of XPM would require the knowledge of not only the channel of interest but also of the surrounding channels, for which impractically large receiver bandwidth (>200GHz) is needed. Another way of performing NLC to compensate for XPM is by using parallel data processing. In this configuration the transmitted WDM signal is first demultiplexed into multiple separate channels, which can then be detected using a set of coherent receiver (one receiver per channel) and post-processed. This post-processing is first carried out on both per-channel basis and then jointly for all channels, as shown in [138].

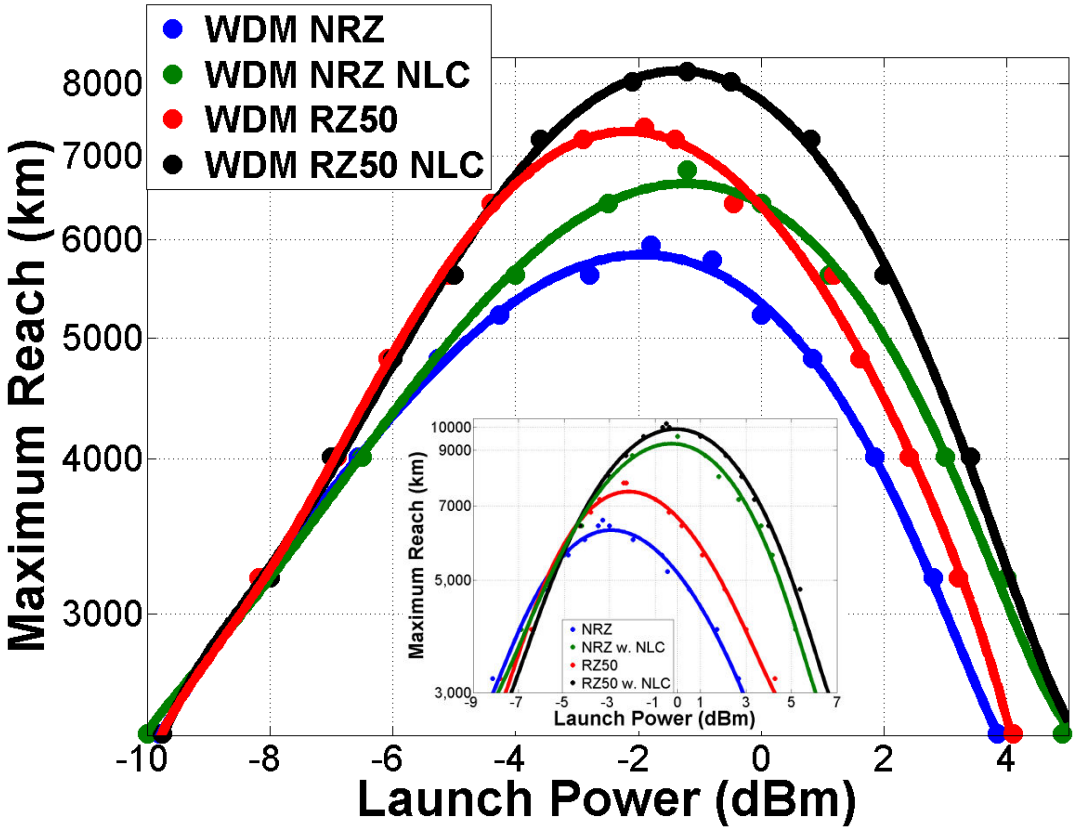

Figure 88: Measured maximum reach of PDM-QPSK transmission, measured at 112Gbit/s, with NRZ and RZ50 pulse shapes and linear and nonlinear compensation. Inset: comparison with single-channel measurements

While in single-channel transmission the use of NRZ with NLC is preferred to RZ50 in terms of the maximum reach, RZ50 outperformed NRZ in the case of WDM. Therefore, from an upgrade point of view, it could be argued that the optimisation of the

transmitter side (from NRZ to RZ50) may be preferred to the optimisation of the receiver side (from NRZ to NRZ with NLC) – both from the performance and complexity point of view. For long-haul transoceanic transmission, where distances exceeding 6000km are required, both RZ50 pulses shape and NLC might be required, potentially in addition to other techniques, like advanced optical fibre and amplification.

5.2 WDM QAM16 Transmission at 112 and 224Gbit/s

5.2.1. Experimental set-up

The results in section 4.2.3 showed that similarly to PDM-QPSK transmission, the use of RZ pulse shape and digital nonlinearity compensation (NLC) can also improve single-channel transmission performance of PDM-QAM16 signals. To experimentally quantify the WDM transmission of QAM16 signals, the set-up shown in Figure **89** was used. In this set-up the central and adjacent channels were first independently modulated, passed through an optional block of pulse carving to obtain RZ pulses, and combined using an interleaver. The rest of the set-up is the same as the one shown in Figure **70** and described in section 5.2.2.1, apart from the gain-flattening optical filter used in this experiment to equalise the WDM comb during transmission. The filter used was the same as that in the QPSK WDM experiments, described in section 5.1.

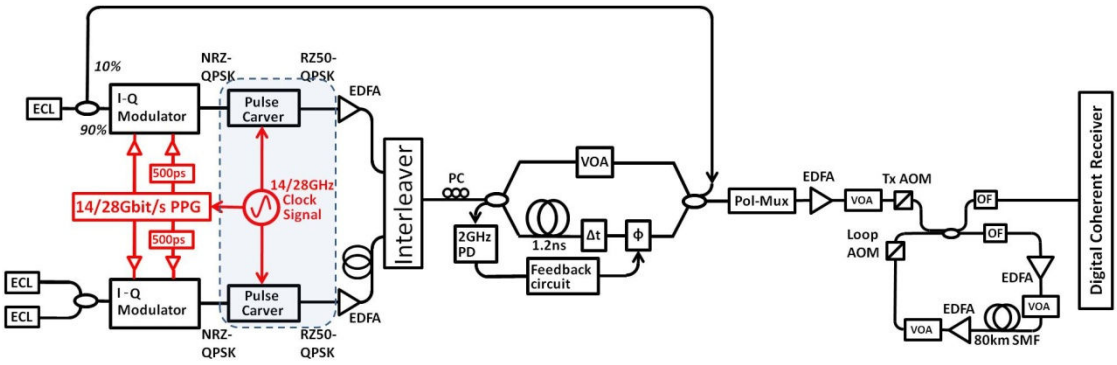

Figure 89: Experimental setup for 3-channel PDM-QAM16 transmission at 112 and 224Gbit/s

When comparing the QAM16 transmission performance to QPSK, it is important to perform it for the same symbol rate (i.e. 28Gbaud) and the same channel spacing (50GHz) to directly study the performance differences in the linear and nonlinear regimes. It is also important to compare QPSK and QAM16 at the same bit rate (i.e. 112Gbit/s) and the same spectral efficiency, for which 28Gbaud QPSK and 14Gbaud QAM16 signals over a 50-GHz WDM grid need to be used. The use of a QAM16 signal

in such a configuration would allow to offset the impact of WDM linear and non-linear cross-talk due to the larger separation between the channels, and would allow the same total capacity but with lower-speed electronics. The WDM experiment in this work was designed for 3 channels, and the system performance was assessed by measuring the BER for the central channel of interest. A higher number of QAM16 WDM channels were not experimentally studied due to the limited experimental resources, as will be described later in the section.

For the central channel under test the phase stabilisation was achieved in the same way as in a single-channel QAM16 experiment – by counter-propagating part of the CW light within the interferometer, detecting the interference product and feeding this onto the phase shifter via a control feedback circuit. Such a phase stabilisation scheme relies on having access to CW light at the transmitter, which inherently means that only one true QAM16 channel can be generated using this technique. To ensure that the adjacent channels also represent QAM16, the wavelengths of the right and left channels were fine-tuned to coincide with the two peaks of the interferometer transfer function. Because of the small free-spectral range of the interferometer (measured to be 6.5pm, as described in section 4.3), two ECLs with high wavelength stability (±100MHz/hour) were used to ensure stable operation over the time required to perform an experiment (1-2 hours). It must be noted that there is no limitation for using more than 3 channels using this technique for the generation of the WDM comb, and the use of 3 channels in the experiment in this work was limited by the availability of ECLs. The concept of the wavelength fine-tuning for the adjacent WDM channels is illustrated in Figure **90**.

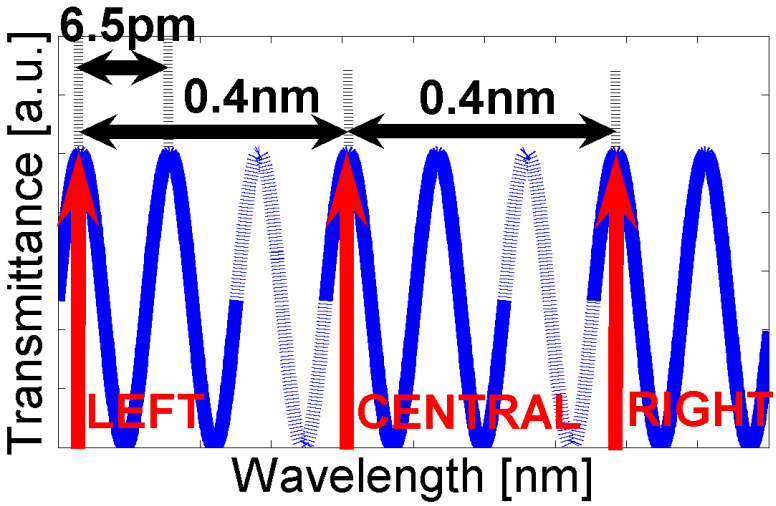

Figure 90: Laser wavelength alignment to the peaks of the interferometer transfer function

5.2.2. Back-to-back measurements: results and discussion

To demonstrate the validity of this approach in generating a WDM-QAM16 signal, the NRZ and RZ50 constellation diagrams for all three channels were measured and are plotted in Figure **91**. Although minor modulation distortions are present in Figure **91(e,f)**, they can be compensated by using the minimum Euclidian distance decision boundaries, as described in section 2.3.2.

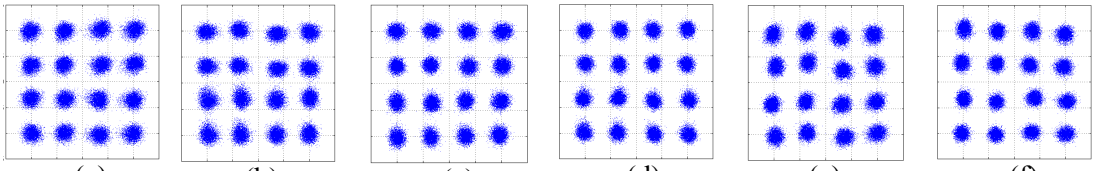

Figure 91: Constellation diagrams for 28Gbaud NRZ-QAM16 (*a – central channel under test, b – left, c – right*) and RZ50-QAM16 (*d – central channel under test, e – left, f –right*)

Next, the receiver sensitivity was measured for 112Gbit/s (14Gbaud) WDM-QAM16 with 50GHz spacing between the channels (Figure **92(a)**). Without the noise loading both NRZ- and RZ50-QAM16 were found to be error free over the 2^{19} symbols estimated. The implementation penalty was measured (at the BER = $3x10^{-3}$) to be 1.7dB and 1.8dB for NRZ- and RZ50-QAM16 signals, respectively. This compares with 1.7dB for NRZ and 1.5dB for RZ50 in the case of a single-channel experiment. These are the lowest values of implementation penalty reported to date.

At 224Gbit/s (28Gbaud) the implementation penalty was measured to be 3.5dB for NRZ-QAM16 and 3.1dB for RZ50-QAM16 (Figure **92(b)**); this compares to 3.4dB (for NRZ) and 3.1dB (for RZ50 with interleaver) in a single-channel experiment. The obtained implementation penalty was slightly worse than previously reported in [68] [85], where 3.4dB at $1x10^{-3}$ and 3.15dB at $2x10^{-3}$ were obtained, respectively. However, it was better than the one reported in [69], where 4.3dB of implementation penalty was obtained at the BER = $1x10^{-3}$. The error floor was found to be $8x10^{-5}$ for NRZ-QAM16, and decreased to $1x10^{-5}$ when using RZ50-QAM16.

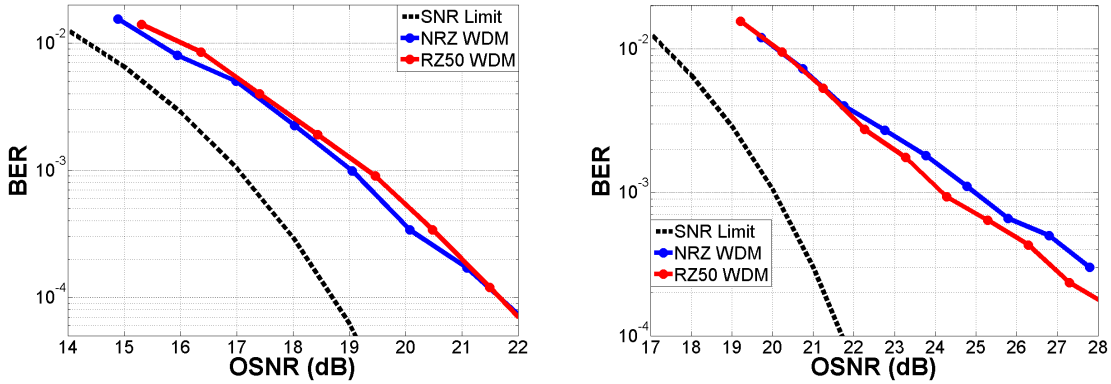

Figure 92: Measured receiver sensitivity for WDM NRZ- and RZ-50 QAM16 at (a) 112Gbit/s (14Gbaud) and (b) 224Gbit/s (28Gbaud).

At 224Gbit/s the Matlab simulations were also used to match the experimentally obtained back-to-back results by adding the appropriate amount of noise to the electrical driving signals at the transmitter. The limited transmitter bandwidth was emulated with a 5th order electrical Bessel filter with a 3dB bandwidth of 19GHz, which was determined by fitting simulated eye diagrams to experimentally obtained eye diagrams in order to obtain similar rise and fall times (Figure **93**). Since the receiver bandwidth in the experiment was limited by the analogue-to-digital converter (ADC), the experimentally measured amplitude-frequency profile of the ADC, as shown in Figure **93(a)**, was also used in the receiver simulation model. The simulation results, shown in Figure **93**, also expanded the experimental work by including the investigation of RZ pulses with 33 and 67% duty cycle (RZ33 and RZ67, respectively). The equivalent back-to-back performance in experiments and simulations allowed to reliably simulate the QAM16 transmission performance, based on the experimentally used link parameters.

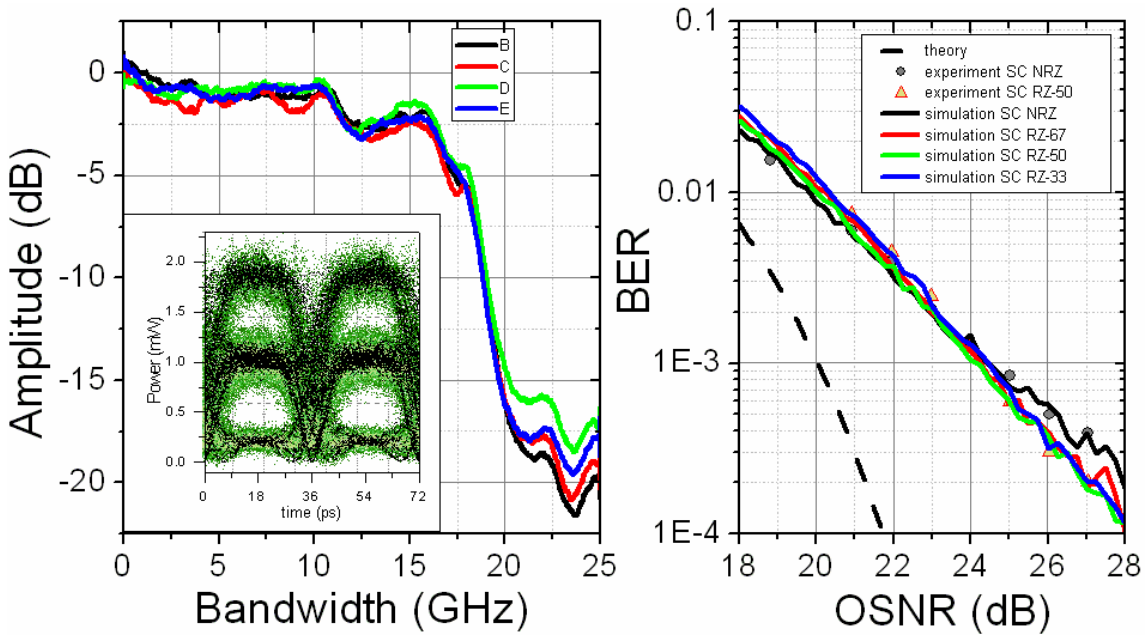

(a) (b)

Figure 93: (a) Frequency response of the four channels of the real-time scope used for ADCs. Inset shows the eye-diagram of a single-polarisation 28Gbaud QAM16 signal; black traces are simulation and green – experiment; (b) experimental and simulated single-channel receiver sensitivity of 224Gbit/s QAM16 signal for various pulse shapes

To characterise the linear and nonlinear transmission performance of 112Gbit/s 3-channel QAM16 signal, the maximum reach was measured as a function of the per channel launch power into the fibre (Figure **94**). The similar back-to-back performance between NRZ- and RZ50-QAM16, as shown in Figure **92**, also means that in the linear transmission regime the NRZ and RZ50 pulses perform in a similar way. This is evident for low launch powers of up to approximately -5dBm, where the four curves overlap, as shown in Figure **94**. Similar to the single-channel experiment, the worse performance is obtained when using the NRZ pulse shape (maximum reach of 2240km, optimum launch power of -3dBm) and the best performance - using the RZ50 pulse shape and digital nonlinearity compensation (NLC) (maximum reach of 3280km, optimum launch power of 0dBm). Because in the WDM regime the transmission is limited by not only SPM but also XPM, the efficiency of NLC is reduced. The compensation of XPM would require knowledge about not only about the channel under test but also about adjacent channels, therefore, requiring a receiver with a bandwidth that is currently technologically impossible to achieve. This consideration becomes apparent when

comparing single-channel and WDM transmission results in Figure **94**; the maximum reach was decreased from 4240km (in the case of single-channel) to 3280km (in the case of WDM). Also, the difference (in terms of the maximum reach) between the two curves: RZ50 vs. NRZ with NLC, is decreased from 29% in the case of the single-channel transmission to a mere 6% in the case of WDM.

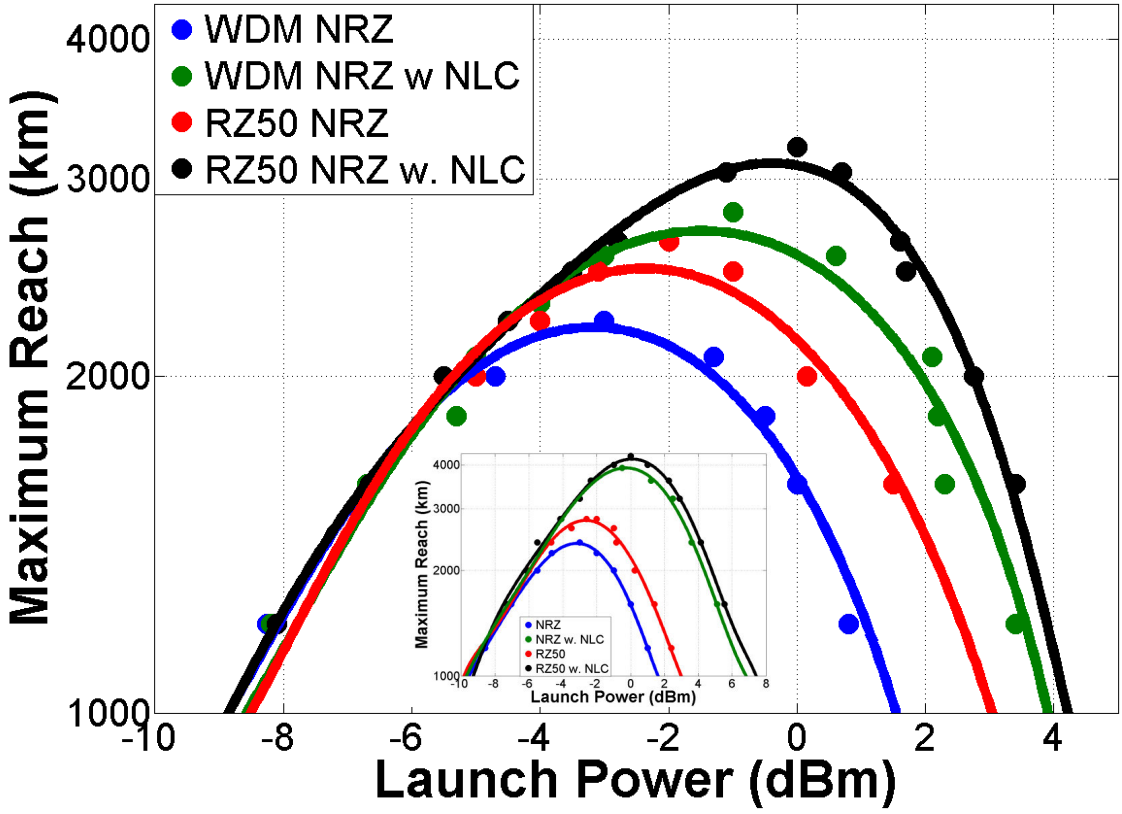

Figure 94: Measured maximum reach of 3-channel PDM-QAM16 transmission at 112Gbit/s with NRZ and RZ50 pulse shapes and linear (solid lines) and nonlinear (dashed lines) compensation. Inset: comparison with single-channel measurements

At 224Gbit/s QAM16 transmission the benefit of using NLC was even further reduced to the extent where NRZ with NLC yielded the same maximum reach as RZ50 – 1360km. Both configurations showed a 13% increase in reach compared to a standard NRZ transmission, where a maximum reach of 1200km was achieved. The use of RZ pulses and NLC only slightly increased the reach to 1520km (by 27%). The transmission results for 224Gbit/s WDM-QAM16 transmission are shown in Figure 95, along with the single-channel transmission results for comparison (inset).

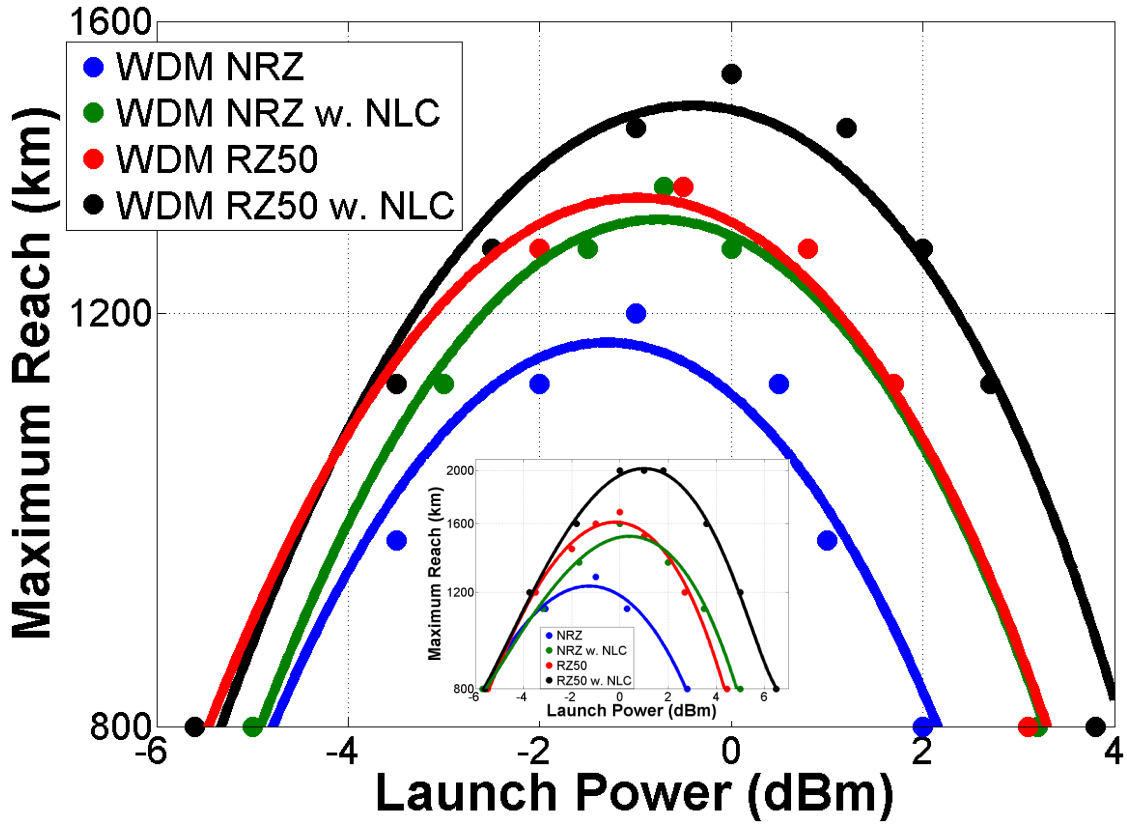

Figure 95: Maximum reach of 3-channel PDM-QAM16 transmission at 224Gbit/s with NRZ and RZ50 pulse shapes and linear (solid lines) and nonlinear (dashed lines) compensation. Inset: comparison with single-channel measurements

The 224Gbit/s QAM16 transmission experiments were then verified by simulations, where the results were also expanded to include RZ33 and RZ67 pulses, and also a varying number of the WDM channels to estimate the minimum number of channels required to reliably simulate the behaviour of a real multi-channel WDM system. The results, shown in Figure **96**, demonstrate that in the case of the single-channel transmission the experiment underestimates the maximum reach by only 2-3 spans, which is a reasonable deviation from the upper bound provided by the simulation. One of the potential sources of deviation is that any other inaccuracies in the EDFA noise figure and nonlinear fibre coefficient tend to accumulate with an increased number of recirculations, and could cause deviation from the simulated performance. Another likely source of such deviation is the fact that changing the launch power into the fibre requires rebalancing the recirculating loop used in the experiment, which changes the effective noise figure of the EDFA in the loop. This effect is extremely difficult and time-consuming to simulate, and could be one of the reasons that the simulation

overestimates the maximum reach of a 3-WDM channel RZ50-QAM16 signal by 6 spans. Nevertheless, both single-channel and WDM simulations show very good agreement in transmission trend for both NRZ- and RZ50-QAM16 modulation formats.

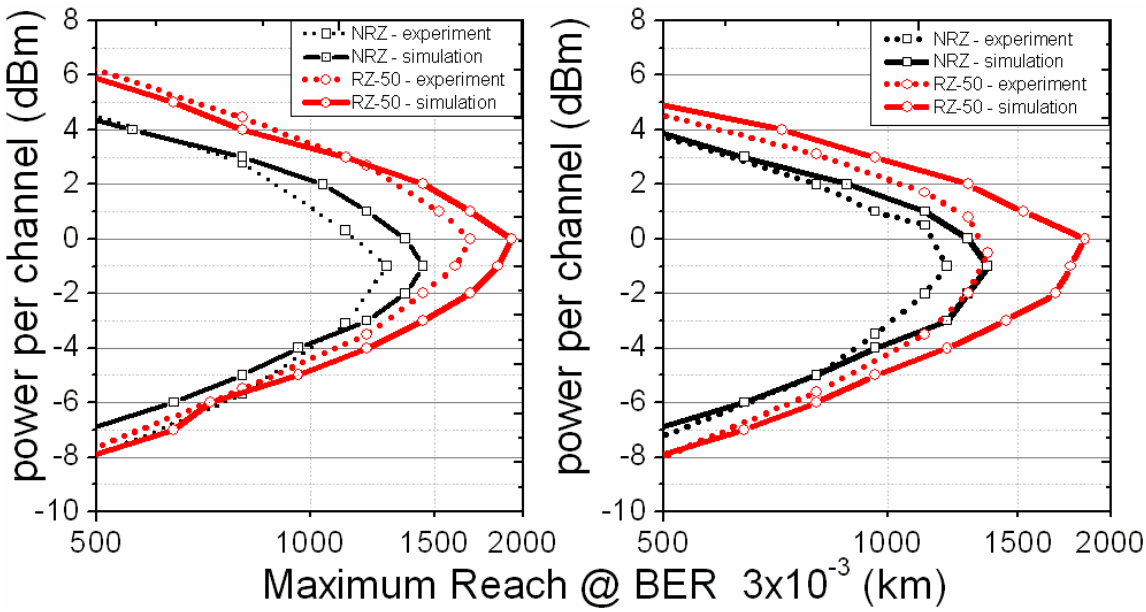

(a) (b)

Figure 96: Comparison of experimentally obtained and simulated maximum reach versus launch power per channel for (a) single-channel and (b) 3-WDM channel configurations

Next, an extensive set of simulations was carried out to determine the impact of XPM in a WDM transmission for NRZ-, RZ33-, RZ50- and RZ67-QAM16 transmission (Figure **97**). Simulations were performed for 3, 5, 7 and 9 WDM channels to study whether 3-channels used in the experiment is sufficient for including most of the XPM effect occurring during transmission. The results show that for WDM transmission without digital nonlinearity compensation (NLC) the simulation of 5 channels was sufficient to capture most of XPM since the maximum reach remains practically unaffected when further increasing the number of channels to 7 or 9. But even when 3 WDM channels were used, the transmission performance was only overestimated by 1-2 spans, compared to 9-channel transmission.

An interesting conclusion is that in the case when NLC with one nonlinear step per span was used, the maximum reach was also more sensitive to additional WDM channels. As pointed out in [139] additional channels not only reduced reach by more

uncompensated nonlinear cross-talk but also reduce the efficiency of the NLC algorithm, which ultimately affects the maximum reach. Therefore, as shown in Figure **97**, the simulation of only 5 WDM channels was no longer sufficient, and 9 or more WDM channels needed to be included.

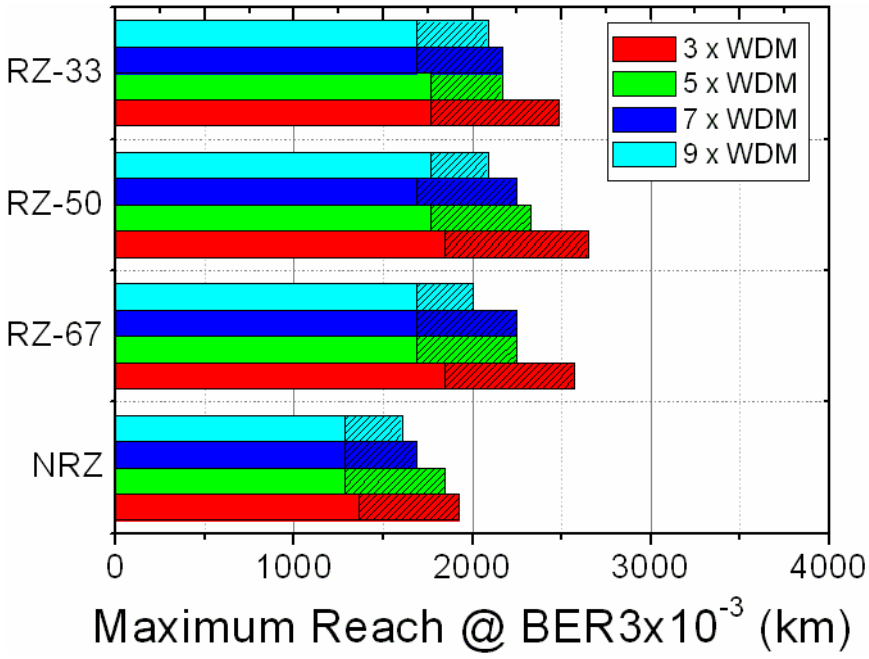

Figure 97: Comparison of the maximum reach for NRZ, RZ67, RZ50 and RZ33 pulse shapes for configurations with multiple WDM channels. Shaded bars show the maximum reach in the case of NLC for the central channel

5.3 Summary

The results in this chapter represent the first comprehensive investigation of the impact of RZ pulse shaping and the use of NLC in the QPSK and QAM16 WDM transmission. The WDM back-to-back and transmission results in this chapter further extend the single-channel QPSK and QAM16 results, previously obtained in chapter 4. Overall, it was seen that the maximum transmission distance in the case of WDM was lower than in single-channel experiments due to additional cross-phase-modulation (XPM) from the neighbouring channels. The results for 112Gbit/s QPSK transmission and 112/224Gbit/s QAM16 transmission are summarised in Tables 4-6.

Single-channel (maximum reach at BER = $3x10^{-3}$)					
	NRZ	**RZ50**	**NRZ/NLC**	**RZ50/NLC**	**Change (%)**
NRZ vs. RZ50	6560km	7760km			18%
NRZ vs. NRZ/NLC	6560km		9600km		46%
RZ50 vs. RZ50/NLC		7760km		10160km	31%
RZ50 vs. NRZ/NLC		7760km	9600km		24%
NRZ vs. RZ50/NLC	6560km			10160km	55%
WDM (maximum reach at BER = $3x10^{-3}$)					
NRZ vs. RZ50	5920km	7360km			24%
NRZ vs. NRZ/NLC	5920km		6800km		15%
RZ50 vs. RZ50/NLC		7360km		8160km	11%
RZ50 vs. NRZ/NLC		7360km	6800km		-8%
NRZ vs RZ50/NLC	5920km			8160km	38%

Table 4. Comparison of maximum reach between single-channel and WDM PDM-QPSK transmission at 112Gbit/s. NRZ and RZ50 pulse shapes, both with and without digital nonlinearity compensation, are also compared.

At 112Gbit/s the presence of the additional 9 WDM channel in the case of QPSK decreased the maximum achievable reach from 10160km to 8160km, compared to the single-channel experiment. The lowest maximum reach of 5920km was obtained when

using NRZ pulses with no digital nonlinearity compensation (NLC); this is 38% less than 8160km of maximum transmission distance obtained using RZ50 pulses and NLC. While in single-channel 112Gbit/s PDM-QPSK experiment the use of NLC for NRZ transmission yielded a significant increase in reach compared with RZ pulses without NLC, in the case of WDM transmission it was the RZ pulses without NLC that yielded a superior performance as shown in Table 4. The reason for this is the reduced efficiency of NLC in dense WDM systems where cross-phase-modulation (XPM) is the dominant source of nonlinearity. To mitigate for XPM the capability to detect adjacent neighbouring channels is required, currently implying impractically wide receiver bandwidth (200GHz or more). Nevertheless, the maximum achievable transmission distance of 8160km in the case of WDM means that 112Gbit/s QPSK solution can be potentially used for transatlantic long-haul transmission

Single-channel (maximum reach at BER = $3x10^{-3}$)					
	NRZ	**RZ50**	**NRZ/NLC**	**RZ50/NLC**	**Change (%)**
NRZ vs. RZ50	2400km	2800km			17%
NRZ vs. NRZ/NLC	2400km		3920km		63%
RZ50 vs. RZ50/NLC		2800km		4240km	51%
RZ50 vs. NRZ/NLC		2800km	3920km		40%
NRZ vs. RZ50/NLC	2400km			4240km	77%
WDM (maximum reach at BER = $3x10^{-3}$)					
NRZ vs. RZ50	2240km	2640km			13%
NRZ vs. NRZ/NLC	2240km		2800km		25%
RZ50 vs. RZ50/NLC		2640km		3280km	24%
RZ50 vs. NRZ/NLC		2640km	2800km		6%
NRZ vs. RZ50/NLC	2240km			3280km	46%

Table 5. Comparison of maximum reach between single-channel and WDM PDM-QAM16 transmission at 112Gbit/s. NRZ and RZ50 pulse shapes, both with and without digital nonlinearity compensation, are also compared.

In 112Gbit/s PDM-QAM16 transmission, the presence of additional two channels decreased the maximum reach from 4240km to 3280km – both obtained using RZ50 pulses with NLC. The lowest transmission distance of 2240km is obtained using NRZ pulses and no NLC, as expected. However, the overall benefit of using NLC reduced compared with single-channel experiment was reduced to 24-25%, as shown in Table 5.

Conversely, the benefit of RZ50 pulse shaping remained virtually unchanged - as a result, the RZ50 only slightly underperformed NRZ with NLC (2640km vs. 2800km). Still, 3280km is the longest transmission distance currently reported for 112Gbit/s WDM-QAM16.

Finally, the 3-WDM channel PDM-QAM16 transmission at 224Gbit/s (28Gbaud) was studied. The maximum achievable reach was found to be 1520km (again, using RZ50 pulses and NLC), down from 2000km obtained in a single-channel transmission. Similar to the previous experiments, the worst case scenario was found to be when using NRZ pulses and no NLC (1200km). One of the most important conclusions is that for both single-channel and 3-channel transmission the use of RZ50 is the preferred upgrade solution compared to NLC over NRZ pulses. This is due to the similar transmission distances achieved in both cases, but much lower complexity associated with RZ50 pulse shaping.

Single-channel (maximum reach at BER = $3x10^{-3}$)					
	NRZ	**RZ50**	**NRZ/NLC**	**RZ50/NLC**	**Change (%)**
NRZ vs. RZ50	1280km	1680km			31%
NRZ vs. NRZ/NLC	1280km		1600km		25%
RZ50 vs. RZ50/NLC		1680km		2000km	10%
RZ50 vs. NRZ/NLC		1680km	1600km		-5%
NRZ vs. RZ50/NLC	1280km			2000km	56%
WDM (maximum reach at BER = $3x10^{-3}$)					
NRZ vs. RZ50	1200km	1360km			13%
NRZ vs. NRZ/NLC	1200km		1360km		13%
RZ50 vs. RZ50/NLC		1360km		1520km	12%
NRZ/NLC vs. RZ50		1360km	1360km		0%
NRZ vs. RZ50/NLC	1200km			1520km	27%

Table 6. Comparison of maximum reach between single-channel and WDM PDM-QAM16 transmission at 224Gbit/s. NRZ and RZ50 pulse shapes, both with and without digital nonlinearity compensation, are also compared.

6. Conclusions and Future Work

The research work described in this thesis was devoted to the experimental investigation of the techniques that could allow for longer reach and higher bit-rate of optical fibre transmission systems. Two ways to increase the bit-rate were studied in this work: optical time-division multiplexing (OTDM) using bit-wise phase control and advanced spectrally-efficient modulation formats with coherent detection.

The first conclusion is that, although the optimisation of the bit-wise phase difference between the OTDM channels can increase the maximum transmission distance by ~70%, the overall use of the OTDM in direct-detected systems is unlikely to provide a practical benefit in terms of capacity-distance product. This is due to the reduced tolerance to chromatic dispersion (CD) and polarisation-mode dispersion (PMD) at higher bit-rates, and the complexity associated with short pulse generation, multiplexing and demultiplexing. A better way of increasing the bit-rate and provide gain in terms of spectral efficiency (SE) is by using advanced modulation formats, where a lower symbol rate (and, hence, less expensive electronics) can be used to obtain an equivalent channel bit-rate. The easiest (and in some cases, the only) way to receive advanced modulation formats is by using coherent reception, which also gives an opportunity to increase the overall bit-rate by a factor of 2 for “free”, using polarisation division multiplexing (PDM). Coherent reception allows for the detection of amplitude, phase and the state of polarisation of the signal, therefore, enabling a full characterisation of the signal field. Thus, very large accumulated CD values can be compensated, allowing transmission over uncompensated dispersion links, which have a better nonlinear tolerance than most dispersion managed links.

The subsequent research work was focused on the study of advanced modulation formats, namely quadrature phase-shift keying (QPSK) and 16-state quadrature amplitude modulation (QAM16), and the use of RZ pulses and digital NLC to improve nonlinear transmission performance and maximum reach of QPSK and QAM16. A key result of this research work was the proposal and use of a novel technique to generate QAM16 signal. This generation technique was based on the modified version of phase-stabilised OTDM multiplexer, used in the experiments described in chapter 4. During

the generation process only binary electrical signals were used, which reduced the complexity of electronics at the transmitter. The use of binary signals also suppressed an electrical noise transfer into the optical domain due to the fact that an I-Q modulator could be driven over the nonlinear part of its transfer function.

It should be noted that this research represents the first comprehensive experimental comparison of the use of RZ and NLC for the two modulation formats at various bit-rates. It was found that in single-channel transmission NLC yields a significant improvement in the maximum reach, particularly when NRZ pulses were used. It is worth highlighting that NLC is effective in dealing with self-phase-modulation (SPM) but cannot undo nonlinear phase noise and ASE due to its stochastic nature. The improvement in the maximum reach when using NLC was found to be 72% for 42.7Gbit/s (10.66Gbaud) QPSK, 46% for 112Gbit/s (28Gbaud) QPSK, 63% for 112Gbit/s (14Gbaud) QAM16, and 25% for 224Gbit/s (28Gbaud) QAM16. Two points are worth noting: first, it was found that the efficiency of the NLC was reduced for higher symbol rates. This is due to the combination of the lower nonlinear threshold (lower tolerance towards nonlinearity) at higher symbol rates and the fact that at higher symbol rates the nonlinearity induced spectrum broadening was more critical due to the limited bandwidth of the analogue-to-digital converters (ADCs) at the receiver. Second, the efficiency of NLC was also reduced for QAM16 compared to QPSK for the same symbol rate because of the lower tolerance to nonlinearity of QAM16 signals, particularly, nonlinear phase noise (which cannot be compensated for).

However, most practical optical transport systems are based on wavelength division multiplexing (WDM), where cross-phase-modulation (XPM) is the dominant source of nonlinearity. While NLC can theoretically compensate for XPM as well, this would require the receiver bandwidth of ~200GHz or more, which is currently technologically impossible to achieve. The reason that such large bandwidth is required is that the receiver must detect not only the channel under test but also adjacent channels to obtain information on the overall contribution of XPM on channel under test. The results of this research work showed that in the case of WDM with 50GHz spacing between the channels, the efficiency of NLC was significantly reduced in terms of the maximum reach: 15% for 112Gbit/s (28Gbaud) QPSK, 25% for 112Gbit/s (14Gbaud) QAM16, and 13% for 224Gbit/s (28Gbaud) QAM16. Since for 28Gbaud signals on a 50GHz grid the effect of XPM is stronger than for 14Gbaud, NLC (which in this work was used to

compensate for SPM only) for 112Gbit/s QAM16 was the most effective amongst the three configurations.

The use of RZ pulse shapes with 50% duty cycle (RZ50) was studied for 112Gbit/s QPSK, and 112 and 224Gbit/s QAM16 transmission. In the single-channel transmission the benefit of using RZ50 pulses instead of NRZ was found to be 18%, 17% and 31% respectively. In the WDM configuration this corresponded to 24%, 13% and 13%, respectively. An interesting conclusion is that for WDM transmission an upgrade from NRZ pulses to RZ50 is a preferred solution compared to an upgrade from NRZ to NRZ with NLC. While both upgrades yielded comparable transmission distances, the use of the RZ50 pulse shape is less complex and is potentially more cost-effective than the use of NLC.

Overall, the longest single-channel transmission distances obtained in this research work were 13600km for 42.7Gbit/s PDM-QPSK, 10160km for 112Gbit/s PDM-QPSK, 4240km for 112Gbit/s PDM-QAM16, and 2000km for 224Gbit/s PDM-QAM16. These are the longest transmission distances reported to date. In the case of WDM transmission these were reduced to 8160km for 112Gbit/s PDM-QPSK, 3280km for 112Gbit/s PDM-QAM16, and 1520km for 224Gbit/s PDM-QAM16. The results of the described research work can be applied in the development of the next generation optical communication system and the trade-offs in system design.

The overall conclusion is that at 100Gbit/s the use of QPSK with coherent detection is a desirable configuration to reach transoceanic transmission distances. Further increase in the bit-rate per carrier using more complex modulation formats can also be desirable to achieve higher spectral efficiencies. The next-generation systems are likely to be based on 400Gbit/s bit-rate (448Gbit/s with FEC), the optimum generation of which is still a question of debate. However, with the advances in the transmitter and receiver components design, PDM-QAM16 becomes feasible in achieving the data rate of 400Gbit/s per carrier.

One of the ideas for future work is the generation of PDM-QAM64 modulation format and investigation of its transmission performance (in terms of the maximum reach) at various bit-rates (9.3Gbaud for 112Gbit/s and 18.7Gbaud for 224Gbit/s). Such QAM64 signal will most likely be generated using two phase-stabilised fibre interferometers in a parallel structure. Similar to QAM16 generation, the generation of a

QAM64 signals will require only binary signals, which reduces the electrical noise transfer into the optical domain and the complexity of the electronics at the transmitter.

Another direction for future work is in the generation of a 448Gbit/s (56Gbaud) PDM-RZ-QAM16 signal with the help of the OTDM technique and investigation of the transmission performance at this bit-rate. The problem with the generation and reception of a 56Gbaud signal using all-electrical means is the limited bandwidth of components at the transmitter and receiver (in particular, ADCs). Therefore, an RZ-QAM16 signal could first be generated at 28Gbaud and then optically multiplexed to 56Gbaud using single-stage OTDM. Finally, a 56Gbaud RZ-QAM16 signal is passed through the polarisation multiplexing stage to obtain an overall bit-rate of 448Gbit/s. At the receiver a 448Gbit/s signal needs to be demultiplexed to 224Gbit/s (28Gbaud) using a pulsed, rather than a continuous wave (CW), local oscillator (LO). The easiest way to obtain a pulsed signal for the LO is from the unmodulated RZ source at the transmitter, but it should also be possible to extract it at the receiver using clock recovery. It must be noted that the use of OTDM cannot not be used to generate NRZ-QAM16 since the RZ pulse shape is the pre-requisite for an OTDM. However, as has been determined previously the use of RZ is preferred to NRZ anyway, due to an increased tolerance towards nonlinearity.

The economic viability of future optical fibre transmission systems, potentially based on QAM16 modulation, will first of all depend on the advances in the sampling rate of ADCs at the receiver (assuming 56Gbaud PDM-QAM16 for an overall bit-rate of 448Gbit/s, which would require the sampling rate of ~80GSamples/s). Secondly, the techniques to develop a high-speed QAM16 transmitter with low implementation penalty still remain a challenge. Finally, the detection and post-processing of QAM16 signals requires the use of source laser and LO with the linewidths lower than the ones for QPSK signals. Reducing the cost of those low-linewidth lasers is essential to the success of future QAM16 transponders.

Appendix A: Recirculating Loop for Long-Haul Transmission

In a real system optical signals are propagated in a straight-line configuration, consisting of many periodically amplified spans of optical fibre (Figure **98**). However, during the stage of test and development of the system a straight-line configuration becomes inconvenient, since the price of building a long-haul experiment is extremely high. For instance, in order to reach transpacific distances (~10000km) 125 spools of 80km fibre and, hence, 125 optical amplifiers and other passive components, must be used.

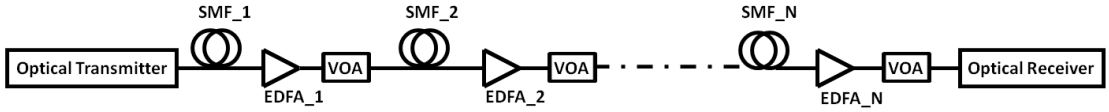

Figure 98: An example of a straight-line transmission experiment

To reduce number of components during an investigation of long-haul transmission involving optical amplifiers, a useful tool called "recirculating loop" can be used. A loop experiment emulates the transmission performance of multi-thousand kilometre long system by reusing or recirculating an optical signal through a modest length amplifier chain of tens to hundreds of kilometres [140]. The UCL recirculating loop test bed was developed ~10 years ago, and the purpose of this Appendix is to give a description of its current configuration, used in the experiments of this research work. A more detailed description of the recirculating loop is given in [123].

The loop operation is determined by the states of acousto-optic modulators (AOMs), which act as optical switches in the loop to create a sequence of 'loading' and 'transmission' stages (Figure **99**).

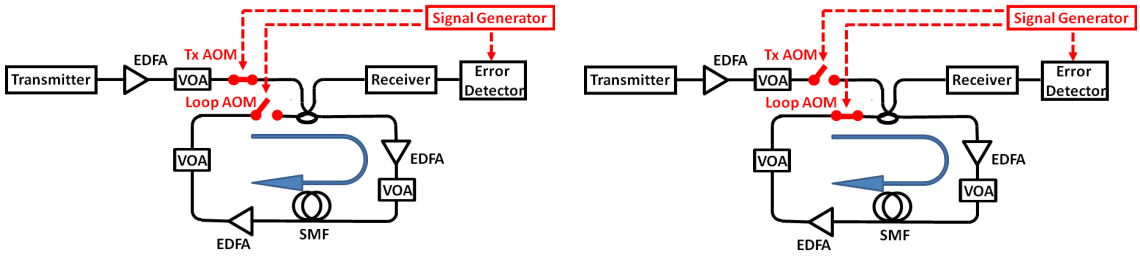

Figure 99: "Loading" and "Transmission" states of a recirculating loop

The choice of AOMs for switching is determined by the optimum combination of switching speed (80ns), high extinction ratio (up to 50dB) and low insertion loss (~ 2dB) [123]. During the loading stage the input optical switch allows the data from the transmitter to feed the loop while the optical switch inside the loop is open (Figure **99(a)**). When the loop is completely loaded with the data signal the state of the two optical switches is reversed, so the burst of the optical signal can start propagating in the loop (Figure **99(b)**) [123]. The process of changing the states of the loop (from 'loading' to 'transmission' and vice versa) is continuous, so light is constantly coupled out of the loop. The length of the loading stage should be equal to at least 2 x τ_{LOOP} to leave sufficient time to fill the loop with the data, where τ_{LOOP} is the time it takes the signal to propagate though a single span of fibre. For conventional span lengths of 80-100km, τ_{LOOP} = 400-500µs. The length of the 'transmission' stage is then equal to (number of recirculations x τ_{LOOP}), so for 800km of reach the duration of the 'transmission' stage is 5ms. To avoid measuring an incorrect part of the signal that is constantly coupled out of the loop, all the measurement equipment including optical spectrum analysers (OSAs), oscilloscopes and error detectors must be capable of performing the measurements only during the time when external gating signal is present (i.e. during the last recirculation) (so called, burst mode operation) [123]. The gating signal should be centred in the middle of the recirculation with a duration chosen to be at least 10% shorter than τ_{LOOP} to exclude measuring transients of EDFAs in the loop. The loop timing diagram is shown in Figure **100**.

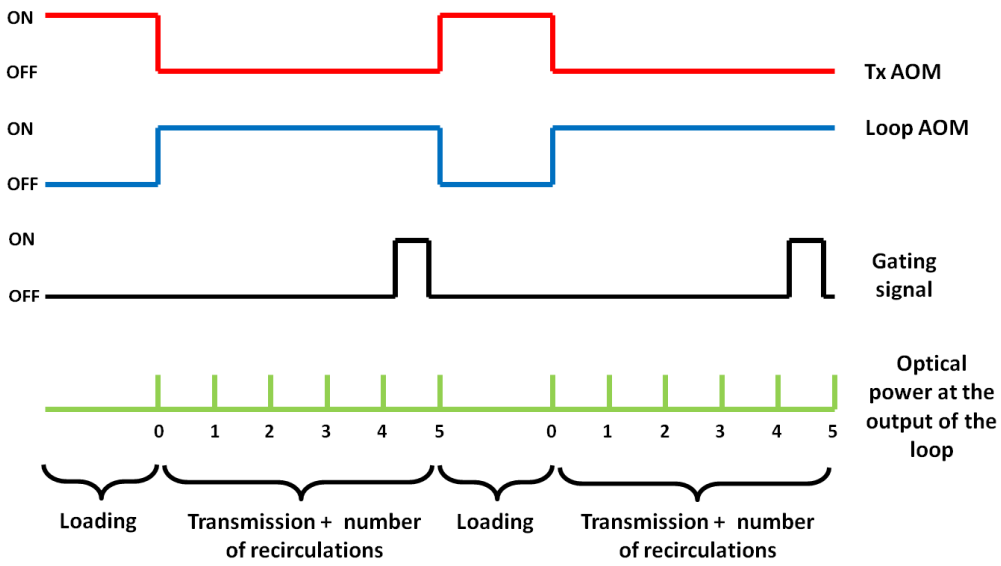

Figure 100: Timing diagrams of a recirculating loop

To allow for reliable measurements, the input power to the fibre must be constant over the required number of recirculations. Variable optical attenuators (VOAs) before the Tx AOM and the Loop AOM, as shown in Figure **99** can be used to equalise (balance) the optical powers after Tx AOM and Loop AOM.

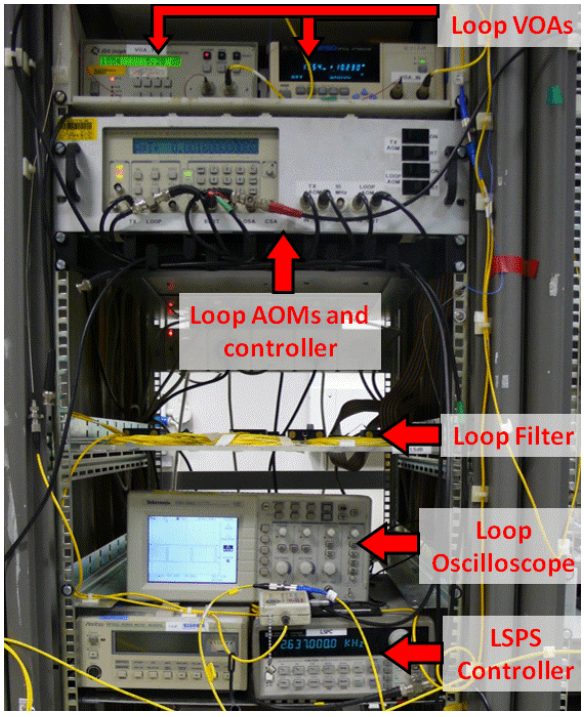

Figure 101: Recirculating loop configuration

Appendix B: List of Abbreviations

ADC	Analogue-to-Digital Converter
AOM	Acousto-Optical Modulator
ASE	Amplified Spontaneous Emission
ASK	Amplitude Shift Keying
AWG	Arbitrary Waveform Generator
BER	Bit Error Rate
BPSK	Binary Phase Shift Keying
CD	Chromatic Dispersion
CMA	Constant Modulus Algorithm
CRU	Clock-Recovery Unit
CS-RZ	Carrier-Suppressed Return-to-Zero
CW	Continuous Wave
DAC	Digital-to-Analogue Converter
DC	Direct Current
DCF	Dispersion Compensating Fibre
DFB	Distributed Feedback Laser
DPSK	Differential Phase Shift Keying
DQPSK	Differential Quadrature Phase Shift Keying
DSP	Digital Signal Processing
EAM	Electro-Absorption Modulator
ECL	External Cavity Laser
EDFA	Erbium-Doped Fibre Amplifier
ERGO-PGL	Erbium Glass Oscillator Pulse Generating Laser
ETDM	Electrical Time-Division Multiplexing
FEC	Forward Error Correction
FFT	Fast Fourier Transform
FIR	Finite Impulse Response
FROG	Frequency-Resolved Optical Gating
FSR	Free-Spectral Range
FWHM	Full Width Half Maximum

FWM	Four Wave Mixing
GT-UNI	Gain-Transparent Ultrafast Nonlinear Interferometer
HI-SMZ	Hybrid Integrated Symmetric Mach-Zehnder
IFWM	Intra-Channel Four Wave Mixing
I-Q	In-phase and Quadrature
ISI	Inter-Symbol Interference
IXPM	Intra-Channel Cross-Phase Modulation
LMS	Least-Mean Square
LO	Local Oscillator
LSPS	Loop-Synchronous Polarisation Scrambler
MIMO	Multiple Input Multiple Output
MLLD	Mode-Locked Laser Diode
ML-FRL	Mode-Locked Fibre Ring Laser
MMA	Multi Modulus Algorithm
MZI	Mach-Zehnder Interferometer
MZM	Mach-Zehnder Modulator
NLC	Nonlinearity Compensation
NOLM	Nonlinear Optical Loop Mirror
NRZ	Non-Return-to-Zero
NZ-DSF	Non-Zero Dispersion Shifted Fibre
OFDM	Optical Frequency-Division Multiplexing
OOK	On-Off Keying
OSA	Optical Spectrum Analyser
OSNR	Optical Signal-to-Noise Ratio
OTDM	Optical Time-Division Multiplexing
PC	Polarisation Controller
PDL	Polarisation Dependent Loss
PDM	Polarisation Division Multiplexed
PIC	Photonic Integrated Circuit
PIN	P-I-N photodiode
PLC	Planar Lightwave Circuit
PMD	Polarisation Mode Dispersion
PPG	Pulse Pattern Generator
PSD	Power Spectral Density

PSK	Phase Shift Keying
PRBS	Pseudo-Random Bit Sequence
PSCF	Pure-Silica Core Fibre
QAM	Quadrature Amplitude Modulation
QPSK	Quadrature Phase Shift Keying
RDE	Radially Directed Equaliser
RF	Radio-Frequency
RZ	Return-to-Zero
SDH	Synchronous Digital Hierarchy
SE	Spectral Efficiency
SER	Symbol Error Rate
SLA	Super-Large Area
SMF	Single Mode Fibre
SNR	Signal-to-Noise Ratio
SOA	Semiconductor Optical Amplifier
SOP	State Of Polarisation
SPM	Self-Phase Modulation
SSM	Split-Step Method
TAT	Trans-Atlantic
VOA	Variable Optical Attenuator
VCO	Voltage-Controlled Oscillator
WDM	Wavelength Division Multiplexing
XPM	Cross-Phase Modulation

C. List of Figures

References

[1] Nakazawa M. Weber H.-G., "Ultrahigh-speed optical transmission technology," *Springer, 2007*.

[2] Nagayama K. et al., "Ultra low loss (0.1484 dB/km) pure silica core fiber and extension of transmission distance," *Electronics Letters*, vol. 38, no. 20, pp. 1168-1169, 2004.

[3] http://www.ciena.com/products/6500/.

[4] Birk M. et al., "Real-time, single-carrier coherent 100 Gbit/s PM-QPSK field trial," *IEEE Journal of Lightwave Technology*, vol. 29, no. 4, pp. 417-425, 2011.

[5] Winzer P.J. et al., "Generation and 1200-km transmission of 448-Gb/s ETDM 56-Gbaud PDM 16-QAM using a single I/Q modulator," *Proceedings of European Conference on Optical Communication*, PD2.2, 2010.

[6] Makovejs S. et al., "Characterisation and comparison of bitwise phase-control OTDM signals in 80Gbit/s transmission," *Proceedings of European Conference on Optical Communication*, We.2.E.7, 2008.

[7] Makovejs S. et al., "Experimental and numerical investigation of bit-wise phase-control OTDM transmission," *Optics Express*, vol. 16, no. 23, pp. 18725-18730, 2008.

[8] Makovejs S. et al., "Novel method of generating QAM-16 signals at 21.3Gbaud and transmission over 480km," *IEEE Photonics Technology Letters*, vol. 22, no. 1, pp. 36-38, 2010.

[9] Torrengo E. et al., "Influence of pulse shape in 112-Gb/s WDM PDM-QPSK transmission," *IEEE Photonics Technology Letters*, vol. 22, no. 23, pp. 1714-1716, 2010.

[10] Makovejs S. et al., "Comparison of pulse shapes in a 224Gbit/s (28Gbaud) PDM-QAM16 transmission experiment," *Technical Digest of Optical Fiber Communication Conference*, OMR5, 2011.

[11] Makovejs S. et al., "Experimental investigation of PDM-QAM16 transmission at 112 Gbit/s over 2400km," *Technical Digest of Optical Fiber Communicaion*

Conference, OMJ6, 2010.

[12] Millar D.S. et al., "Experimental comparison of nonlinear compensation in long-haul PDM-QPSK transmission at 42.7 and 85.4 Gb/s," *Proceedings of European Conference on Optical Communication*, Paper 9.4.4, 2009.

[13] Stark J. B. Mitra P. P., "Nonlinear limits to the information capacity of optical fibre communications," *Nature*, vol. 411, pp. 1027-1030, 2001.

[14] Cai J.-X. et al., "112x112 Gb/s transmission over 9360 km with channel spacing set to the baud rate (360% spectral efficiency)," *Technical Digest of Optical Fiber Communication Conference*, PD2.1, 2010.

[15] Cai J.-X. et al., "20 Tbit/s capacity transmission over 6860 km," *Technical Digest of Optical Fiber Communication Conference*, PDPB4, 2011.

[16] Qian D. et al., "101.7-Tb/s (370x294-Gb/s) PDM-128QAM-OFDM transmission over 3x55-km SSMF using pilot-based phase noise mitigation," *Technical Digest of Optical Fiber Communication Conference*, PDPB5, 2011.

[17] Trebino R., "Frequency-resolved optical gating," *Kluwer academic publishers*, 2002.

[18] Ellis A.D., "All optical networking beyond 10 Gbit/s," *PhD Thesis*, 1997.

[19] Jepsen K.S. et al., "Investigation of cascadability of add-drop multiplexers in OTDM systems," *Proceedings of European Conference on Optical Communication*, pp. 619-620, 1998.

[20] Kroh M. et al., "Transmitter enabling ultra-high speed transmission of phase modulated data signals up to 640 Gbit/s," *Technical Digest of Optical Fiber Communication Conference*, OWW1, 2006.

[21] Nakazawa M. et al., "1.28Tbit/s-70km OTDM transmission using third- and fourth-order simultaneous dispersion compensation with a phase modulator," *Electronics Letters*, vol. 36, no. 24, pp. 2027-2029, 2000.

[22] Richter T. et al., "Single wavelength channel 10.2 Tb/s TDM-Data capacity using 16-QAM and coherent detection," *Technical Digest of Optical Fiber Communication Conference*, PDPA9, 2011.

[23] Chraplyvy A. R. Boivin L., "Testing optical time-division multiplexed transmission systems with interleaved bit sequences," *Technical Digest of Optical Fiber Communication Conference*, WM35, 2000.

[24] Kaminow I.P., "Optical fiber telecommunications B: systems and networks," *Academic Press*, 2008.

[25] Molle L. et al., "Polarization multiplexed 20 Gbaud square 16QAM long-haul transmission over 1120 km using EDFA amplification," *Proceedings of European Conference on Optical Communication*, Paper 8.4.4, 2009.

[26] Yu J. Zhou X., "200-Gb/s PDM-16QAM generation using a new synthesizing method," *Proceedings of European Conference on Optical Communication*, Paper 10.3.5, 2009.

[27] Ludwig R. et al., "Unrepeatered transmission of 160 Gb/s RZ-DPSK over 240km dispersion managed fiber," *Proceedings of European Conference on Optical Communication*, 2007.

[28] Kagawa M. et al., "Control and stabilization of bit-wise phase correlation in 160 (4 x 40) Gbit/s OTDM signal and its impact on transmission," *Optics Express*, vol. 16, no. 14, pp. 10039-10050, 2008.

[29] Schilling M. et al., "OTDM planar lightwave components (PLCs) for multiplexing from 40 Gb/s to 80-640 Gb/s," *Proceedings of Lasers and Electro-Optics Society Conference*, ThBB5, 2002.

[30] Hirano A. et al., "Dispersion tolerant 80 Gbit/s optical-time-division multiplexing using a duty- and phase-control technique," *Proceedings of European Conference on Optical Communication*, We C1, 1999.

[31] Schubert C. et al., "Comparison of interferometric all-optical switches for demultiplexing applications in high-speed OTDM systems," *IEEE Journal of Lightwave Technology*, vol. 20, no. 4, pp. 618-624, 2002.

[32] Mortimore D. B., "Fiber loop reflectors," *IEEE Journal of Lightwave Technology*, vol. 6, no. 7, pp. 1217-1224, 1988.

[33] Verdurmen E.J.M. et al., "OTDM demultiplexing using HNLF in a NOLM at 160 Gb/s," *Proceedings of Lasers and Electro-Optics Society Conference*, 2004.

[34] Schubert C. et al., "160-Gb/s all-optical demultiplexing using a gain-transparent ultrafast-nonlinear interferometer (GT-UNI)," *IEEE Photonics Technology Letters*, vol. 13, no. 5, pp. 475-477, 2001.

[35] Weber H.G. et al., "Single channel 1.28 Tbit/s and 2.56 Tbit/s DQPSK transmission," *Electronics Letters*, vol. 42, no. 3, 2006.

[36] Boerner C. et al., "320 Gbit/s clock recovery with electro-optical PLL using a bidirectionally operated electroabsorption modulator as phase comparator," *Technical Digest of Optical Fiber Communication Conference*, OTuO3, 2005.

[37] Kawanishi S. Kamatani O., "Prescaled timing extraction from 400 Gb/s optical signal using a phase lock loop based on four-wave mixing in a laser diode amplifier," *IEEE Photonics Technology Letters*, vol. 8, no. 8, pp. 1094-1096, 1996.

[38] Turkiewicz J.P. et al., "160 Gbit/s OTDM networking using deployed fiber," *IEEE Journal of Lightwave Technology*, vol. 23, no. 1, pp. 225-235, 2005.

[39] Denton R. T. Kinsel T. S., "Terminals for a high-speed optical pulse code modulation communication systems: 2. Optical multiplexing and demultiplexing," *Proceedings of IEEE*, vol. 56, no. 2, pp. 146-154, 1968.

[40] Tucker R.S. et al., "Optical time-division multiplexing for very high bit-rate transmisison," *IEEE Journal of Lightwave Technology*, vol. 6, no. 11, pp. 1737-1749, 1988.

[41] Nakazawa M. et al., "160 Gbit/s soliton data transmission over 200 km," *Electronics Letters*, vol. 31, no. 7, pp. 565-566, 1995.

[42] Kawanichi S. et al., "1.4 Tbit/s (200 Gbit/s x 7 ch) 50 km optical transmission experiment," *Electronics Letters*, vol. 33, no. 20, pp. 1716-1717, 1997.

[43] Kawanichi S. et al., "3 Tbit/s (160 Gbit/s x 19 ch) OTDM/WDM transmission experiment," *Technical Digest of Optical Fiber Communication Conference*, PD1, 1999.

[44] Schmidt M. et al., "8x170 Gbit/s DWDM field transmission experiment over 430 km SSMF using adaptive PMD compensation," *Proceedings of European Conference on Optical Communication*, Th4.1.12, 2004.

[45] Gnauck A.H. et al., "1-Tb/s (6*170.6 Gb/s) transmission over 2000-km NZDF using OTDM and RZ-DPSK format," *IEEE Photonics Technology Letters*, vol. 15, no. 11, pp. 1618-1620, 2003.

[46] Suzuki A. et al., "10x320 Gb/s (3.2 Tb/s) DWDM/OTDM transmission in C-band by semiconductor based devices," *Proceedings of European Conference on Optical Communication*, Th4.1.7, 2004.

[47] Murai H. et al., "Single channel 160 Gbit/s CS-RZ transmission over 640 km

with EA modulator based OTDM module," *Proceedings of European Conference on Optical Communication*, Mo3.6.4, 2003.

[48] Daikoku M. et al., "160-Gb/s four WDM quasi-linear transmission over 225-km NZ-DSF with 75-km spacing," *IEEE Photonics Technology Letters*, vol. 15, no. 8, pp. 1165-1167, 2003.

[49] Weisser S. et al., "Single- and alternating-polarization 170-Gb/s transmission up to 4000 km using dispersion-managed fiber and all-Raman amplification," *IEEE Photonics Technology Letters*, vol. 18, no. 12, pp. 1320-1322, 2006.

[50] Feiste U. et al., "160 Gbit/s transmission over 116 km field-installed fiber using 160 Gbit/s OTDM and 40 Gbit/s ETDM," *OFC Proceedings*, ThF3, 2001.

[51] Richter T. et al., "Single wavelength channel 10.2 Tb/s TDM-Data capacity using 16-QAM and coherent detection," *OFC Proceedings*, PDPA9, 2011.

[52] Zhang C. et al., "Demodulation of 480-Gbit/s 8PSK OTDM signal with digital coherent receiver," *Proceedings of European Conference on Optical Communcation*, Mo.4.D.6, 2008.

[53] Schmidt-Langhorst C. et al., "Generation and coherent time-division demultiplexing of up to 5.1 Tb/s single-channel 8-PSK and 16-QAM signals," *Technical Digest of Optical Fiber Communication Conference*, PDPC6, 2009.

[54] Zhang C. et al., "Straight-line 1073-km transmission of 640-Gbit/s dual-polarization QPSK signals on a single carrier," *Proceedings of Eurooean Conference on Optical Communication*, PD2.8, 2009.

[55] Schmidt-Langhorst C. et al., "Terabit/s single-carrier transmission systems based on coherent time-division multiplexing," *Technical Digest of Optical Fiber Communication Conference*, OThV3, 2010.

[56] Lach E. et al., "Application of electroabsorption modulators for high-speed transmission systems," *Journal of Optical Fiber Communication, Rep. 2*, pp.140-170, 2005.

[57] Evans P. et al., "Multi-channel coherent PM-QPSK InP transmitter photonic integrated circuit (PIC) operating at 112 Gb/s per wavelength," *Technical Digest of Optical Fiber Communication Conference*, PDPC7, 2011.

[58] Boivin L. et al., "Receiver sensitivity improvement by impulsive coding," *IEEE Photonics Technology Letters*, vol. 9, no. 5, pp. 684-686, 1997.

[59] Kalmar A. Winzer P.J., "Sensitivity enhancement of optical receivers by impulsive coding," *IEEE Journal of Lightwave Technology*, vol. 17, no. 2, pp. 171-177, 1999.

[60] Renaudier J. et al., "Experimental analysis of 100Gb/s coherent PDM-QPSK long-haul transmission under constraints of typical terrestrial networks," *Proceedings of European Conference on Optical Communication*, Th.2.A.3, 2008.

[61] Renaudier J. et al., "8 Tb/s long haul transmission over low dispersion fibers using 100 Gb/s PDM-QPSK channels paired with coherent detection," *Bell Labs Technical Journal*, vol. 14, no. 4, pp. 27-45, 2010.

[62] Behrens C. et al., "Nonlinear distortion in transmission of higher-order modulation formats," *IEEE Photonics Technology Letters*, vol. 22, no. 15, pp. 1111-1113, 2010.

[63] Xie C. et al., "Comparison of RZ and NRZ formats in 112-Gb/s PDM-QPSK long haul coherent transmission systems," *Technical Digest of Optica Fiber Communication Conference*, JThA, 2011.

[64] Lyubomirsky I. Wang Y.-H., "Impact of DP-QPSK pulse shape in nonlinear 100 G transmission," *IEEE Journal of Lightwave Technology*, vol. 28, no. 18, pp. 2750-2756, 2010.

[65] Carter A.C. Griffin R.A., "Optical differential quadrature phase-shift jey (oDQPSK) for high capacity optical transmission," *Technical Digest of Optical Fiber Communication Conference*, WX6, 2002.

[66] Salehi M. Proakis J.G., "Digital Communications," *McGraw-Hill*, 2008.

[67] Gnauck A.H. Winzer P.J., "112-Gb/s polarisation-multiplexed 16-QAM on a 25-GHz WDM grid," *Proceedings of European Conference on Optical Communication*, Th.3.E.5, 2008.

[68] Nolle M. et al., "8x224 Gbit/s PDM 16QAM WDM transmission with real-time processing at the transmitter," *Proceedings of European Conference on Optical Communication*, We.8.C.4, 2010.

[69] Alfiad M.S. et al., "Transmission of 11x224-Gb/s Polmux-RZ-16QAM over 1500 km of longline and pure-silica SMF," *Proceedings of European Conference of Optical Communication*, We.8.C.2, 2010.

[70] Sakamoto T. et al., "50-km SMF transmission of 50-Gb/s 16 QAM generated by

quad-parallel MZM," *Proceedings of European Conference on Optical Communication*, Tu.1.E.3, 2008.

[71] Sano A. et al., "Ultra-high capacity WDM transmission using spectrally-efficient PDM 16-QAM modulation and C- and extended L-band wideband optical amplification," *IEEE Journal of Lightwave Technology*, vol. 29, no. 4, pp. 578-586, 2011.

[72] Lu G.-W. et al., "40-Gbaud 16-QAM transmitter using tandem IQ modulators with binary driving electronic signals," *Optics Express*, vol. 18, no. 22, pp. 23062-23069, 2010.

[73] Yamada E. et al., "Demonstration of 50 Gbit/s 16QAM signal generation by novel 16QAM generation method using a dual-drive InP Mach-Zehnder modulator," *Tehnical Digest of Optical Fiber Communication Conference*, OMU1, 2011.

[74] Doerr C.R. et al., "28-Gbaud InP square or hexagonal 16-QAM modulator," *Technical Digest of Optical Fiber Communication Conference*, OMU2, 2011.

[75] Gnauck A.H. et al., "Generation and transmission of 21.4-Gbaud PDM 64-QAM using a high-power DAC driving a single I/Q modulator," *Technical Digest of Optical Fiber Communication Conference*, PDPB2, 2011.

[76] Griffin R.A. et al., "Integrated DQPSK transmitter for dispersion-tolerant and dispersion-managed DWDM transmission," *Technical Digest of Optical Fiber Communication Conference*, FP6, 2003.

[77] Foursa D. et al., "Coherent 40 Gb/s transmission with high spectral efficiency over transpacific distances," , OMI4, 2011, p. Technical Digest of Optical Fiber Communication Conference.

[78] Sjodin M. et al., "Comparison of polarization-switched QPSK and polarization-multiplexed QPSK at 30 Gbit/s," *Optics Express*, vol. 19, no. 8, pp. 7839-7846, 2011.

[79] Millar D.S. et al., "Generation and long-haul transmission of polarization-switched QPSK at 42.9 Gb/s," *Optics Express*, vol. 19, no. 10, pp. 9296-9302, 2011.

[80] Yu J. Zhou X., "Multi-level, multi-dimensional coding for high-speed and high-spectral-efficiency optical transmission," *IEEE Journal of Lightwave Technology*,

vol. 27, no. 16, pp. 3641-3653, 2009.

[81] Yu J. et al., "17 Tb/s (161x114Gb/s) PolMux-RZ-8PSK transmission over 662 km of ultra-low loss fiber using C-band EDFA amplification and digital coherent detection," *Proceedings of European Conference on Optical Communication*, Th.3.E.2, 2008.

[82] Freund R. et al., "30 Gbit/s RZ-8-PSK transmission over 2800 km standard single mode fibre without inline dispersion compensation," *Technical Digest of Optical Fiber Communication Conference*, OMI5, 2008.

[83] Zhou X. et al., "Transmission of 32-Tb/s capacity over 580km using RZ-shaped PDM-8QAM modulation format and cascaded multimodulus blind equalization algorithm," *IEEE Journal of Lightwave Technology*, vol. 28, no. 4, pp. 456-465, 2010.

[84] Winzer P.J. et al., "Spectrally efficient long-haul networking using 112-Gb/s polarization-multiplexed 16-QAM," *IEEE Journal of Lightwave Technology*, vol. 28, no. 4, pp. 547-556, 2010.

[85] Gnauck A.H. et al., "Spectrally efficient long-haul WDM transmission using 224-Gb/s polarization-multiplexed 16-QAM," *IEEE Journal of Lightwave Technology*, vol. 29, no. 4, pp. 373-377, 2011.

[86] Liu X. et al., "Single coherent detection of a 606-Gb/s CO-OFDM signal with 32-QAM subcarrier modulation using 4 x 80-Gsamples/s ADCs," *Technical Digest of Optical Fiber Communication Conference*, PD2.6, 2010.

[87] Okamoto S. et al., "512 QAM (54 Gbit/s) coherent optical transmission over 150 km with an optical bandwidth of 4.1 GHz," *Proceedings of European Conference on Optical Communication*, PD2.3, 2010.

[88] Zhou X. et al., "64-Tb/s (640x107-Gb/s) PDM-36QAM transmission over 320km using both pre- and post-transmission digital equalization," *Technical Digest of National Fiber Optic Engineers Conference*, PDPB9, 2010.

[89] Zhou X. et al., "8x450-Gb/s, 50-GHz-Spaced, PDM-32QAM transmission over 400km and one 50GHz-grid ROADM," *Technical Digest of Optical Fiber Communication Conference*, PDPB3, 2011.

[90] Kobayashi T. et al., "120-Gb/s PDM 64-QAM transmission over 1280 km using multi-staged nonlinear compensation in digital coherent receiver," *Technical*

Digest of Optical Fiber Communication Conference, OThF, 2011.

[91] Sano A. et al., "69.1-Tb/s (432 × 171-Gb/s) C- and extended L-band transmission over 240 km using PDM-16-QAM modulation and digital coherent detection," *Technical Digest of Optical Fiber Communication Conference*, PDPB7, 2010.

[92] Jansen S.L. et al., "Optical OFDM, a hype or is it for real," *Proceedings of European Conference on Optical Communications*, Mo.3.E.3, 2008.

[93] Barbieri A. et al., "Is optical OFDM a viable alternative to single-carrier transmission for future long-haul optical systems," *Proceedings of International Conference on Communications*, 2010.

[94] Bosco G. et al., "Performance limits of Nyquist-WDM and CO-OFDM in high-speed PM-QPSK systems," *Photonics Technology Letters*, vol. 22, no. 15, pp. 1129-1231, 2010.

[95] Bosco G. et al., "On the performance of Nyquist-WDM terabit superchannels based on PM-BPSK, PM-QPSK, PM-8QAM or PM-16QAM subcarriers," *IEEE Journal of Lightwave Technology*, vol. 29, no. 1, pp. 53-61, 2011.

[96] Savory S.J., "Digital filters for coherent optical receivers," *Optics Express*, vol. 16, no. 2, pp. 804-817, 2008.

[97] Lyubomirsky I., "Coherent detection for optical duobinary communication systems," *IEEE Photonics Technology Letters*, vol. 18, no. 7, pp. 868-870, 2006.

[98] Savory S.J., "Digital coherent receivers: key concepts and subsystems," *IEEE Journal of Selected Topics in Quantum Electronics*, vol. 16, no. 5, pp. 1164-1179, 2011.

[99] Savory S.J., Ives D. Fatadin I., "Compensation of quadrature imbalance in an optical QPSK coherent receiver," *IEEE Photonics Technology Letters*, vol. 20, no. 20, pp. 1733-1735, 2008.

[100] Leven A. et al., "Real-time implementation of digital signal processing for coherent optical digital communication systems," *IEEE Journal of Selected Topics in Quantum Electronics*, vol. 16, no. 5, pp. 1227-1234, 2010.

[101] Winzer P.J. et al., "Spectrally efficient long-haul networking using 112-Gb/s polarization-multiplexed 16-QAM," *Journal of Lightwave Technology*, vol. 28, no. 4, pp. 547-556, 2010.

[102] Fatadin I. et al., "Blind equalization and carrier phase recovery in a 16-QAM optical coherent system," *Journal of Lightwave Technology*, vol. 27, no. 15, pp. 3042-3049, 2009.

[103] Makovejs S. et al., "Characterisation of long-haul 112Gbit/s PDM-QAM16 transmission with and without digital nonlinearity compensation," *Optics Express*, vol. 18, no. 12, pp. 12939-12947, 2010.

[104] Fatadin I. et al., "Blind equalization and carrier phase recovery in a 16-QAM optical coherent system," *IEEE Journal of Lightwave Technology*, vol. 27, no. 15, pp. 3042-3049, 2009.

[105] Li G. Yaman F., "Nonlinear impairment compensation for polarization-division multiplexed WDM transmission using digital backward propagation," *Photonics Journal*, vol. 1, no. 2, pp. 144-152, 2009.

[106] Millar D.S. et al., "Mitigation of fiber nonlinearity using a digital coherent receiver," *IEEE Journal of Selected Topics in Quantum Electronics*, vol. 16, no. 5, pp. 1217 - 1226, 2010.

[107] Kahn J.M. Ip E., "Compensation of dispersion and nonlinear impairments using digital backpropagation," *IEEE Journal of Lightwave Technology*, vol. 26, no. 20, pp. 3416-3425, 2008.

[108] Savory S.J. et al., "Impact of interchannel nonlinearities on a split-step intrachannel nonlinear equalizer," *IEEE Photonics Technology Letters*, vol. 22, no. 10, pp. 673-675, 2010.

[109] Mateo E.F. et al., "Improved digital backward propagation for the compensation of inter-channel nonlinear effects in polarization-multiplexed WDM systems," *Optics Express*, vol. 19, no. 2, pp. 570-83, 2011.

[110] Mateo E.F. et al., "Efficient compensation of inter-channel nonlinear effects via digital backward propagation in WDM optical transmission," *Optics Express*, vol. 18, no. 14, pp. 15144-15154, 2010.

[111] Agrawal G.P., *Nonlinear Fiber Optics*.: Academic Press, 2001.

[112] Eiselt M. et al., "Contribution of timing jitter and amplitude dispersion to XPM system penalty in WDM systems," *IEEE Photonics Technology Letters*, vol. 11, no. 6, pp. 748-750, 1999.

[113] Mamysheva N.A. Mamyshev P.V., "Pulse-overlapped dispersion-managed data

transmission and intra-channel four-wave-mixing," *Optics Letters*, vol. 24, no. 21, pp. 1454-1456, 1999.

[114] Breuer D., "Network upgrade from telecom operators view," *Technical Digest of Optical Fiber Communication Conference*, OThS7, 2007.

[115] Pitois S., "Optimisation of phase alternation in 160 Gbit/s transmission systems," *Optics Communications*, vol. 242, pp. 457-461, 2004.

[116] Johanisson P. et al., "Suppression of nonlinear effects by phase alternation in strongly dispersion-managed optical transmission," *Optics Letters*, vol. 27, no. 12, pp. 1073-1075, 2002.

[117] Appathurai S. et al., "Investigation of the optimum alternate-phase RZ modulation format and its effectiveness in the suppression of intrachannel nonlinear distortion in 40-Gbit/s transmission over standard single-mode fiber," *IEEE Journal of Selected Topics in Quantum Electronics*, vol. 10, no. 2, pp. 239-249, 2004.

[118] Edagawa N. Morita I., "Study on optimum OTDM signals for long-distance 40 Gbit/s transmission," *Technical Digest of Optical Fiber Communication Conference*, TuA4, 2002.

[119] Gill D.M. et al., "Pi/2 alternate-phase on-off keyed 42.7 Gb/s long-haul transmission over 1980 km of standard single-mode fiber," *IEEE Photonics Technology Letters*, vol. 16, no. 3, pp. 906-908, 2004.

[120] Randel S. et al., "Influence of bitwise phase changes on the performance of 160 Gbit/s transmission systems," *Technical Digest of Optical Fiber Communication Conference*, P3.31, 2002.

[121] Kagawa M. et al., "Performance comparison of bitwise phase-controlled 160 Gbit/s signal transmission using an OTDM multiplexer with phase-correlation monitor," *Proceedings of European Conference on Optical Communication* , We4.P.109, 2004.

[122] O'Sullivan M. Hui R., "Fiber optic measurement techniques," *Academic Press*, 2009.

[123] Mikhailov V., "Investigation of high-speed wavelength-division-multiplexed (WDM) optical fibre transmission systems and devices using recirculating loop techniques," *PhD Thesis*, 2003.

[124] Turkiewicz J.P. et al., "Clock recovery and demultiplexing performance of 160-Gb/s OTDM field experiments," *IEEE Photonics Technology Letters*, vol. 16, no. 6, pp. 1555-1557, 2004.

[125] Boerner C. et al., "160 Gbit/s clock recovery with electro-optical PLL using bidirectionally operated electrobsorption modulator as phase comparotor," *Electronics Letters*, vol. 39, no. 14, pp. 1071-1073, 2003.

[126] Winzer P.J. et al., "Optimum filter bandwidths for optically preamplified NRZ receivers," *IEEE Journal of Lightwave Technology*, vol. 19, no. 9, pp. 1263-1273, 2001.

[127] Fonseca D. et al., "Influence of the extinction ratio on the intrachannel nonlinear distortion of 40-Gb/s return-to-zero transmission systems over standard fiber," *IEEE Journal of Lightwave Technology*, vol. 25, no. 6, pp. 1447-1457, 2007.

[128] Nortel. (2008) Nortel meets bandwidth explosion with new, revolutionary 40G to 100G optical solution. [Online]. http://www2.nortel.com/go/news_detail.jsp?cat_id=-8055&oid=100237560

[129] Nortel. (2009) Nortel unveils industry's first commercially available 100G optical solution. [Online]. http://www2.nortel.com/go/news_detail.jsp?cat_id=-8055&oid=100237560

[130] Verizon. (2011) Verizon first service provider to announce 100G deployment on U.S. network. [Online]. http://newscenter.verizon.com/press-releases/verizon/2011/verizon-first-service.html

[131] Laperle C. et al., "WDM performance and PMD tolerance of a coherent 40-Gbit/s dual-polarization QPSK transceiver," *IEEE Journal of Lightwave Technology*, vol. 26, no. 1, pp. 168-175, 2008.

[132] He G. Gariepy D., "Measuring OSNR in WDM systems - effects of resolution bandwidth and optical rejection ratio," *098 Application note*, 2009.

[133] Behrens C. et al., "Nonlinear transmission performance of higher-order modulation formats," *IEEE Photonics Technology Letters*, vol. 23, no. 6, pp. 377-379, 2011.

[134] Winzer P.J. Phennigbauer M., "Choice of MUX/DEMUX filter characteristics for NRZ, RZ, and CSRZ DWDM systems," *IEEE Journal of Lightwave Technology*, vol. 24, no. 4, pp. 1689-1696, 2006.

[135] Alfiad M.S. et al., "Transmission of 11x224-Gb/s Polmux-RZ-16QAM over 1500 km of longline and pure-silica SMF," *ECOC Proceedings*, We.8.C.2, 2010.

[136] Gnauck A.H. et al., "Spectrally efficient long-haul WDM transmission using 224-Gb/s polarization-multiplexed 16-QAM," *Journal of Lightwave Technology*, vol. 29, no. 4, pp. 373-377, 2011.

[137] Gavioli G. et al., "Ultra-narrow-spacing 10-channel 1.12 Tb/s D-WDM long-haul transmission over uncompensated SMF and NZDSF," *IEEE Photonics Technology Letters*, vol. 22, no. 19, pp. 1419-1421, 2010.

[138] Rafique S. et al., "Digital back-propagation for spectrally efficient WDM 112 Gbit/s PM m-ary QAM transmission," *Optics Express*, vol. 19, no. 6, pp. 5219-5224, 2011.

[139] Makovejs S., Killey R.I., Savory S.J., Chen M., Bayvel P. Behrens C., "Pulse-shaping versus digital backpropagation in 224Gbit/s PDM-16QAM transmission," *Optics Express*, vol. 19, no. 14, pp. 12879-12884, 2011.

[140] Davidson C.R. Bergano N.S., "Circulating loop transmission experiments for the study of long-haul transmission systems using erbium-doped fiber amplifiers," *IEEE Journal of Lightwave Technology*, vol. 13, no. 5, pp. 879-888, 1995.

[141] Kylia. (2011) [Online]. http://kylia.com/QAM.html

[142] Birk M. et al., "Real-time, single-carrier coherent 100 Gbit/s PM-QPSK field trial," *Journal of Lightwave Technology*, vol. 29, no. 4, pp. 417-425, 2011.

[143] Ferber S. et al., "640 Gbit/s DQPSK single-channel transmission over 480 km fibre link," *Electronics Letters*, vol. 41, no. 22, 2005.

[144] Woodward S.L. et al., "Cross-polarization modulation: theory and experiment of a multiple-wavelength system," *OFC Proceedings*, OWI15, 2006.

[145] Xie C. et al., "Nonlinear polarization scattering impairments and mitigation in 10-Gbaud polarization-division-multiplexed WDM systems," *OFC Proceedings*, OTuD6, 2009.

[146] Xie C. et al., "Effect of cross-phase-modulation-induced polarization scattering on optical polarization mode dispersion compensation in wavelength-division-multiplexed systems," *Optics Letters*, vol. 28, no. 23, pp. 2303-2305, 2003.

[147] Feiste U. et al., "160 Gbit/s transmission over 116 km field-installed fiber using 160 Gbit/s OTDM and 40 Gbit/s ETDM," *Technical Digest of Optical Fiber*

Communication Conference, ThF3, 2001.

[148] Mikhailov V. et al., "Investigation of intra-channel nonlinear distortion in 40 Gbit/s transmission over standard fibre," *Proceedings of European Conference on Optical Communication*, Mo.L.3.4, 2001.

[149] Moller L. et al., "Generation of 160 Gb/s carrier-suppressed return-to-zero signals," *Proceedings of European Conference on Optical Communication*, Mo3.6.3, 2003.

[150] Schmidt M. et al., "8x170 Gbit/s DWDM field transmission experiment over 430 km SSMF using adaptive PMD compensation," *ECOC Proceedings*, Th4.1.12, 2004.